Orientation and Phase Behavior of Block Copolymers in External Electric Fields

DISSERTATION

zur Erlangung des akademischen Grades eines
Doktors der Naturwissenschaften
- Dr. rer. nat. -
der Fakultät Biologie, Chemie und Geowissenschaften
der Universität Bayreuth

vorgelegt von
Kristin Schmidt
geboren in Bad Salzungen

Bayreuth, 2007

Vollständiger Abdruck der von der Fakultät Biologie, Chemie und Geowissenschaften der Universität Bayreuth genehmigten Dissertation zur Erlangung des akademischen Grades Doktor der Naturwissenschaften (Dr. rer. nat.).

Die vorliegende Arbeit wurde in der Zeit von November 2003 bis Juni 2007 am Lehrstuhl für Physikalische Chemie der Universität Bayreuth in der Arbeitsgruppe von Herrn Prof. Dr. Georg Krausch und Herrn Prof. Dr. Alexander Böker angefertigt.

Die Arbeit wurde eingereicht am: 14. Juni 2007

Das Kolloquium fand statt am: 14. November 2007

Der Prüfungsausschuss bestand aus:
Prof. Dr. Alexander Böker (Erstgutachter)
Prof. Dr. Axel Müller (Zweitgutachter)
Prof. Dr. Helmut Alt (Vorsitzender)
Prof. Dr. Thomas Hellweg

Meiner Familie

Jede Lösung eines Problems ist ein neues Problem.
Johann Wolfgang von Goethe.

Contents

Introduction

In this thesis a discussion of electric field induced effects on block copolymer microdomains is presented. The mechanism and kinetics as well as the driving forces of the alignment process are investigated. Furthermore, the influence of an electric field on the phase behavior is studied.

Many applications of ordered mesophases in soft materials have emerged during the recent years. Block copolymers have gained considerable potential for nanotechnological applications, such as nanostructured networks and membranes, nanoparticle templates, and high-density data storage media [Has97, Bat90a, Bat99, Urb00]. Block copolymers composed of incompatible components self-assemble into microphase separated domains and, hence lead to well-ordered structures on the mesoscale. However, in the absence of external fields, typically an isotropic grain structure is obtained, which is characterized by a random distribution of microdomain orientations. In view of potential applications the control of long-range order and the removal of defects remains a crucial issue. Therefore, numerous routes have been devised to align the microdomains over large scales by use of external fields such as shear fields [Kel70, Win93, Alb94, Che97], temperature gradients [Has99] and electrical fields (see section 1.2.2).

Both lamellar and cylindrical microdomain structures were oriented macroscopically by virtue of a DC electric field. Experiments in the melt, however, are limited by the high viscosities typical for high molecular weight copolymers or copolymers of more complex architectures. These limitations can be circumvented by using concentrated block copolymer solutions in nonselective solvents [Bök02b, Bök03b].

While the aligning effect of DC electric fields on non-cubic block copolymer microphases is indisputable, its physical origin is still somewhat contentious. Two potential driving forces are being discussed. A commonly used argument is based on the fact that the dielectric contrast between the copolymer blocks will lead to a minimum in electrostatic free energy whenever the interfaces between the two dielectrics are oriented parallel to the electric field vector [Amu93]. As an alternative

driving force the potential existence of mobile ions has been discussed, which may contribute to the reorientation process via the creation of an effective polarization of the anisotropic block copolymer structure [Tso03b]. While the free energy penalty can be eliminated by reorientation of lamellae and cylinders, it cannot be eliminated in cubic phases, such as the gyroid or spherical phase, but only reduced by distorting the phase.

In the first part of this thesis experiments examining the mechanism and kinetics of the alignment of lamellar forming diblock copolymer solutions are presented. The influence of the degree of initial order on the microscopic route towards domain alignment is studied. Furthermore, to clarify the driving force of reorientation, a first quantitative study of the reorientation kinetics of various model block copolymers exposed to an electric field is presented. Moreover, first kinetic experiments in high frequency AC electric field are described.

In the second part the influence of an electric field on the phase behavior of block copolymers is studied. It is shown that a gyroid phase exposed to an electric field is first distorted and then undergoes a phase transition to cylinders. Furthermore, anisotropic deformation of the chain conformation in various block copolymer solutions via electric fields is demonstrated. These deformations lead to fully reversible and extremely fast changes in the characteristic spacings of the block copolymer microstructure. The dependence of this process on electric field strength, segregation power, block copolymer composition, and polarity of the solvent as well as the kinetics are investigated.

1.1 Microphase Separation of Block Copolymers

Block copolymers belong to the class of ordered fluids exhibiting crystal like order on a mesoscopic scale, e. g. on a length scale of several tens of nanometers, and fluid like order at a microscopic scale. They are build from two or more immiscible blocks covalently attached to each other. The incompatibility of the different blocks provides a short range repulsive interaction, which drives a phase segregation of the blocks into domains rich of only one component, i. e. they self-assemble into ordered microstructures [Bat99]. A macroscopic phase separation cannot occur since the blocks are chemically linked at a junction point.

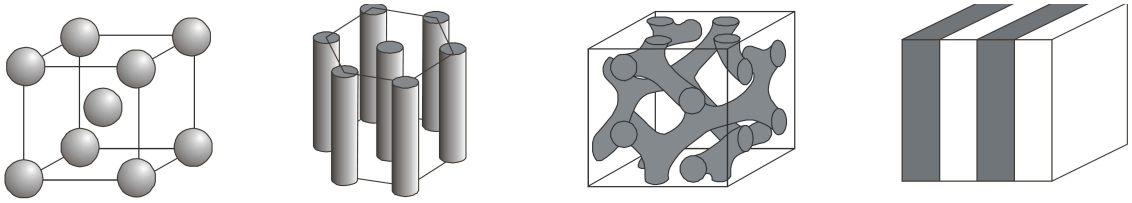

Figure 1.1: *Microphase separated morphologies of diblock copolymers. From left to right: body-centered spheres (S), hexagonally packed cylinders (C), gyroid (G), and lamellae (L) [Abe00].*

1.1.1 Morphologies in Diblock Copolymers

The tendency of block copolymers to separate into microdomains is governed by two competing driving forces. On one hand, the system tends to minimize the enthalpic unfavorable interface between the incompatible blocks via the formation of A-rich and B-rich regions. Thereby, the smallest possible interface-to-volume ratio is achieved. On the other hand, the microphase separation results in a significant stretching of the respective block chains while the conformational entropy tends to a random coil conformation. The loss in entropic energy has to be balanced by the gain in enthalpic energy. Thus, the formed morphology within the block copolymer is determined by the interplay of these contributions. As a result, a morphology with a larger interface between the blocks than the minimal interface is formed.

The different thermodynamically stable microphases for AB diblock copolymers are presented in Figure 1.1 [Abe00]. The equilibrium morphologies are depicted from left to right with increasing volume fraction ϕ_A of the minority component. Symmetric diblock copolymers arrange into a lamellar phase (L), with alternating layers of the constituent blocks. The increase of the volume fraction of one component leads to more asymmetrical copolymers, for which a bicontinuous cubic gyroid phase (G) is observed. With further increase of the matrix component, i. e. with further asymmetry, a hexagonal phase in which the minority component forms cylinders (C) and a body-centered cubic phase with spheres formed from the minority component (S) occurs. Furthermore, on changing the morphology from the lamellar phase to the spherical phase the interfacial curvature increases and thereby reduces the elastic energy of the chains.

While the spherical, cylindrical and lamellar microstructure have been known for a long time, the double gyroid phase was discovered independently by Hajduk [Haj94] and Schulz [Sch94] in the 1990's. Recently, it turned out that the gyroid phase

is the only thermodynamically stable phase between lamellae and cylinders. In the gyroid phase ($Ia\bar{3}d$ symmetry) the minority component forms two three-coordination lattices which interpenetrate and are mirror images of one another. Other identified morphologies, such as ordered bicontinuous double diamond (OBDD) or hexagonally perforated lamellae (HPL), are considered as metastable phases [Haj95, Vig98].

1.1.2 Theoretical Models for the Microphase Separation

The simplest block copolymer consists of two blocks A and B linearly attached to each other. On the level of mean field theory, the following parameters control the phase behavior: The overall degree of polymerization N, the volume fractions of the individual blocks ϕ_A and ϕ_B, the individual segment length of the monomers a_A and a_B, and the A-B segment-segment interaction, described by the Flory-Huggins parameter χ_{AB}. As every chain segment contributes to the enthalpy of mixing, the incompatibility of the two blocks is not only proportional to χ_{AB} but also to the number of segments N. Therefore, the product $\chi_{AB}N$ is used to express the incompatibility [Bat90a, Oht86, Mat94]. If there are no strong specific interactions between the different monomers like hydrogen bonding or coulomb forces, the interaction parameter χ_{AB} is usually small compared to unity and positive indicating a net enthalpic repulsion of the monomers. The Flory-Huggins parameter is derived from experiments or can be calculated from the solubility parameters of both components using the van-Laar-Hildebrand equation

$$\chi_{AB} = \frac{V}{RT} \cdot (\delta_A - \delta_B)^2$$

where δ is the solubility parameter of the respective segments and V is the molar segment volume. χ_{AB} is typically inversely proportional to the temperature, therefore mixing of the blocks is enhanced at higher temperatures. As soon as $\chi_{AB}N$ is large enough the system tries to minimize the nonfavorable contacts between A and B monomers by microphase separation. If the temperature of the system increases and thus χ_{AB} decreases, the entropic factors will dominate and the system will become disordered. This process is called order-disorder transition (ODT).

The amount of segregation and the molecular conformation of a block copolymer melt can be divided into five regimes with increasing interaction $\chi_{AB}N$. Figure 1.2 shows from top to bottom the density profile perpendicular to the formed structure, the lateral structure formed in the system, and the definition of regimes depending on order, theoretical treatment and chain conformation as a function of $\chi_{AB}N$ [Ros95].

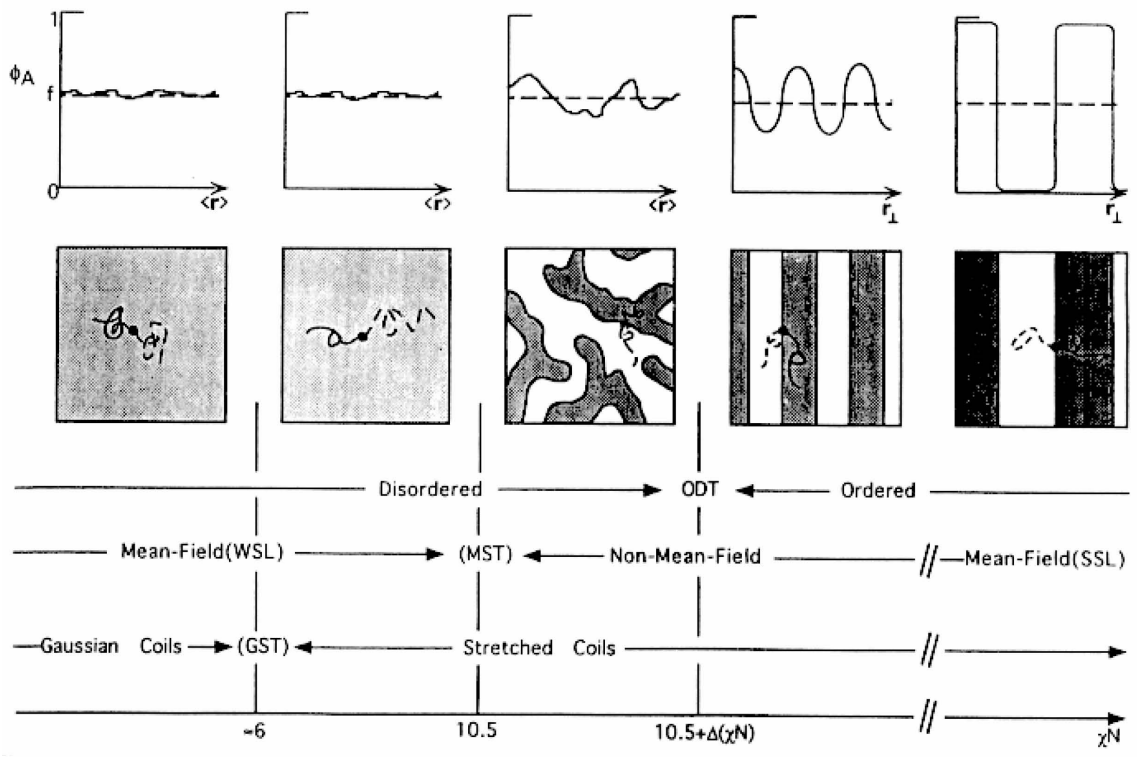

Figure 1.2: *Five regimes of block copolymer segregation and molecular conformation. The borders are marked by the Gaussian to stretched (coil) transition (GST), the microphase separation temperature (MST), the order-disorder transition (ODT), and the limit of strong segregation (SSL). Depicted are from top to bottom the composition profile, the state of order, and the definition of regimes depending on order, theoretical treatment and chain conformation as a function of the interaction* $\chi_{AB}N$ *[Ros95].*

Weak Segregation Limit

For $\chi_{AB}N \ll 10$ the entropic contributions overwhelm the enthalpic term, resulting in the formation of a mixed, isotropic phase whereas the chain segments of both components penetrate into each other. With an increase of $\chi_{AB}N$ to $\chi_{AB}N < 10$ by either a higher incompatibility or a larger degree of polymerization, a correlation hole occurs in the polymer melt with fluctuations on a length scale proportional to the radius of gyration R_g. These fluctuations can be regarded as the origin of the formation of a microphase separated structure ($\chi_{AB}N = 10.5$) [Oht86]. The composition profile is sinusoidal, i. e. a broad smeared interface separates neighboring microdomains. This regime is referred to as the "weak segregation limit" (WSL).

Considerably below $\chi_{AB}N = 10.5$, at the Gaussian-to-stretched (coil) transition

(GST), the diblock chains become stretched [Alm90]. Rosedale *et al.* experimentally found this transition to occur at $\chi_{AB}N \sim 6$ [Ros95], while Fried and Binder reported a GST at $\chi_{AB}N \sim 4$ based on Monte Carlo simulations [Fri91].

A phase diagram for weakly segregated diblock copolymers was first calculated by Leibler [Lei80] using Landau's mean field approximation. For symmetric diblock copolymers a second-order transition between the lamellar and disordered phase was predicted. At other compositions a first-order transition between the disordered state and a spherical phase was predicted, followed by a change into the cylindrical phase and finally into the lamellar phase upon further increase of $\chi_{AB}N$. The chain statistics are Gaussian, which implies that the radius of gyration R_g scales with $N^{1/2}$ [Ros95]. The microphase separation transition (MST) occurs at $\chi_{AB}N = 10.5$ and does not necessarily coincide with the order-disorder transition (ODT). This region is strongly influenced by composition fluctuations, which have been found responsible for the shift of the ODT away from the MST. However, in Leibler's approach fluctuation effects are not included.

Fredrickson and Helfand [Fre87] expanded the theory of Leibler by incorporation of compositional fluctuations into the mean field theory, by also taking the degree of polymerization into account. Figure 1.3 shows a comparison of phase diagrams calculated for a diblock copolymer using the approach of Leibler and of Fredrickson

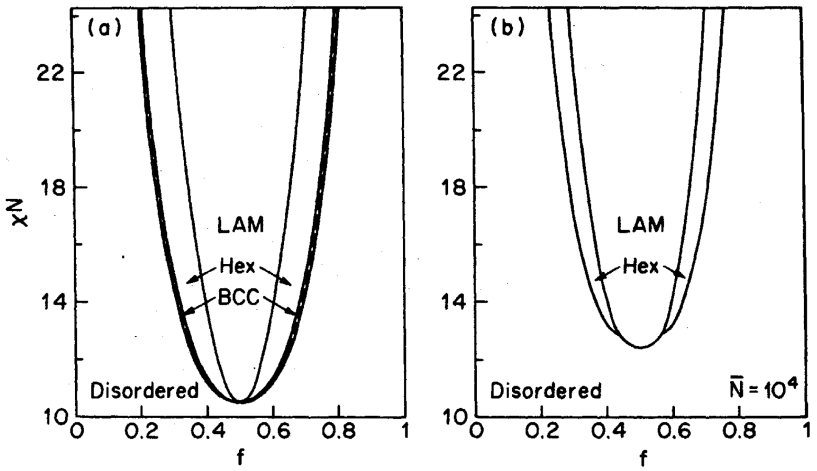

Figure 1.3: *(a) Phase diagram of a diblock copolymer according to Leiblers theory and (b) including fluctuation corrections according to Fredrickson and Helfand. (LAM) lamellar phase, (HEX) hexagonal phase, (BCC) body-centered cubic phase [Bat90b].*

and Helfand. In contrast to Leiblers theory, a direct transition from the disordered state to lamellae or cylinders was found. Moreover, a first-order transition between lamellar and disordered state was predicted for symmetric diblock copolymers.

Strong Segregation Limit

Diblock copolymers belonging to the regime of the "strong segregation limit" (SSL), show a strong incompatibility of the two segments, which is indicated by a large value for χ_{AB} ($\chi_{AB}N \gg 10$). Phase separation does occur even for small N, the interphases between the domains are narrow and well separated, and nearly pure A and B microdomains form.

This regime has been first theoretically investigated by Helfand [Hel76] and Semenov [Sem93]. However, this theory does not extend to the WSL. Therefore, calculations on phase diagrams are limited to $\chi_{AB}N > 100$. Nevertheless, SSL calculations are qualitatively correct, provide analytical expressions for the quantities of interest, and offer intuitive explanations for the phase behavior. In the SSL, the free energy $\mathcal{F}$ of the melt takes the form [Mat97a]

$$\frac{\mathcal{F}}{nk_BT} = \mathcal{F}^A_{entropic} + \mathcal{F}^B_{entropic} + \mathcal{F}_{interfacial} \tag{1.1}$$

$$= \alpha^A \left(\frac{D}{a\sqrt{N}}\right)^2 + \alpha^B \left(\frac{D}{a\sqrt{N}}\right)^2 + \beta\sqrt{\chi_{AB}N}\left(\frac{D}{a\sqrt{N}}\right)^{-1} \tag{1.2}$$

where n is the number of molecules in the melt, D the characteristic domain size. The coefficients α^A, α^B, and β are quantities that depend on the molecular composition ϕ and the geometry of the microstructure. The first two terms $\mathcal{F}^A_{entropic}$ and $\mathcal{F}^B_{entropic}$ account for entropic losses from stretching the A and B blocks, respectively. They are proportional to D^2 because the polymer chains are Gaussian. The last term $\mathcal{F}_{interfacial}$ represents the interfacial energy and is proportional to D^{-1}. Minimizing this free energy amounts to balancing entropic stretching energy against interfacial energy. This determines the equilibrium domain size, which exhibits the scaling form

$$D = a\left(\frac{\beta}{2\left(\alpha^A + \alpha^B\right)}\right)^{1/3} \chi^{1/6} N^{2/3}$$

The coefficients α^A, α^B and β take the values $\frac{\pi^2\phi}{8}$, $\frac{\pi^2(1-\phi)}{8}$ and $\frac{1}{\sqrt{6}}$ for the lamellar phase, respectively.

Intermediate Regime

Starting with the self-consistent field theory (SCFT) developed by Helfand and Wasserman [Hel80], Matsen and Bates [Mat96, Mat97a] developed a theory that

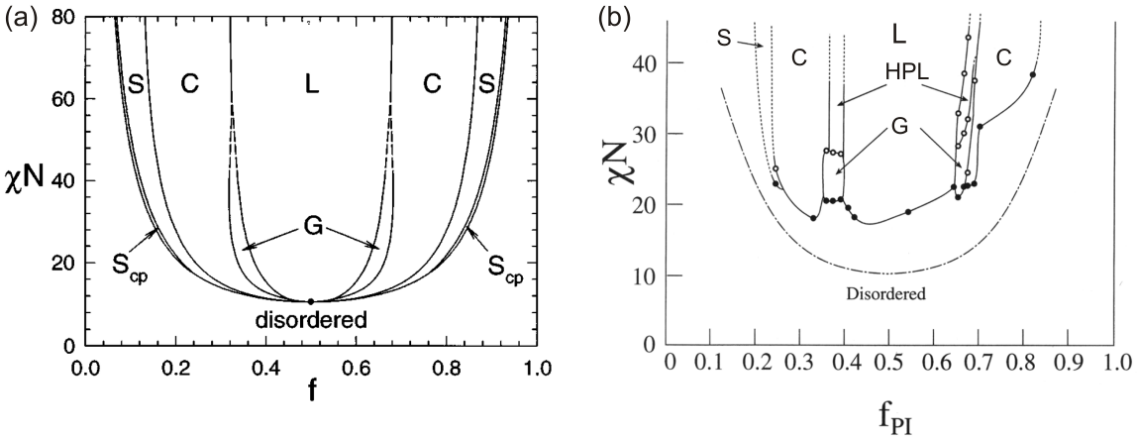

Figure 1.4: *(a) Phase diagrams predicted by SCFT calculations [Mat94] and (b) measured for the a polystyrene-b-polyisoprene system [Kha95]. (L) lamellar phase, (HPL) hexagonal perforated lamellae phase, (G) gyroid phase, (C) cylindrical phase, (S) spherical phase, and (S_{CP}) closed packed spheres phase.*

covers the bridge between the WSL and SSL. This theory allows the calculation of the phase diagram of diblock copolymers starting from the disordered state, going through the WSL and ending in the SSL.

Figure 1.4 shows the phase diagram calculated with this method in comparison with an experimentally measured phase diagram for polystyrene-*b*-polyisoprene (PS-*b*-PI) diblock copolymers [Kha95]. The experimental diagram has been established by mapping the order-order transitions (OOT) (open symbols) and the ODT (solid symbols) for ten different PS-*b*-PI diblock copolymers as the temperature was increased. The lowest line in the phase diagram represents the mean field result of Leibler. The theoretical results compare rather well with the experimental phase diagram. The sequence of phases is predicted correctly with an exception of the hexagonally perforated lamellar phase (HPL), which is only seen in the experiment. As mentioned above, this phase is not thermodynamically stable, but rather a long-lived transient structure. Another difference is the asymmetry of the experimental diagram with respect to $\phi_A = 1/2$. The reason is the different size of styrene and isoprene monomers and also some asymmetry in their interactions. The asymmetry of the statistical segment lengths a_A and a_B of the two blocks has been theoretically examined by Matsen and Bates [Mat97b]. They found that the ratio of a_A/a_B does not only change the order-order phase boundaries but also affects the relative stability of the phases. A third discrepancy is the behavior close to the ODT. While the

theory predicts all phases to converge to a critical point at $\chi_{AB}N = 10.5$, the experimental diagram shows ODTs only at larger values of $\chi_{AB}N$. The SCFT theory is a mean field theory and does not account for compositional fluctuations, which become important near the ODT curve and destabilize ordered structures.

1.1.3 Block Copolymers and Solvents

Solvents play an important role in the preparation of block copolymer samples. A solvent is called a good solvent, if a homopolymer chain effectively swells in solution. If it keeps a Gaussian shape the solvent is called theta solvent and if it shrinks the solvent is a bad solvent. For block copolymers the solvent can be selective or nonselective, whether the solvent prefers one of the blocks or not. In a strict sense a solvent is always selective, since it typically slightly prefers one of the blocks [Hua98].

The influence of a nonselective solvent of good quality on the block copolymer behavior is often approximated by the so called "dilution approximation" [Hel72, Lod03]. In this approximation the phase diagram of a block copolymer solution is obtained by rescaling χ_{AB} to $\phi_P\chi_{AB}$, where ϕ_P is the polymer volume fraction of the polymer solution. The accumulation of solvent at the interfaces, i. e. the existence of a solvent-rich and a polymer-rich phase, is neglected [Fre89]. This two-phase region is predicted to be very narrow and therefore of no experimental consequence for nonselective solvents.

The SCFT theory for block copolymer melts has been extended to block copolymer solutions [Hon83, Whi90, Whi92]. It has been shown that the dilute approximation is valid for the construction of the phase diagram. As already discussed, the SCFT calculations neglect the influence of composition fluctuations, which turn out to be even more important in the presence of solvent.

A series of experiments studying the influence of solvents and the validity of the dilution approximation has been performed in the group of Lodge [Lod95, Han98, Han00, Lod03]. The experiments show that the dilution approximation is valid for the OOTs but fails to describe the ODT in block copolymer solutions, i. e. the approximation correctly describes the phase diagram except in a close range near the ODT. Dilution expands the stability of the disordered state, since the presence of solvent enhances compositional fluctuations.

1.2 Electric Field Induced Alignment of Block Copolymers

Designed control of material properties in the submicrometer range has drawn considerable interest during the recent years because of its importance in applications as well as in basic research. For block copolymers electric fields are effective in aligning microdomains in a desired direction, as has been shown experimentally and theoretically (see section 1.2.2).

It seems unlikely that alignment by an electric field can compete with well-known shear alignment methods for achieving strong alignment of lamellar structures. However, electric field induced alignment offers means of orienting block copolymer microstructures in ways not possible by flow methods. By applying a voltage difference across the electrodes, alignment of the microstructure in the direction orthogonal to the flow or surface induced alignment direction can be achieved. By choosing the placement and the size of the electrodes, it is possible to align only certain regions of the sample. Finally, the physics of electric field induced alignment is simpler than of flow induced alignment. Therefore, electric field induced orientation may offer a convenient way to study materials properties such as defect mobility and interaction between defects.

1.2.1 Electrothermodynamics

When a material with inhomogeneous dielectric constant is placed in an electric field, there is an electrostatic free energy penalty for having interfaces of different dielectric constants perpendicular to the field.

In the following, a block copolymer filling the gap between two parallel planar electrodes is considered. The free energy of a dielectric material in an electric field is given by [Amu93]

$$\mathcal{F} = \mathcal{F}_0 - \frac{1}{8\pi} \int_{\mathcal{V}} \varepsilon(\mathbf{r}) \, |\mathbf{E}(\mathbf{r})|^2 \, \mathrm{d}^3\mathbf{r}$$

for the condition of constant potential at the boundaries. $\mathcal{F}$ is the total free energy, $\mathcal{F}_0$ the free energy without an external electric field, $\varepsilon(\mathbf{r})$ the local dielectric constant, and $\mathbf{E}(\mathbf{r})$ the electric field. The integration is over the volume $\mathcal{V}$ of the polymer. Different composition patterns within a block copolymer material and the associated spatially varying local dielectric constant produce different patterns of electric field. The consequence is a composition-pattern-dependent electrostatic contribution to the free energy. Certain orientations of the composition pattern are thermodynamically favored over others.

When a body with a dielectric constant ε is placed in an electric field $\mathbf{E}_0$, the difference in polarization between the body and the surroundings will induce polarization charges on the surface of the body. These surface charges give rise to a depolarization field $\mathbf{E}_p$ superposed to the external field $\mathbf{E}_0$. The forces that give rise to preferred orientation originate from these surface charges [DeR04].

The local dielectric constant in a block copolymer sample is a function of the local composition and can be expressed as an expansion in the composition pattern $\overline{\Psi}$, associated with the ordered state[Amu93]

$$\varepsilon(\mathbf{r}) = \varepsilon_D(\mathbf{r}) + \beta\overline{\Psi}(\mathbf{r}) + \frac{1}{2}\frac{\delta^2\varepsilon}{\delta\Psi^2}\left[\overline{\Psi}(\mathbf{r})\right]^2$$

where ε_D is the dielectric constant in the limit of a vanishing stationary composition pattern and includes effects of dynamic composition fluctuations. $\Psi(\mathbf{r})$ is the local volume fraction of one component minus its mean value. The effect of dynamic fluctuations is separated from the effect of the compositional pattern $\overline{\Psi}(\mathbf{r})$, associated with the ordered phase. Since the dynamic fluctuations have a short correlation length, they will not significantly couple to an electric field. The stationary composition pattern can have a much larger correlation length and can couple more effectively to an electric field. β measures the sensitivity of the dielectric constant to composition changes, $\beta = \delta\varepsilon/\delta\Psi$.

Using Maxwells equation, $\nabla \cdot [\varepsilon(\mathbf{r})\mathbf{E}(\mathbf{r})] = 0$, the electrostatic contribution to the free energy is

$$\mathcal{F} - \mathcal{F}_0 = \frac{1}{8\pi}\varepsilon_D \left|\mathbf{E}_0\right|^2 \left[-\left(\frac{\langle\varepsilon\rangle}{\varepsilon_D}\right)\mathcal{V} + \left(\frac{\beta}{\varepsilon_D}\right)^2 \frac{1}{(2\pi)^3}\int \widetilde{\Psi}(\mathbf{k})\widetilde{\Psi}(-\mathbf{k})(\widehat{\mathbf{e}}_k \cdot \widehat{\mathbf{e}}_z)^2 \mathrm{d}^3\mathbf{k}\right]$$

with $\widehat{\mathbf{e}}_k$ the unit wave vector, $\widehat{\mathbf{e}}_z$ the unit vector in the direction of the applied field $\mathbf{E}_0$, and $\widetilde{\Psi}(\mathbf{k})$ the Fourier transform of $\overline{\Psi}(\mathbf{r})$. The second term on the right can yield an anisotropic contribution to the free energy of the ordered state and is the basis of electric field induced alignment.

For microstructures with at least two distinct axes of threefold or greater rotational symmetry, the integral is isotropic, and the electric field is unable to align the microstructure. Into this class fall the body-centered cubic spherical and the ordered bicontinuous gyroid microstructures. On the other hand, cylindrical and lamellar microstructures do interact anisotropically with an electric field. Since the anisotropic electric energy term is nonnegative, it is minimized by orientations for patterns with the wave vector orthogonal to the applied field.

The cylindrical morphology is made up of six hexagonally arranged wave vectors. Here, the electric field contribution to the free energy density is

$$\frac{\mathcal{F}-\mathcal{F}_0}{\mathcal{V}} = \frac{1}{8\pi}\varepsilon_D \left|\mathbf{E}_0\right|^2 \left[\frac{1}{2}\left(\frac{\beta}{\varepsilon_D}\right)^2 \left\langle \overline{\Psi}^2 \right\rangle \left[1-(\widehat{\mathbf{e}}_c\cdot\widehat{\mathbf{e}}_z)^2\right] - \frac{\langle\varepsilon\rangle}{\varepsilon_D}\right]$$

where $\widehat{\mathbf{e}}_c$ is the unit vector in the direction of the cylindrical axes. The free energy is minimized for any orientation where the six wave vectors are in the plane perpendicular to the applied electric field, i. e. the cylindrical axes are parallel to the field.

For lamellar microstructures the free energy is minimized whenever $\mathbf{E}$ lies in the plane of the lamellae. This condition does not specify a single minimum energy orientation, but a set of states along a ring. The electric contribution to the free energy density is

$$\frac{\mathcal{F}-\mathcal{F}_0}{V} = \frac{1}{8\pi}\varepsilon_D \left|\mathbf{E}_0\right|^2 \left[\left(\frac{\beta}{\varepsilon_D}\right)^2 \left\langle \overline{\Psi}^2 \right\rangle (\widehat{\mathbf{e}}_q\cdot\widehat{\mathbf{e}}_z)^2 - \frac{\langle\varepsilon\rangle}{\varepsilon_D}\right]$$

Here, $\widehat{\mathbf{e}}_q$ is the unit vector of the lamellar pattern. Only the first term is anisotropic and contributes to an alignment force. The force is proportional to the applied field strength squared $|\mathbf{E}_0|^2$, to the the mean-square of the composition pattern strength $\left\langle \overline{\Psi}^2 \right\rangle$, and to the material parameter β^2/ε_D.

The size of the anisotropic component of the electric energy is rather small. To put it on a relative basis, for the energy difference between aligned and misaligned orientations of a region of the order of k_BT, the region must be of the order of a couple of hundred nanometers on a side. Only because the electric field is acting on an organized state with long-range order it does have important effects.

The free energy expression neglects the contribution to the electric field energy from the alignment and stretching of chains and the difference of polarizability of these chains in the direction along and perpendicular to the bonds. In a very different theory Gurovich [Gur94b, Gur94a, Gur95] has examined the effects of chain deformation on the microphase transition due to anisotropy in the electric polarizability tensor. He has developed a microscopic statistical theory of diblock copolymer melts in an electric field within the framework of the random phase approximation. His theory explains the shift in phase transitions under the influence of an electric field.

The main point of his theory is that - in the presence of a monomer orienting field - it is not the simple composition ϕ, but rather an effective composition ϕ^*, describing the configurational entropy of the chains. Chains with non-randomly oriented segments are not Gaussian. For instance, an electric field polarizes monomers, interacts

with induced polar moments, and orients them. If the anisotropic polarizabilities of A and B monomers are the same, the chains will be elongated by the applied field in the same way. In general, blocks are deformed differently by an applied field. The stiffness of a chain depends on its local orientation with respect to the electric field. As a result, the composition of a copolymer related with the conformational properties cannot be defined unambiguously. For instance, the effective composition associated with the statistical segments measured along and perpendicular to the electric field are different.

In isotropic diblock copolymer melts, critical fluctuation wave vectors form a sphere at the spinodal point. An applied field breaks this isotropic symmetry. Gurovich has predicted that near the spinodal point copolymer melts reveal four different universal types of behavior. The only relevant parameters turn out to be the composition ϕ, and the parameters S_A and S_B characterizing how much the radii of gyration of blocks A and B increase along an applied field. Class $\mathcal{A}$ represents copolymers strongly degenerated in electric fields, for which the anisotropic parts of the A and B monomer polarizabilities are equal. Experimentally, this situation can be hardly realized. For class $\mathcal{B}$, critical fluctuations are concentrated in q-space on two rings perpendicular to the electric field. The transition temperature does not depend on the intensity of the applied field. For class $\mathcal{C}$, only fluctuations with wave vectors oriented strictly along the electric field lines diverge at the spinodal point, the fluctuations are concentrated on two points. A second-order transition to a lamellar phase oriented perpendicular to the electric field appears from the homogeneous melt. The effective composition ϕ^* seems to be a more relevant parameter than the composition ϕ. The ODT and the pattern periodicity depend on the intensity of the electric field. The values of χN for ODT are shifted by the electric field to smaller values of χN in comparison with those calculated for a zero electric field. For class $\mathcal{D}$, the critical wave vectors form a ring perpendicular to the electric field. A lamellar phase oriented strictly parallel to the electric field appear by first-order transition. The pattern periodicity has the same dependence on the applied electric field as for class $\mathcal{C}$-copolymers.

Onuki and Fukuda [Onu95] have investigated effects of the electric field on diblock copolymers by assuming an induced dipolar interaction among the composition fluctuations. They have shown that, upon application of an electric field perpendicular to lamellae, undulations start to grow. Subsequently, the undulations grow into larger spatial structures, eventually leading to a final square lattice pattern. As

in the theory of Amundson *et al.* [Amu93] Gurovich's theory neglects the dipolar interaction. Onuki and Fukuda have shown that these dipolar interactions are the dominant mechanism of electric field induced alignment.

1.2.2 Overview of Recent Studies

The effect of an electric field on diblock copolymers was first discussed by Amundson *et al.* [Amu91]. They reported on a macroscopic alignment of a lamellar microstructure upon cooling a melt through the order-disorder transition. The experimental SAXS results were supported by a theoretical model. The alignment process was described in terms of nucleation and reorientation of ordered domains. Since then the study of diblock copolymers under the influence of external electric fields has attracted increasing interest. Experimental studies were carried out mostly in thin films but also in bulk or concentrated solutions. *In-situ* studies that follow the pathway of alignment are scarce, though mechanisms of alignment have been suggested on the basis of indirect evidence. Theoretical investigations were performed using self-consistent theories.

Alignment of Lamellar Structures

Amundson *et al.* [Amu94] considered two mechanisms of alignment in symmetric diblock copolymer bulk samples: selective electric field induced disordering and alignment through movement of defects. Electron micrographs of an aligned block copolymer gave convincing evidence that alignment is achieved by movement and annihilation of disclination lines and defect walls. Based on calculations using the thermodynamic potential of Fredrickson and Helfand [Fre87] they concluded that the effect of selective disordering is far too weak to be operative. Employing the dynamic density functional theory simulations, Kyrylyuk *et al.* [Kyr02] provided real space images of lamellar phase transitions in diblock copolymer melts in an electric field. They found that the transition proceeds through lamellar undulations as predicted by Onuki and Fukuda [Onu95]. They did not observe selective disordering, which is in agreement with the predictions by Amundson.

Böker *et al.* [Bök02b, Bök03b] identified two distinct microscopic mechanisms of electric field induced lamellar alignment in concentrated diblock copolymer solutions: nucleation and growth of domains and grain rotation (see Figure 1.5). These mechanisms are intrinsic to the degree of microphase separation of the system. Additionally, self-consistent field theory simulations were used to provide detailed insight and yielding indications supporting both mechanisms [Zve03].

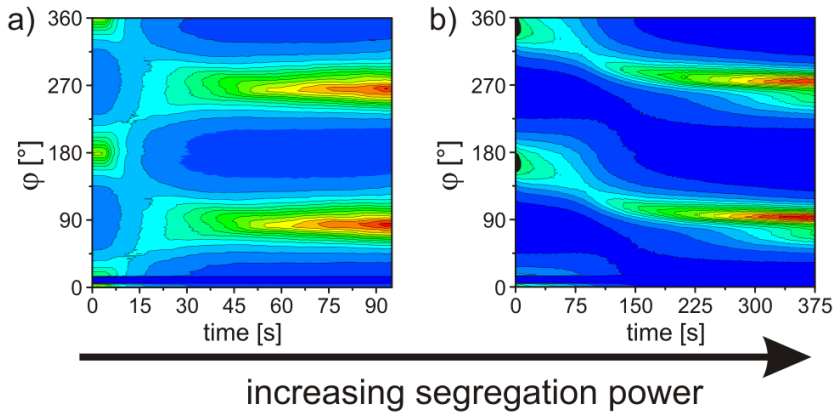

Figure 1.5: *Microscopic mechanisms of electric field induced alignment of lamellar forming diblock copolymer solutions: Time development of the scattering intensity as a function of the azimuthal angle φ in the presence of an electric field strength of $E = 1\ kV/mm$. (a) nucleation and growth of domains for weakly segregated systems, (b) grain rotation for strongly segregated systems [Bök02b].*

Experiments in thin films as a function of film thickness and interfacial energy were performed by Xu *et al.* [Xu03b, Xu04b, Xu05a]. Pereira *et al.* [Per99] and Tsori *et al.* [Tso02] described theoretically the orientation of lamellar microdomains in symmetric block copolymer films taking into account the competition between the applied field and the surface interactions. They found, that the response of weakly-segregated lamellae is different than the response of strongly-segregated lamellae. In the former case, the applied field dimishes the amplitude of the parallel state. Above a critical field, a first-order phase transition occurs from the parallel into the perpendicular state. In the strong segregation regime, a few parallel lamellae exist near the surface, while the rest of the film is oriented perpendicular. A T-junction defect is therefore created. Two threshold fields E_1 and E_2 exist, separating the parallel, the mixed, and the perpendicular orientations. With the use of quasi *in-situ* SFM imaging Olszowka *et al.* [Ols06] were able to follow the details of the reorientation process from an initially disordered structure to a highly ordered one. In a first, rather fast step, grains of ordered microdomains which are already aligned parallel to the field are formed. In a second step, the defects accumulated at the grain boundaries are removed by well-known defect annihilation steps.

Alignment of Cylindrical Structures

Electric field induced reorientation of a cylinder forming block copolymer film was first studied by Thurn-Albrecht *et al.* [TA00, TA02] for different initial situations with *in-situ* SAXS measurements. The electric field was found to orient composition fluctuations in the disordered state, resulting in a preferred growth of oriented nuclei. An electric field applied to a microphase separated copolymer led to a disruption of grains into smaller pieces that were able to rotate. This disruption occurred via the growth of undulations at the cylinder interface. Similar results were identified by Xu *et al.* [Xu05b].

Influence of Ions

Most studies to date have given little or no attention to the ions in block copolymers. Some fraction of these ions move under the influence of an electric field. This motion, in turn, changes the field and exerts forces on the system. Tsori *et al.* [Tso03b] showed that the presence of ions may increase the alignment effect markedly. They concluded that orientation can in principle be achieved without a dielectric contrast if there is a mobility contrast. The effect of ions vanishes for high frequency ($> 50\,\mathrm{Hz}$) AC electric fields. They argued that the presence of ions can also induce strong morphological changes and even lead to a phase transition [Tso03a].

Wang *et al.* [Wan06] and Xu *et al.* [Xu04a] showed an enhanced alignment for PS-*b*-PMMA diblock copolymers contaminated with lithium ions. The lithium ions coordinate with the carbonyl group in the PMMA block, thereby increasing the dielectric constant of the respective block leading to an increased dielectric contrast between the two blocks.

Use of Orthogonal Fields

Electric fields are unidirectional, causing a high degree of orientation along the field line direction but lacking any preferred orientation in the plane normal to this direction. Consequently, a second orthogonal field is required in order to achieve a morphology where the microdomain orientation can be controlled in three dimensions. Zvelindovsky *et al.* [Zve05] and Feng *et al.* [Fen04] investigated the structure of diblock copolymer melts with large scale computer simulations and cell dynamic simulations, respectively. They showed that long-range lamellae alignment can be achieved by applying simultaneously orthogonal electric and shear fields.

Long-range order of a lamellar forming diblock copolymer was achieved by Xu *et al.* [Xu03a]. An elongation flow field was applied to obtain an in-plane orientation of the microdomains, and an electric field, applied normal to the surface was then used

for further alignment of the microdomains. Olszowka *et al.* [Ols06] created stripe pattern exhibiting long-range order of a lamellar forming diblock copolymer film via the combination of an electric field oriented within the plane of the film and surface interactions tailored to favor a perpendicular orientation of the lamellae.

Shift in Phase Transitions

The electrostatic free energy penalty associated with dielectric interfaces which are not parallel to the electric field lines is the driving force for structures to reorient so that their interfaces are parallel to the field. By reorientation of lamellae and cylinders, the free energy penalty can be eliminated. On the other hand, cubic phases, such as the gyroid or spherical phase, cannot be aligned in field direction. The free energy penalty can only be reduced by distorting the cubic phase. Thus, the free energy of this distorted phase, whose symmetry is reduced, increases with respect to the other phases, a circumstance which can lead to a phase transition.

Lin *et al.* [Lin05], Tsori *et al.* [Tso06], and Pinna *et al.* [Pin06] showed, based on self-consistent field theory, that spheres elongate in the applied field direction to an extent which is a balance between electrostatic and elastic forces. At a threshold value of the electric field, a first-order transition to a hexagonal phase occurs. This threshold value is found to be considerably lower for ion containing block copolymers with respect to ion free ones [Tso03a].

The electric field induced sphere to cylinder transition in thin films was observed experimentally by Xu *et al.* [Xu04c]. TEM imaging indicated that, under an electric field, the asymmetric diblock copolymer formed spherical microdomains that were deformed into ellipsoids and, with time, interconnected to cylindrical microdomains oriented in the direction of the applied electric field.

Lyakhova *et al.* [Lya06b] studied the behavior of confined systems of sphere, cylinder, and lamellae forming block copolymers under an applied electric field by means of dynamic self-consistent theory. They found that the kinetic pathway taken by a system near a phase transition can be very different from one that is far from a phase transition (see Figure 1.6). Sphere forming systems close to ODT undergo a sphere-to-cylinder transition with partial disordering of a system in a transient state (pathway 1). Sphere forming systems further away from ODT transform into cylinders via elongation and merging of spheres (pathway 2). Cylinder forming systems close to the boundary with spheres transform into the spherical phase on their way to the perpendicular cylindrical structure (pathway 3). Cylinder forming systems close to the boundary with the bicontinuous phase transform via an intermediate

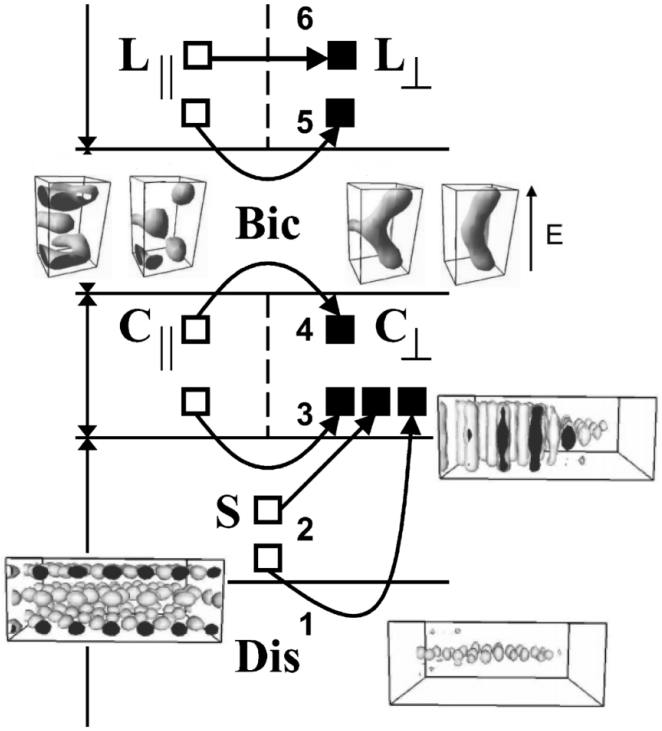

Figure 1.6: *Schematic diagram summarizing kinetic pathways (denoted by arrows) for sphere (S), cylinder (C), and lamellae (L) forming systems under an electric field. Open squares denote initial positions; black squares denote positions after the phase transition. (Dis) denotes disordered phase and (Bic) a bicontinuous phase. The insets show the structural evolution of a sphere and a cylinder forming block copolymer film [Lya06b]. See text for details about the pathways 1-6.*

bicontinuous structure (pathway 4). In a lamellae forming system they found two distinctly different mechanisms for the parallel-to-perpendicular lamellar transition. In a system relatively close to the ODT the transition proceeds via a transient bicontinuous phase (pathway 5). The transition via a local rotation of lamellar grains caused by defect movement was observed in a system further away from ODT (pathway 6). The system remains in the lamellar phase during the whole transition. They found that structural defects and undulation instability play an important role in the phase transition in systems close to any phase boundary. Ly *et al.* [Ly07] investigated the gyroid-to-cylinder transition under an electric field. They showed details of the kinetics of the transition, which includes intermediate structures with increased connectivity compared to the gyroid phase. This type of transformation

has not been studied experimentally yet.

The influence of an electric field on the composition fluctuations has not been considered. Gunkel *et al.* [Gun07] generalized the Fredrickson-Helfand theory of the microphase separation in symmetric diblock copolymer melts by taking into account the influence of a time-dependent homogeneous electric field on the composition fluctuations within the self-consistent Hartree approximation. They predicted that electric field suppresses composition fluctuations, and consequently weaken the first-order transition, i. e. the field favors demixing with respect to the free field case. They found a shift of 2.5 K for PS-*b*-PMMA and 40 kV/mm. A shift in ODT of diblock copolymers was not observed in experiments yet.

1.3 Structure of this Thesis

This thesis is organized as follows:

- Chapter 2 includes fundamentals of the synthetic methods, the characterization methods as well as the simulation model.
- An overview of the investigated materials is given in Chapter 3. It considers both the synthesis and characterization of these materials, the sample preparation, experimental setup, and the data evaluation.
- The microscopic mechanisms and the kinetics of alignment depending on the initial order of the system are discussed in Chapter 4.
- The driving force of the alignment process is investigated in Chapter 5. It describes the scaling behavior of the reorientation kinetics and first experiments in AC electric fields.
- The order-order-transitions of different phases under the influence of an electric field is investigated in Chapter 6.
- Chapter 7 covers the electric field induced changes in the periodicity of diblock copolymer systems.

Methods

2.1 Synthesis

Block copolymers can be synthesized in different ways. The most common procedures are living polymerization techniques. One important aspect of the term "living" refers to the fact that these polymerizations occur in the absence of irreversible termination and chain transfer. Therefore, the molecular weight in a living polymerization is controlled by the stoichiometry of the reaction and the degree of conversion. The living anionic and cationic polymerization as well as the group transfer polymerization (GTP) mainly meet these conditions. Furthermore, in so called controlled polymerizations chain transfer and termination is theoretically possible but can be suppressed experimentally. Techniques such as atom transfer free radical polymerization (ATRP) and reversible addition fragmentation chain transfer (RAFT) are examples.

2.1.1 Anionic Polymerization

Anionic polymerization of styrene and dienes initiated by alkali metals has been known since the early 1900's. The interest in these reactions has increased over the last decades since Szwarc first reported the "living" nature of the anionic polymerization in 1956 [Szw56]. This method allows the control over various properties of the synthesized block copolymers such as the molecular weight, molecular weight distribution, composition, microstructure, stereochemistry and functionality of the chain ends. Figure 2.1 illustrates a general reaction scheme for an anionic polymerization initiated by metal organic compounds.

The anionic polymerization starts with a nucleophilic attack of the initiator on the double bond of the monomer. The initiator that is required to polymerize a monomer depends on the reactivity of the monomer towards this attack. The monomer reactivity increases with increasing ability to stabilize the carbanion charge. Very strong nucleophiles such as amide anions or alkyl carbanions are needed to poly-

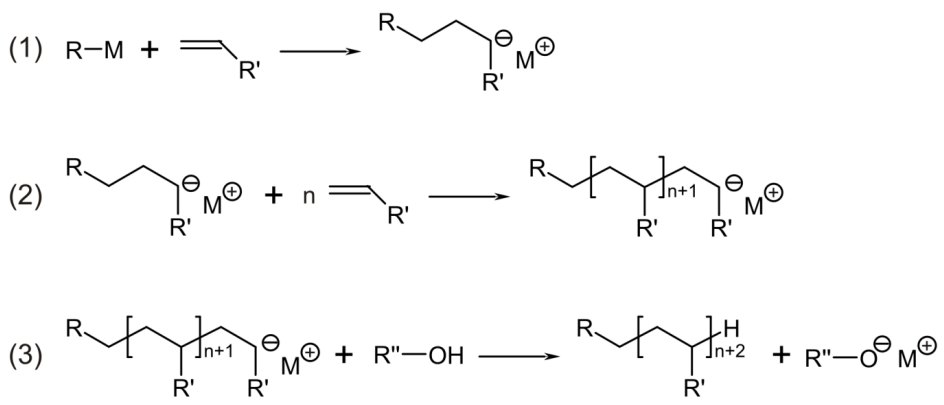

Figure 2.1: *Reaction scheme of an anionic polymerization: (1) initiation, (2) propagation, (3) termination (R-M: metal organic compound).*

merize monomers with relatively weak electron-withdrawing substituents, such as styrene and butadiene. Weaker nucleophiles, such as alkoxide or hydroxide ions, can initiate the polymerization of monomers with strongly electron-withdrawing substituents, such as acrylonitrile, methyl methacrylate and methyl vinyl ketone. The rate of propagation for an anionic polymerization is strongly affected by the nature of both the solvent and the counterion. A strong solvating power of the reaction medium increases the fraction of solvent-separated ion pairs relative to contact ion pairs and thus increases their reactivity. The reaction is terminated by addition of a hydrogen transfer agent, e. g. methanol or water. A disadvantage of the anionic polymerization is the sensitivity of the initiator and the living chain end to impurities. In order to prevent uncontrolled termination the monomers and the solvents have to be extremely clean and the polymerization has to be carried out in the absence of water and air [Bök02a].

The living nature of the propagating chain allows the synthesis of block copolymers by sequential addition of different monomers. The living chain end of one polymer has to initiate the polymerization of the following block. Therefore, it is necessary that the reactivity of the blocks decreases. The synthesis is carried out in a Buechi reactor, see Figure 2.2. The temperature-controlled reactor is equipped with a riser pipe for the withdrawal of samples or the end product, with an access for addition of the initiator, and with a manifold for different capillaries made of steel.

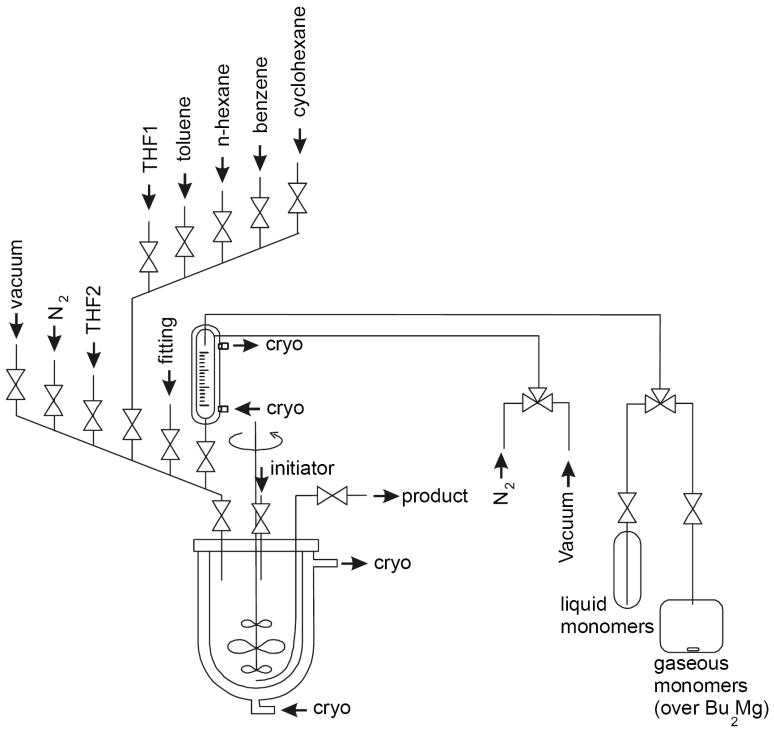

Figure 2.2: *Scheme of a Buechi reactor for anionic polymerization [Gol99].*

These capillaries provide vacuum, clean nitrogen, different solvents and access for the monomer ampoules [Gol99].

Molecular weight distribution

As described above, the molecular weight in a living polymerization is controlled by the stoichiometry of the reaction and by the degree of conversion. Therefore, a living anionic polymerization only consists of initiation and propagation steps in the absence of termination and chain transfer. As a consequence, the concentration of propagating chains c^* is constant during the course of the reaction and the number-average molecular weight depends linearly on the conversion p. Hence, for the number-average degree of polymerization $\overline{X}_n$ at full conversion is given by

$$\overline{X}_n = \frac{[M]_0}{[I]_0}$$

where $[M]_0$ is the initial concentration of monomer and $[I]_0$ the initial concentration of initiator. A consequence of the absence of termination and chain transfer in a polymerization is that the resulting polymer should be nearly monodisperse ($\overline{M}_w \cong \overline{M}_n$). This is true when the following experimental conditions are fulfilled: The

initiation must be fast compared to the propagation so that all propagations centers begin to grow simultaneously. Efficient mixing throughout the polymerization is required and depropagation must be slow relative to propagation. Moreover, there must be a fast equilibrium between propagating species of different reactivity. With these assumptions, the size distribution is given by a Poisson distribution and the polydispersity index (PDI) can be expressed as

$$\frac{\overline{X}_w}{\overline{X}_n} = 1 + \frac{\overline{X}_n - 1}{\overline{X}_n^2} \cong 1 + \frac{1}{\overline{X}_n}$$

where $\overline{X}_n$ is the number-average degree of polymerization and $\overline{X}_w$ the weight-average degree of polymerization. For a sufficiently high degree of polymerization, the size distribution will be narrow with PDI close to unity. Practically, living anionic systems under ideal conditions yield PDI$<$ 1.1.

2.1.2 Gel Permeation Chromatography

Size exclusion chromatography is a chromatographic method in which particles are separated based on their size or on their hydrodynamic volume. The name gel permeation chromatography is used when an organic solvent is used as the mobile phase. GPC is a widely used technique for the analysis of polymers in order to obtain the molecular weight distribution.

The underlying principle of GPC is that particles of different hydrodynamic volumes will elute through a stationary phase at different rates. This results in the separation of the particles based on their size. Provided that all the particles are loaded simultaneously, particles of the same size elute together. This is usually achieved with a column, consisting of a hollow tube tightly packed with extremely small porous beads designed to have pores of different sizes. As the solvent travels down the column some particles enter into the pores. Larger particles cannot enter into as many pores as small particles can. The larger the particle, the less overall volume to traverse over the length of the column, and the faster the elution. Practically, particles in solution are not of constant size, resulting in the probability that a particle which would otherwise be hindered by a pore may pass right by it. The stationary phase particles are not ideally defined, both particles and pores may vary in size. Therefore, elution curves resemble Gaussian distributions. For analysis the eluent is monitored constantly and examined by spectroscopic techniques. The common spectroscopy detection methods are refractive index (RI), evaporative light scattering (ELS), and ultraviolet (UV) measurements. Calibration curves

for the determination of molecular weights can be obtained by using well-defined standards.

2.1.3 NMR Spectroscopy

NMR spectroscopy is one of the principal techniques used to obtain physical, chemical, electronic and structural information about molecules. The absolute composition of the block copolymer can be determined with NMR spectroscopy. The different polymers yield characteristic signals in the ^{1}H-spectrum and by means of the intensity of these signal it is possible to calculate the composition of the different blocks.

For example, the composition of PS-*b*-PI block copolymers can be determined by the assignment of the following signals. The characteristic signals at 6.3 ppm and 7.2 ppm for polystyrene arise from the five aromatic protons. Due to the two double bonds isoprene has, unlike styrene, different configurations in the polymer chain, i. e. the double bond can be in the backbone of the chain (1,4-polyisoprene) or in the side chain (1,2-polyisoprene and 3,4-polyisoprene). The characteristic signals for polyisoprene at 5.2 ppm and at 4.7 ppm arise from the vinyl proton from 1,4-polyisoprene and from the vinyl proton from 3,4-polyisoprene, respectively. From the ratio of these signals not only the composition of the block copolymer can be determined but also the percentage of 1,4-polyisoprene.

2.2 Small-Angle X-Ray Scattering

X-Ray scattering and diffraction are among the principal tools for studying polymers, with their utility proven since the very beginning of polymer science. While direct imaging methods allow the investigation of the microphase in local areas of a few micrometers, x-ray scattering provides average information on bulk properties of the segregated microdomains within the sample. The technique of small-angle scattering is used to study polymer structures on a scale of 2 - 200 nm. The scattering of x-rays at small angles originates from the spatial fluctuations of the electron density within the material. Due to the interaction of the beam with the electrons, segments of the block copolymers need to be different in their electron density in order to allow a monitoring of the morphology by SAXS. The amount of structural information obtained from the scattering experiment depends to some extent on the

degree of supermolecular order within the sample. For example, this can be the radius of gyration in the case of a dilute polymer solution, while a structural model may be derived in the case of a highly-ordered copolymer system.

X-Rays are electromagnetic radiation occupying the spectrum from about 10^{-2} to 10^{2} Å in wavelength, but those used for the study of the structure of materials have wavelengths more narrowly confined to the approximate range of 0.5 - 2.5 Å. Studies on polymers are performed mostly with the K_α characteristic radiation from a copper target tube having a wavelength of 1.54 Å. Time-resolved experiments down to the millisecond range can be performed with synchrotron radiation. The spectral brilliance of modern synchrotron sources is more than 10 orders of magnitude higher than the copper K_α line of a rotating anode source and thus allows real time studies with high temporal and spatial resolution [Roe00, Nar07].

2.2.1 Basics of Scattering

Figure 2.3 shows the scattering geometry of a typical SAXS experimental setup. An incident beam of monochromatic radiation with a wavelength λ and an intensity I_0 is partly absorbed or scattered by a sample while the rest is transmitted unchanged. The scattered intensity $I(q)$ is recorded with a two dimensional detector at a distance d. The transmitted primary beam is fully absorbed by the beamstop placed in front of the detector and the entire flight path before and after the sample is in vacuum to avoid absorption and scattering by air.

The number of photons scattered as a function of the scattering angle θ is measured. For x-rays, the scattering originating from electrons is nearly independent of

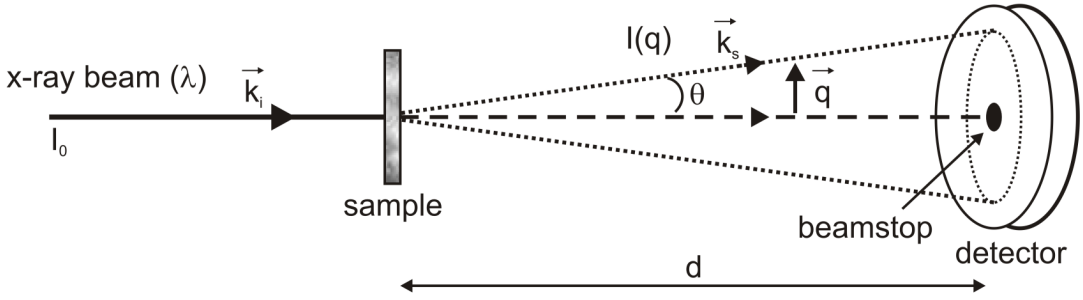

Figure 2.3: *Schematic layout of a SAXS setup illustrating the incident, scattered and transmitted x-ray beams, the 2-D detector, and the definition of the scattering vector q.*

λ except close to the absorption edge of the constituent elements. The scattering at small angles is fully elastic because of the high energy of the radiation relative to typical excitations in the sample. Therefore, the magnitude of the incident and scattered wave vector are identical

$$\left|\vec{k_i}\right| = \left|\vec{k_s}\right| = \frac{2\pi}{\lambda}$$

The scattering vector $\vec{q}$ is defined as the difference between the wave vector of the incident, and the scattered plane waves, $\vec{k_i}$ and $\vec{k_s}$.

$$\vec{q} = \vec{k_s} - \vec{k_i}$$

with the magnitude q given by

$$q = |\vec{q}| = \frac{4\pi \sin\theta}{\lambda}$$

The scattering vector has a unit of reciprocal length and indicates the typical length scales investigated by the scattering experiment.

The diffraction of x-rays by matter results from the combination of two different phenomena: scattering of x-rays by individual electrons in the sample, and interference among the waves scattered by these primary events. The interference is constructive when the phase shift is proportional to 2π, this condition can be expressed by Bragg's law

$$n\lambda = 2d_{hkl} \cdot \sin\theta$$

Thus, the spacing d_{hkl} from the diffraction pattern of a crystal can be determined by

$$d_{hkl} = \frac{2\pi n}{q}$$

2.2.2 Diffraction by Crystals

The scattered intensity pattern arising from a microphase separated block copolymer is similar to the diffraction pattern obtained from a crystal. However, the Bragg diffraction peaks show a broadening of the peaks due to the diminished regularity as compared to a regular crystalline lattice. In order to understand the scattering pattern of a microphase-separated block copolymer it is necessary to know the fundamentals about diffraction by crystals.

A crystal consists of a large number of unit cells arranged regularly in three-dimensional space, with each unit cell having the identical atomic content. The

shape and size of the unit cell are defined by the three unit cell vectors a, b, c and the angles α, β, and γ. The content of the unit cell is defined by specifying the positions of all the atoms it contains. It is more convenient to specify the unit cell content by the distribution $\rho_u(r)$ of the appropriate scattering length density. The convolution of the unit cell content $\rho_u(r)$ with the lattice $z(r)$ produces an infinite repetition of the unit cell pattern $\rho(r)$. The amplitude $A(q)$ of scattered x-rays is equal to the Fourier transform of $\rho(r)$,

$$A(q) = \int_V \rho(r) \mathrm{e}^{iqr} \mathrm{d}r$$

By using the convolution theorem, it can be obtained

$$A(q) = F(q) \cdot Z(q)$$

where $F(q)$, called the structure factor of the unit cell, is the Fourier transform of $\rho_u(r)$, and $Z(q)$, called the lattice factor, is the Fourier transform of $z(r)$. $Z(q)$ is itself a lattice in reciprocal space, and its lattice points are given by

$$r^*_{hkl} = ha^* + kb^* + lc^*$$

where h, k, l are integers. The three vectors a^*, b^*, and c^* in reciprocal space define the reciprocal lattice and are related to the unit cell vectors a, b, and c in real space. The basis vectors a^*, b^*, and c^* of the reciprocal lattice are defined as

$$a^* = \frac{1}{V_u}(b \times c), \quad b^* = \frac{1}{V_u}(a \times c), \quad c^* = \frac{1}{V_u}(b \times a)$$

where V_u is the unit cell volume given by

$$V_u = a(b \times c) = b(c \times a) = c(a \times b)$$

The structure factor $F(q)$ is in general a smoothly varying function defined over the whole range of reciprocal space. Its product with the lattice factor $Z(q)$, however, produces the amplitude function $A(q)$ that is nonzero only at the reciprocal lattice points. The scattered beam intensity $I(q)$, which is given by the square of $A(q)$, is therefore also nonzero only at the reciprocal lattice points. It is thus seen that in diffraction by crystals, the scattering vector q and hence the direction in which finite diffraction intensity is observed is determined solely by the lattice factor $Z(q)$, which in turn depends uniquely on the lattice structure represented by the unit cell vectors a, b, and c. The scattering intensities observed at these various reciprocal

lattice points are "modulated" by the structure factor $F(q)$, which is governed by the atomic content, represented by $\rho_u(r)$, of the unit cell only. Thus the interpretation of diffraction patterns from crystals cleanly separates into two aspects, the diffraction directions giving information about the lattice structure and the intensities of diffraction at various q giving information about the placement of atoms in the unit cell.

Given the diffraction data, information can be derived on the crystal structure. From the set of diffraction angles at which Bragg peaks occur, the lattice parameter and the symmetry can be determined. The first step in the determination of lattice parameters is to index the observed diffraction peaks, that is, to identify the Miller indices h, k, and l for each of the crystallographic planes d_{hkl} that gave rise to the reflections.

In a unit cell the positions of many of the atoms are related to each other by symmetry relationships. The various symmetry elements that can be present in a crystal with three-dimensional lattices are n-fold rotation axes, n-fold rotation-inversion axes, mirror planes, n-fold screw axes and glide planes. These symmetry elements can be combined to give a three-dimensional infinite lattice in one of 230 space groups. Detailed description of each of these space groups is found in the International Tables for Crystallography, Vol. A [Hah87]. Some of the hkl reflections are missing from the observed reflections. These reflections have certain simple relationships among the h, k, and l indices and these relationships depend on the particular space group. By examination of systematic absences of Bragg reflection the space group can be determined.

2.2.3 Scattering on Microphase Separated Block Copolymers

The different blocks of a block copolymer tend to segregate from each other and aggregate with their own kind, forming periodic microphases on the order of 1 to 100 nm. The most important block copolymer structures are lamellae, gyroid, hexagonally packed cylinders and body-centered spheres. These structures are accessible to study by small-angle scattering. The methods developed for the analysis of diffraction from crystals are directly applicable to the study of the periodic microdomains. The peaks arising from a scattering experiment on block copolymers are broadened because of the limited size of the domains and due to the diminished regularity. As a consequence, usually only the first few Bragg reflections are recognizable as separate peaks.

Table 2.1: *Ratios of successive Bragg peaks for different model morphologies: Body-centered spheres, hexagonally packed cylinders, gyroid and lamellae.*

Morphology Space group		**Scattering Maxima**					
		1	2	3	4	5	6
Spheres	(hkl)	110	200	211	220	310	222
$Im\bar{3}m$	q_{hkl}/q_{100}	1	$\sqrt{2}$	$\sqrt{3}$	$\sqrt{4}$	$\sqrt{5}$	$\sqrt{6}$
Cylinders	(hkl)	100	110	200	210	300	320
$P6mm$	q_{hkl}/q_{100}	1	$\sqrt{3}$	$\sqrt{4}$	$\sqrt{7}$	$\sqrt{9}$	$\sqrt{12}$
Gyroid	(hkl)	211	220	321	400	420	332
$Ia\bar{3}d$	q_{hkl}/q_{100}	$\sqrt{3}$	$\sqrt{4}$	$\sqrt{7}$	$\sqrt{8}$	$\sqrt{10}$	$\sqrt{11}$
Lamellae	(hkl)	100	200	300	400	500	600
Pm	q_{hkl}/q_{100}	1	2	3	4	5	6

In order to examine the structure of the formed microdomains the observed values for the Bragg peaks can be compared with the characteristic sequences of the model lattices. Table 2.1 presents the ratios of Bragg spacings for different spatial arrangements.

The distance d_{100} resulting from the scattering peak q_{100} corresponds directly to the shortest distance between two parallel neighboring lattice planes. For lamellar structures d_{100} is equivalent to the lamellar distance and for hexagonal structures, d_{100} and the cylinder distance L are correlated by

$$d_{100} = \frac{\sqrt{3}}{2} L$$

Orientation of anisotropic samples

The 2-D scattering pattern from an isotropic sample consists of a series of concentric circles, each circle corresponding to a Bragg peak. If, on the other hand, the block copolymer has been aligned in some way, the microdomains may no longer be randomly oriented in all directions. The presence of such a preferred orientation is recognized from the scattering pattern. The scattering circles are no longer of uniform intensity along their circumferences and may even brake up into longer or shorter arcs, depending on the degree of preferred orientation. By measuring

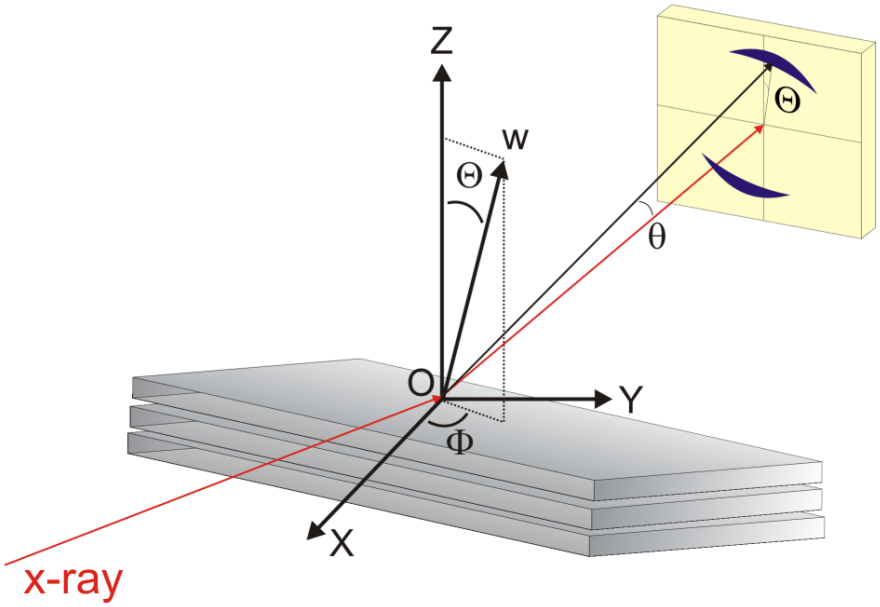

Figure 2.4: *Definition of the angles defining the orientation of a pole (normal to a lamella plane) within a sample. The coordinate system $O - XYZ$ is fixed to the sample. The two angles Θ and Φ, defined as illustrated, are used to specify the direction.*

the variation in the intensities along one scattering arc the degree and direction of preferred orientation can be determined.

A vector $\vec{w}$ is defined to be a unit vector normal to the lamella plane in a lamella forming block copolymer. The orientation of $\vec{w}$ can be specified by reference to a coordinate system $O-XYZ$ fixed to the sample. Two angles are required to specify the orientation of $\vec{w}$ within the coordinate system. The most common practice is to choose the polar and azimuthal angles Θ and Φ, as they are used in the spherical polar coordinate system (see Figure 2.4). The statistical distribution of the orientation of $\vec{w}$ in the sample can be represented by a function $t(\Theta, \Phi)$ defined for $0 \leq \Theta \leq \pi$ and $0 \leq \Phi \leq 2\pi$. $t(\Theta, \Phi)$ is called the pole distribution. For a sample having uniaxial orientation, e. g. a lamella forming system, directions having the same Θ but different Φ are all equivalent, and therefore the pole distribution can be written as a function of Θ only, $t(\Theta)$, defined for $0 \leq \Theta \leq \pi$. The pole distribution

is normalized so as to fulfill

$$\int_0^{\pi} t(\Theta) \sin \Theta \mathrm{d}\Theta = 1$$

The scattering phenomenon is unable to distinguish the scattering by a lamella with a positive direction of the pole from the scattering by a lamella with a negative direction of the pole. As a result, the pole distribution $t(\Theta)$ as determined experimentally is centrosymmetric, that is, $t(\Theta) = t(-\Theta)$. The pole distribution therefore needs to be determined in practice only for the range $0 \leq \Theta \leq \pi/2$.

It is often desirable that the degree of orientation of a pole is designated by a single number rather than by a complete distribution function. Since the pole distribution function is centrosymmetric the average of $\cos \Theta$ is equal to zero. The most natural choice for representing the average orientation of a pole is therefore to evaluate the average of $\cos^2 \Theta$. In view of the normalization of $t(\Theta)$ the averaging is performed according to

$$\left\langle \cos^2 \Theta \right\rangle = \int_0^{\pi} \cos^2 \Theta t(\Theta) \sin \Theta \mathrm{d}\Theta$$

Hermans and Platzek [Her39] proposed using, in place of $\langle \cos^2 \Theta \rangle$, the second-order Legendre function of $\cos \Theta$, i. e.,

$$\langle P_2(\cos \Theta) \rangle = \frac{3}{2} \left\langle \cos^2 \Theta \right\rangle - \frac{1}{2}$$

The parameter P_2 is called the Hermans orientation parameter or simply the orientation parameter. The value of P_2 is equal to 1, 0, or $-1/2$ when the pole is parallel to Z, random, or perpendicular to Z, respectively.

2.2.4 Experimental Setup

Traditionally x-rays are generated in the laboratory by means of a filament tube, originally invented by Coolidge in 1913. Electrons released from a hot tungsten filament are accelerated towards a metal target in an evacuated tube, and x-rays are generated on impact of the electrons at the target. The quest for ever intense x-ray beams led to the development of synchrotron radiation sources in recent years. In a synchrotron high-energy electrons, circulating in a storage ring at speeds approaching the speed of light on a closed orbit, are led to emit intense beams of x-rays and other electromagnetic radiations.

The closed orbit is achieved by bending the path with a series of bending magnets placed along the ring circumference. The circumference of the storage ring ranges from about 50 to over 1000 m, and the electron beams are accelerated typically to an energy on the order of some GeV. A charged particle that is accelerated emits electromagnetic radiation, and bending is a form of acceleration. The radiation emitted by the orbiting electrons covers an extremely broad range of the electromagnetic spectrum. The flux of x-rays emitted is many orders of magnitude greater than that obtainable with conventional x-ray tubes, making the required time for a single measurement very short and therefore allowing rapid time series measurements with samples undergoing dynamic evolution.

Figure 2.5 illustrates schematically the major components of the storage ring:

- The injection system (IS), generates electrons, accelerates them, and injects

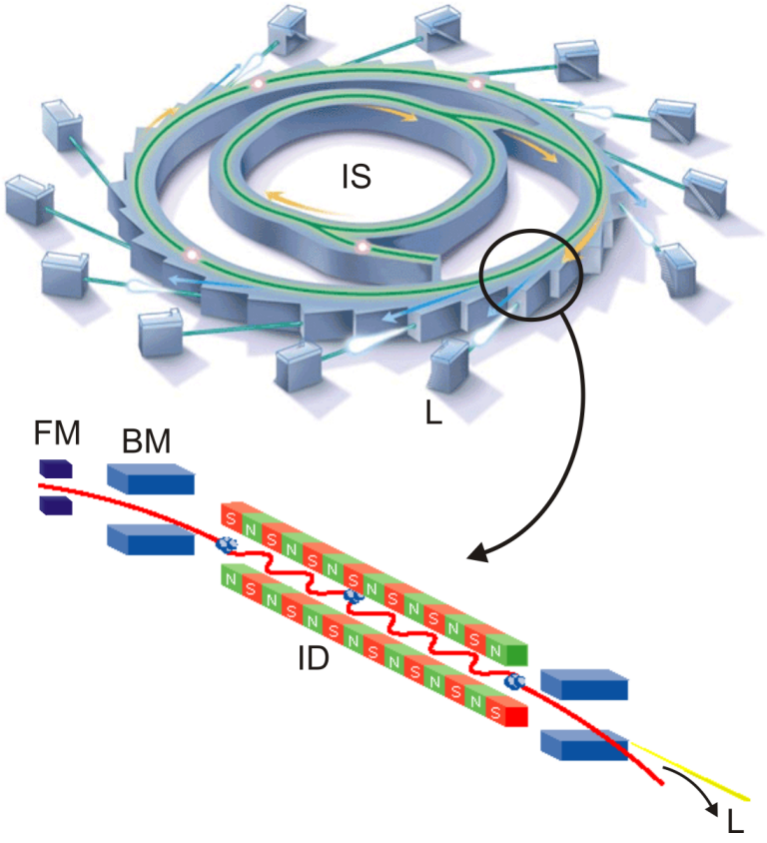

Figure 2.5: *Schematic setup of a synchrotron radiation facility: IS: injection system; L: beamline; BM: bending magnets; FM: focusing magnets; ID: insertion device [Oxf07, Spr05].*

them into the vacuum chamber.

- The vacuum chamber, i. e. the metal tube in which the electrons circulate along a closed trajectory. The vacuum is maintained at 10^{-10} to 10^{-11} Torr.
- The radiofrequency cavity system, which acts on the circulation electrons and restores the energy they lose through the emission of electromagnetic radiation.
- The bending magnets (BM), bend the trajectory of the electrons and force them to circulate in a closed orbit.
- The focusing magnets (FM), fine tunes the electron beam trajectory to keep the electrons within a narrow range of a defined path.
- The beam lines (L) through which the electromagnetic radiation exits into the user's experimental chambers.
- The insertion devices (ID), which are additional devices, such as wigglers and undulators, inserted into straight sections of the ring. They further modify the electron trajectories from a straight line, and thereby induce emission of additional synchrotron radiation. The periodic magnetic structures of the insertion device produce a sinusoidally varying magnetic field in the vertical direction. As a result, the electron beam takes a sinusoidal path in the horizontal direction when passing through an insertion device.

Monochromator and Focusing Mirror

The synchrotron is a polychromatic source and therefore requires a monochromator. The desired collimation can be obtained by a combination of focusing elements and slits. To avoid absorption and scattering by air, the entire path of the beam (except the sample section) is under vacuum. The remaining parasitic background scattering originates from the optical elements before the sample, windows which separate the vacuum before and after the sample, and the intervening air path. The full undulator harmonic is not sufficiently monochromatic for most applications. Therefore, a monochromatic beam is usually obtained by a crystal monochromator. A narrowly limited range of wavelengths can be selected by reflecting the beam from a selected crystallographic plane in a single crystal. When a beam of white radiation impinges on a crystal with its surface cut parallel to a crystallographic plane, reflection can take place only for the component of the beam having a single wavelength that

satisfies the Bragg relation. The wavelength can be selected, as desired, by setting the crystal so that the incident beam strikes it at a glancing angle that meets the condition of Braggs law. The crystal should be able to withstand the high heat load resulting from the absorbed power of the full radiation. The most commonly used monochromator at undulator sources is liquid nitrogen cooled Si-111.

The focusing mirror is an essential component for SAXS instrumentation at synchrotron beamlines. First of all, it serves as an efficient cut-off filter for the higher harmonics reflected by the crystal monochromator. Typically, the sample is placed 30-60 meters away from the source and the sample-to-detector distance can be another 10 meters. X-Ray mirrors are usually made of a highly polished light material such as silicon, zerodur glass ceramic or fused quartz. The reflecting surface is coated by a heavy metal such as rhodium, platinum or gold to increase the electron density and thereby increase the critical angle and reduce the length of the mirror.

Detector

The detector should cover a large dynamic range in intensity ($> 10^6$) and a large q range ($q_{max}/q_{min} \sim 100$). To match the source characteristics, the detector should be able to count at very high rates ($> 10^8$ counts per second) and have a good spatial resolution ($< 50\,\mu$m). However, such a detector does not exist as of this date.

Historically fluorescent screens and photographic films have long been the primary means of detecting x-rays. An alternative to a primary-photon counting is a phosphor-based integrating detector. The phosphor (similar to scintillators used in photon-counting detector) converts x-ray photons to visible photons which are then detected by a slow-scan scientific CCD. Usually the light pattern in the phosphor screen is first enhanced by passing it through an image intensifier, which works on the principle of a photo multiplier tube. The active sensing area of a CCD chip is usually fairly small. The light image pattern from the phosphor screen is therefore reduced in size by use of either an optical fiber taper or an optical lens system before it is sent to the sensing device. The dynamic range is limited by the pixel well capacity and the dark current of the CCD, digital resolution of the analog-to-digital converter, the noise from the CCD readout electronics and the time required to read out the CCD.

2.2.5 Data Reduction

The raw data measured in a SAXS experiment is usually not adequate to make any quantitative conclusion concerning the issues under investigation. First of all,

detectors are invariably imperfect requiring many specific corrections, such as the intensity response function (flat-field), spatial distortion, dead time (for counting detectors), dark current and ADC offset. Secondly, the spatial coordinates have to be transformed to scattering angle ϕ and scattering vector q. In order to make the different data sets comparable, the measured intensity need to be normalized by the incident number of photons I_0, sample transmission T_r, and the solid angle subtended by the detector pixels. The data can be azimuthally averaged over the whole angle range (for isotropic samples) or over a certain angle range (for anisotropic samples) to obtain better intensity statistics. This step requires masking of some detector regions such as the beamstop, detector edges, dead pixels, etc. which for geometrical or electronical reasons do not receive the proper number of photons.

The first step in the data reduction procedure is to apply corrections concerning the readout electronics of the detector which are independent of the scattering geometry. This is the dead time, the minimum time required to separate two events, in the case of counting detectors. For integrating detectors corrections are required for the CCD dark current, the readout noise and the ADC offset. This detector specific background counts can be measured directly for the same duration as the actual acquisition without the shutter being opened. This is referred to as the dark image of the CCD. The next step involves corrections for geometrical distortion which arise from the non-uniformity of the electric field inside these devices. The spatial sensitivity (flat field) also needs to be carefully calibrated in advance, this is done by illuminating the detector by a uniform flux of photons. In order to compare the scattered intensity for different sample-to-detector distances and acquisition times, it is necessary to normalize by the solid angle subtended by the pixel elements and the number of incident photons. A commonly used intensity calibration standard is low-density unoriented semi-crystalline polyethylene (Lupolen ®) which has a broad peak around $q \sim 0.38\,\mathrm{nm}^{-1}$ according to the lamellar spacing. The intensity of this peak has been well calibrated to the scattering cross section of $d\Sigma/d\Omega \sim 0.6\,\mathrm{mm}^{-1}$. Unlike in small angle neutron scattering, the wavelength smearing is not significant in SAXS when a crystal monochromator is employed.

The azimuthal averaging of the normalized 2-D scattering pattern involves transformation of the pixel coordinates from Cartesian (x, y) to polar coordinates (r, Φ), where r is the pixel distance from the beam center and Φ the azimuthal angle. The scattering vector q is calculated from r, d and λ. After masking the unusable pixels, intensity corresponding to the same r values can be averaged to obtain $I(q)$.

For anisotropic scattering patterns, the range of azimuthal integration has to be restricted to a small sector of Φ. In the SAXS range, the sample-to-detector distance d can be measured precisely ($< 1\,\mathrm{mm}$) and detector pixel size is known from the grid calibration thereby allowing Φ and q to be calculated precisely.

2.3 Simulation

There are many approaches to simulate the behavior of polymers. One possibility is to describe the polymer as a fluid with atomic resolution. These calculations are typically based on molecular dynamics or Monte Carlo simulations [Fre96]. These procedures are limited to systems with a low or medium degree of complexity. In order to simulate macroscopic properties of block copolymers an approach based on molecular mean-field theories is therefore more suitable.

For the simulations the MesoDyn code was used, which is based on the dynamic self-consistent field theory and which describes the dynamic behavior of each molecule in the mean field of all other molecules. This code was introduced by Fraaije in 1993 [Fra93, Fra97]. As a molecular model an ideal Gaussian chain is used. In this "spring and beads" model, springs mimic the stretching behavior of a chain fragment and different kinds of beads correspond to different components in the block copolymer.

A block copolymer melt with the volume $\mathcal{V}$ containing n linear freely jointed chains is considered. The chains are of type $\mathrm{A}_{N_\mathrm{A}}\mathrm{B}_{N_\mathrm{B}}$ so that each chain has a block of N_A segments of type A connected to N_B segments of type B. The total length of the chain is $N = N_\mathrm{A} + N_\mathrm{B}$. The type of A or B segment is indexed by I or J. The microstructure patterns are described by coarse-grained variables, which are the density fields $\rho_\mathrm{I}(\mathbf{r})$ of the different species I. Given these density fields, a free energy functional $F[\rho]$ can be defined as follows

$$F[\rho] = -\beta^{-1} \ln \frac{\Phi^n}{n!} - \sum_\mathrm{I} \int_\mathcal{V} U_\mathrm{I}(\mathbf{r}) \rho_\mathrm{I}(\mathbf{r}) \mathrm{d}\mathbf{r} + F^{ind}[\rho] \tag{2.1}$$

where $\beta^{-1} = k_B\,T$, F^{ind} is the contribution due to the nonideal mean-field interactions and Φ is the partition function for the ideal Gaussian chain of length N in the external fields U_I, given by

$$\Phi\left(\mathbf{R}_1 \ldots \mathbf{R}_N\right) = \exp - \left[\frac{3}{2a^2} \sum_{s=2}^{N_i} \left(\mathbf{R}_s - \mathbf{R}_{s-1}\right)^2 + \sum_{s'=1}^{N_i} U_{s'}(\mathbf{R}_{s'}) \right]$$

$\mathbf{R_s}$ describes the coordinate of bead s. The external potentials U_I and the density fields ρ_I are bijectively related in a self-consistent way via a density functional for Gaussian chains

$$\rho_\mathrm{I} = N' \int_{V_N} \delta(\mathbf{r} - \mathbf{R}_s) e^{-\beta\left(\mathcal{H}+\sum_{s'} U_{s'}(\mathbf{R}')\right)} \mathrm{d}\mathbf{R}_1 ... \mathrm{d}\mathbf{R}_N$$

with the normalization constant N'. The Hamiltonian $\mathcal{H}$ describes a set of connected harmonic springs

$$\mathcal{H} \equiv \frac{3\beta^{-1}}{2a^2} \sum_{s=2}^{N} (\mathbf{R}_s - \mathbf{R}_{s-1})^2$$

with a being the Gaussian chain bond length.

The strength of interaction between different components is characterized by the interaction parameter ε_IJ, which is typically expressed in units of kJ/mol.

$$\varepsilon_\mathrm{IJ}(|\mathbf{r} - \mathbf{r}'|) = \varepsilon_\mathrm{JI}(|\mathbf{r} - \mathbf{r}'|) \equiv \varepsilon_\mathrm{IJ} \left(\frac{3}{2\pi a^2}\right)^{\frac{3}{2}} e^{-\frac{3}{2a^2}(\mathbf{r}-\mathbf{r}')^2}$$

This parameter can be related to the conventional Flory-Huggins parameter ($\chi_\mathrm{IJ} = \varepsilon_\mathrm{IJ}/N_A k_b T$). A positive ε_IJ parameter corresponds to a repulsion between the components I and J. The contribution of ε_IJ to the free energy is given by

$$F^{coh}[\rho] = \frac{1}{2} \sum_{\mathrm{I,J}} \int_{\mathcal{V}^2} \varepsilon(|\mathbf{r} - \mathbf{r}'|) \rho_\mathrm{I}(\mathbf{r}) \rho_\mathrm{J}(\mathbf{r}') \mathrm{d}\mathbf{r}\mathrm{d}\mathbf{r}'$$

Furthermore, there is an extra contribution to F^{ind} due to the interaction of the wall with the polymer

$$F^{surf}[\rho] = \frac{1}{2} \sum_{\alpha} \sum_{\mathrm{I}} \int_{\mathcal{V}^2} \varepsilon_{\mathrm{I}M_\alpha}(|\mathbf{r} - \mathbf{r}'|) \rho_\mathrm{I}(\mathbf{r}) \rho_{M_\alpha}(\mathbf{r}') \mathrm{d}\mathbf{r}\mathrm{d}\mathbf{r}'$$

F^{ind} also includes contributions due to excluded volumes and the compressibility of the system

$$F^{e}[\rho] = \frac{\kappa}{2} \int_{\mathcal{V}} \left(\sum_{\mathrm{I}} \nu_\mathrm{I} \left(\rho_\mathrm{I}(\mathbf{r}) - \rho_\mathrm{I}^0\right) \right)^2 \mathrm{d}\mathbf{r}$$

where ρ_I^0 is the averaged concentration of component I, ν_I is the volume of a single bead and κ is the compressibility.

Several methods can be employed to find the minimum of the free energy and the equilibrium density fields $\rho_\mathrm{I}(\mathbf{r})$. They can roughly be divided into static and

dynamic methods, although a number of hybrids exist that are generally referred to as quasi-dynamic methods. Here, a dynamic scheme that has been developed by the group of Fraaije was used. An advantage of this scheme is that it intrinsically considers dynamic pathways towards a free energy minimum, including visits to long-living metastable states. The thermodynamic driving forces for the pattern formation are the gradients of the chemical potential

$$\mu_{\mathrm{I}}(\mathbf{r}) = \frac{\delta F}{\delta \rho_{\mathrm{I}}(\mathbf{r})}$$

The time evolution of the system is modeled by diffusion dynamics

$$\frac{\partial \rho_{\mathrm{I}}}{\partial t} = M_{\mathrm{I}} \nabla^2 \mu_{\mathrm{I}} + \eta_{\mathrm{I}} \tag{2.2}$$

where M_{I} is a constant mobility for bead I and η_{I} is a noise field distributed according to the fluctuation-dissipation theorem [Gar90].

$$\begin{aligned} \langle \eta_{\mathrm{I}}(\mathbf{r},t) \rangle &= 0 \\ \langle \eta_{\mathrm{I}}(\mathbf{r},t) \eta_{\mathrm{J}}(\mathbf{r}',t') \rangle &= -2\beta^{-1}\, \delta_{\mathrm{IJ}}\, M_{\mathrm{I}}\, \nabla \cdot \rho_{\mathrm{I}}\, \nabla\, \delta(\mathbf{r}-\mathbf{r}')\, \delta(t-t') \end{aligned}$$

The time evolution of the system as described by equation 2.2 assumes that the system is in quasi-equilibrium, so that there exists a free energy functional (equation 2.1). This free energy functional does not explicitly depend on time. At each time step of the system's evolution all intramolecular degrees of freedom are assumed to be equilibrated. This is a good approximation in case that the internal dynamics of a single chain is faster than the collective dynamics of the ensemble of chains. Although the free energy description (equation 2.1) incorporates spatial resolution on the level of single beads, the time evolution described by equation 2.2 is coarse-grained, and the smallest physical volume entering it is the volume of a single polymer chain v. This volume is used to introduce a dimensionless variable $\Psi = v(\rho_{\mathrm{A}} - \rho_{\mathrm{A}}^0)$. Here A stands for the material component A. One variable is sufficient in the case of incompressible copolymer melts with only two block types. The variable Ψ is an order parameter, which describes the local deviation of the volume fraction of blocks A from their uniform distribution. It is small for weakly segregated systems [Lya06a, Lya06b].

In the presence of an electric field $\mathbf{E}(\mathbf{r})$ the chemical potential can be split into two terms [Lan84]

$$\begin{aligned} \mu &= \mu^0 + \mu^{el}, \\ \xi &= \frac{\mu^{el}}{v} = -\frac{E^2}{8\pi} \frac{\partial \epsilon}{\partial \Psi} \end{aligned} \tag{2.3}$$

where $E = |\mathbf{E}|$, $\epsilon(\mathbf{r})$ is the dielectric constant of the dielectric, and the CGS system of units is used. The dielectric constant can be modeled by

$$\epsilon(\mathbf{r}) \approx \bar{\epsilon} + \epsilon_1 \Psi(\mathbf{r})$$

The electric field inside the material can be expressed by an auxiliary potential ϕ:

$$\mathbf{E} = \mathbf{E_0} - \nabla\phi$$

where $\mathbf{E_0} = (0, 0, E_0)$ is the uniformly applied electric field along the $\hat{\mathbf{z}}$-axis. The electric part of chemical potential, equation 2.3, can be written as

$$\xi = -\frac{\epsilon_1}{8\pi}\left({E_0}^2 - 2E_0\nabla_z\phi + (\nabla\phi)^2\right)$$

It is assumed that $\epsilon_1\Psi \ll 1$. Therefore, $|\nabla\phi|/E_0 \ll 1$, and the last term can be omited in the treatment. Note that the second term vanishes if $\nabla_z\phi = 0$. This happens in a structure that is fully aligned with the field direction (the very last stages of an alignment process). Using the Maxwell equation $\nabla\epsilon\mathbf{E} = 0$, it can be found in the leading powers of $\nabla\phi$ and Ψ

$$\bar{\epsilon}\nabla^2\phi(\mathbf{r}) = E_0\epsilon_1\nabla_z\Psi$$

Finally, we get

$$\nabla^2\xi = \frac{{E_0}^2}{4\pi}\frac{{\epsilon_1}^2}{\bar{\epsilon}}\nabla_z^2\Psi$$

and for the time evolution of the order parameter

$$\dot{\Psi} = b\Delta\mu^0 + \alpha\Delta_z\Psi + \tilde{\eta}$$

where $b = Mv$ is the mobility in the Einstein sense, associated with the volume of one polymer chain, $\alpha = bvg_e$, Δ is the Laplacian, $\Delta_z \equiv \partial^2/\partial z^2$, and $\tilde{\eta}$ is the properly redefined noise term. The coefficient g_e describes the strength of the electrostatic contribution to the free energy of the system [Onu95]

$$\begin{aligned} g_e &= (4\pi\bar{\epsilon})^{-1}{\epsilon_1}^2{E_0}^2 \qquad \text{(CGS)}, \\ g_e &= \epsilon_0\bar{\epsilon}^{-1}{\epsilon_1}^2{E_0}^2 \qquad \text{(SI)} \end{aligned}$$

where ϵ_0 is the dielectric constant of vacuum. In the numerical simulations the electric field strength is parametrized by the dimensionless variable

$$\tilde{\alpha} = \frac{\alpha}{k_B T b}$$

The studied model system is a symmetric A_4B_4 copolymer melt. The simulations have been performed in either two-dimensional on a 256 x 256 grid or three-dimensional in a box occupying 32 x 32 x 32 and 64 x 64 x 64 grid points. Moreover periodic boundary conditions have been chosen [Sev99]. Prior to the electric field, the samples were shear-aligned with the dimensionless shear rate $\tilde{\dot{\gamma}} = 0.001$ [Zve98].

Experimental Section

3.1 Synthesis

During this thesis five different block copolymers were studied. All block copolymers consist of polystyrene as the first block linked to either polyisoprene, poly(2-vinyl pyridine), poly(2-hydroxyethyl methacrylate)-*b*-poly(methyl methacrylate)*, poly-(*tert*-butyl methacrylate) or poly(methyl methacrylate) as a second block, respectively. The block ratio and overall molecular weight were determined by ^{1}H-NMR in combination with the GPC results of the corresponding polystyrene precursor. GPC of the final block copolymers yielded the polydispersities. SAXS measurements were performed to analyze the bulk structures. Table 3.1 summarizes the molecular weight, composition, polydispersity and morphology of all materials.

Synthesis of Polystyrene-b-polyisoprene

The synthesis of PS-*b*-PI diblock copolymers was accomplished by sequential anionic polymerization of styrene and isoprene in benzene at 40°C with *sec*-BuLi as initiator. The use of benzene as a solvent results in a high 1,4-addition for isoprene.† Benzene was purified by successive destillation over CaH_2 and potassium and kept in a dry nitrogen atmosphere until use. Styrene was stirred over Bu_2Mg and condensed into storage ampoules. Isoprene was stirred over Bu_2Mg under purified nitrogen for 12 h, condensed onto *n*-BuLi followed by stirring at 0°C for 1 h before being condensed into glass ampoules. *sec*-BuLi (1.3 M in cyclohexane/hexan), *n*-BuLi (1.6 M in hexane), Bu_2Mg (1 M in heptane) were used as received.

The freshly distilled benzene was heated to 40°C, *sec*-BuLi was injected before styrene was added, which results in a yellow color of the reaction mixture. After 2 h polyisoprene was added quickly and polymerized for another 2 h, leading to

∗ The two blocks, PHEMA and PMMA, are known to form a mixed phase and can be treated as a single block [Bök02c].

† The fraction of the 1,4-microstructure is more than 90% for all polystyrene-*b*-polyisoprene block copolymers.

Table 3.1: *Molecular weight M_n, polydispersity M_w/M_n, volume fraction ϕ_S of polystyrene, weight fraction w_S of polystyrene, and bulk morphology of the studied block copolymer systems.*

Polymer ‡	$M_n[kg/mol]$	M_w/M_n	$\phi_S[\%]$	$w_S[\%]$	Morphology
$S_{46}I_{54}{}^{108}$	108	1.05	43	46	Lamellae
$S_{50}I_{50}{}^{100}$	100	1.02	48	50	Lamellae
$S_{64}I_{36}{}^{78}$	78	1.05	61	64	Lamellae
$S_{55}I_{45}{}^{51}$	51	1.04	52	55	Lamellae
$S_{58}I_{42}{}^{48}$	48	1.04	55	58	Lamellae
$S_{64}I_{36}{}^{47}$	47	1.03	61	64	Lamellae
$S_{67}I_{33}{}^{75}$	75	1.05	64	67	Gyroid
$S_{69}I_{31}{}^{72}$	72	1.05	66	69	Gyroid
$S_{72}I_{28}{}^{69}$	69	1.05	69	72	Cylinder
$S_{75}I_{25}{}^{66}$	66	1.04	72	75	Cylinder
$S_{76}I_{24}{}^{76}$ §	76	1.02	73	76	Cylinder
$S_{50}V_{50}{}^{78}$ §	78	1.05	52	50	Lamellae
$S_{54}V_{46}{}^{99}$	99	1.05	56	54	Lamellae
$S_{50}T_{50}{}^{100}$ ¶	100	1.03	53	50	Lamellae
$S_{47}H_{10}M_{43}{}^{82}$ §	82	1.04	50	47	Lamellae
$S_{46}H_4M_{50}{}^{134}$ §	134	1.06	49	46	Lamellae
$S_{49}M_{51}{}^{100}$ §	100	1.03	52	49	Lamellae

immediate disappearance of the color. Finally, the reaction was terminated with 1 ml degassed methanol.

The polymer was precipitated in isopropanol. Then the product was redissolved in THF and reprecipitated two more times into water and isopropanol and dried under

‡ The subscripts denote the weight fraction of the respective blocks and the superscript gives the number-average molecular weight in kg/mol.

§ synthesized by Alexander Böker [Bök02a]

¶ synthesized by Thorsten Goldacker [Gol99]

‖ synthesized by Gabi Cantea [Can05]

vacuum at room temperature. The precipitation in water removes the remaining ions.

Synthesis of Polystyrene-b-poly(2-vinyl pyridine)

The synthesis of PS-*b*-PVP was carried out in THF at -78°C with *sec*-BuLi as initiator. THF was distilled over CaH_2 for 48 h and finally refluxed over potassium under nitrogen for another 2 days. 2-Vinylpyridine was treated with Et_3Al for 3 h and condensed into storage ampoules.

For the preparation of PS-*b*-PVP a similar procedure like the synthesis of PS-*b*-PI was chosen. After THF was cooled down to -78°C, *sec*-BuLi was injected and polystyrene was added. After 1 h the styryl anions were capped with 1,1-diphenylethylene (DPE), resulting in a deep red color of the mixture. After another 1 h the 2-vinylpyridine was added and polymerized for 1 h. The reaction was terminated with 1 ml degassed methanol.

The polymer was precipitated two times in water and dried under vacuum at 40°C.

3.2 Sample Preparation

Block copolymer solutions of different concentrations in toluene or THF were prepared. The alignment experiments were performed in a home built capacitor with gold electrodes with a sample depth of 5 mm and variable electrode distance between 0.3 and 3.8 mm at room temperature. The capacitor was filled via a syringe directly connected to the cell. Therefore, the block copolymer is exposed both to the shear fields occurring during this sample preparation and to the surface fields favoring parallel alignment of the microstructure. In consequence, the initial microdomain orientation is not random, but is preferentially aligned parallel to the capacitor plates, i. e. perpendicular to the electric field lines. A DC voltage up to 11 kV/mm or an AC voltage up to 2 kV/mm and 5 kHz can be applied across the capacitor resulting in a homogeneous field pointing perpendicular to the x-ray beam direction (see Figure 3.1). The DC voltage power supply was a commercial Heinzinger PNC 60000. The AC electric fields with high voltage and high frequency were provided by a novel setup consisting of a cascade connection of field effect transistors. Both the voltage at the electrodes and the current through the sample were monitored during the course of the experiment. Within the sensitivity of the setup ($I \approx 0.01$ mA), no leakage currents were detected after the electric field was applied.

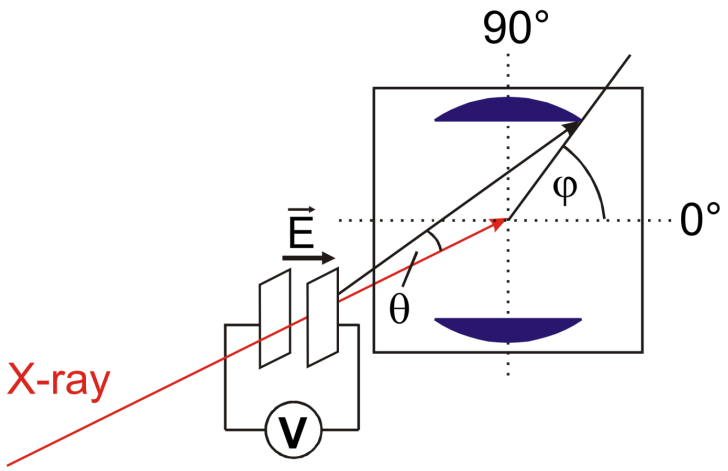

Figure 3.1: *Experimental setup for the in-situ SAXS measurements.*

3.3 SAXS Setup

The *in-situ* SAXS measurements were carried out at the ID2 beamline at the European Synchrotron Radiation Facility (ESRF, Grenoble, France). A schematic depiction is shown in Figure 3.2 [Eur06]. The source is located at a high-β-section of the storage ring. The undulators provide high photon flux with a low divergence. The beamline optics consist of a cryogenic cooled Si-111 monochromator and a focusing toroidal mirror. The beam size is 100 μm × 100 μm with divergence of 10 μrad × 10 μrad. The maximum photon flux at the sample position is of the order of $3.0 \cdot 10^{13}$ photons/s/100 mA with $\Delta\lambda/\lambda = 0.015\%$ at 12.4 keV. The operating energy range is 12.4 keV, corresponding to a wavelength of 0.1 nm.

The detector system is housed in a 10 m evacuated flight tube. The detector is a fiber optically coupled FReLoN (Fast-Readout, Low-Noise) CCD based on Kodak KAF-4320 image sensor. It has an input field of 100 mm × 100 mm, nominal dynamic range of 16 bit and full frame rate of 3 frames/s (2048 × 2048). With 2 × 2 binning, the readout rate is about 6 frames/s and at still higher binning (8 × 8) up to 20 frames/s can be obtained. The spatial resolution determined by the point spread function is about 80 μm.

Prior to data analysis the raw data have to be corrected. The raw data is first corrected for detector artifacts, i. e. subtraction of dark current and readout noise, division by flatfield, and spatial distortion correction. Then, the data is normal-

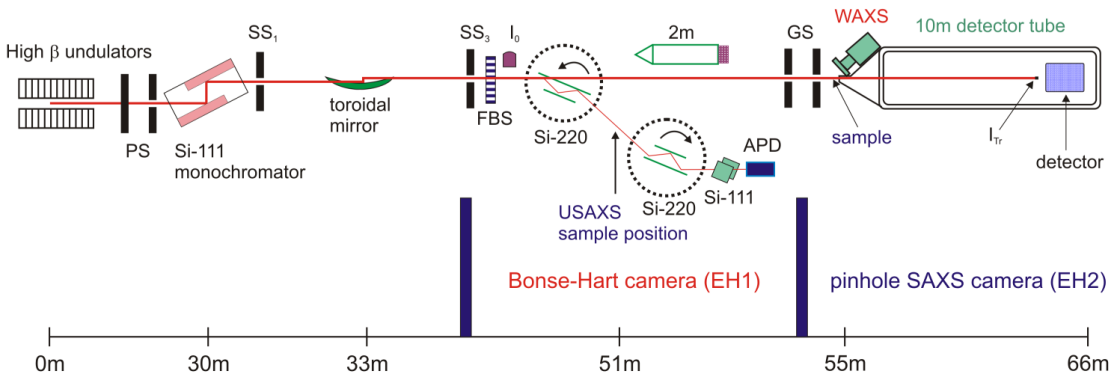

Figure 3.2: *Setup of the ID2 beamline at the ESRF [Eur06].*

ized to absolute scattering intensities. After this step all detector and beamline dependent features are corrected and the sample background is subtracted.

3.4 Data Evaluation

As mentioned above, the microstructure is prealigned due to shear forces occurring during the filling procedure. The microdomains are subjected to two competing external fields of different symmetry, i. e. the interfacial field between polymer solution and the electrode surface and the external electric field. In order to quantify the microdomain alignment, the order parameter P_2 was calculated by integrating the scattering intensity $I(q, \varphi)$ over the azimuthal angle φ from $\varphi = 0°$ to $360°$.

$$P_2 = \frac{3\left\langle \cos^2 \varphi \right\rangle - 1}{2} \tag{3.1}$$

with

$$\left\langle \cos^2 \varphi \right\rangle = \frac{\int_0^{2\pi} \mathrm{d}\varphi (I(q,\varphi) \cos^2 \varphi \left|\sin \varphi\right|)}{\int_0^{2\pi} \mathrm{d}\varphi (I(q,\varphi) \left|\sin \varphi\right|)}$$

Depending on the position of the maxima of the scattering intensity the calculation yields two different ranges of the order parameter. For lamellar alignment parallel to the electrodes (maximum at $\varphi = 0°$), P_2 ranges from 0 to 1 with $P_2 = 1$ corresponding to perfect lamellar alignment where all lamellar normals are oriented perpendicular to the surfaces, i. e. the electrodes. For alignment of the lamellae along the electric field direction (maximum at $\varphi = 90°$), P_2 ranges from 0 to -0.5 with $P_2 = -0.5$ corresponding to the case where all lamellae are aligned parallel

to the electric field vector, however, with the lamellar normals being isotropically oriented in the plane of the electrodes.

In the following step, to quantify the orientation kinetics, the orientational order parameter P_2 was calculated for each single scattering pattern acquired during the course of the experiment. The behavior of P_2 as a function of time t has been fitted by a single exponential as described by

$$P_2(t) = P_{2,\infty} + (P_{2,0} - P_{2,\infty})\mathrm{e}^{-\frac{t}{\tau}} \tag{3.2}$$

with $P_{2,0}$ and $P_{2,\infty}$ being the limiting values of the order parameter before application of the electric field and at later times, respectively, and τ being the time constant. A typical data set is shown in Figure 3.3 [Bök03a].

As found in earlier studies [Bök02b, Bök03b] the reorientation can proceed via two different microscopic mechanisms, i. e. *nucleation and growth of domains* and *grain rotation*. The procedure of calculating only one characteristic time is not satisfactory as it neglects the fact mentioned above. In order to quantify the overall kinetics in more detail two Voigt-based fitting models were used, separately describing the characteristics of *nucleation and growth* and *rotation of grains* to simultaneously fit the overall azimuthal scattering pattern. The Voigt fitting model constitutes a

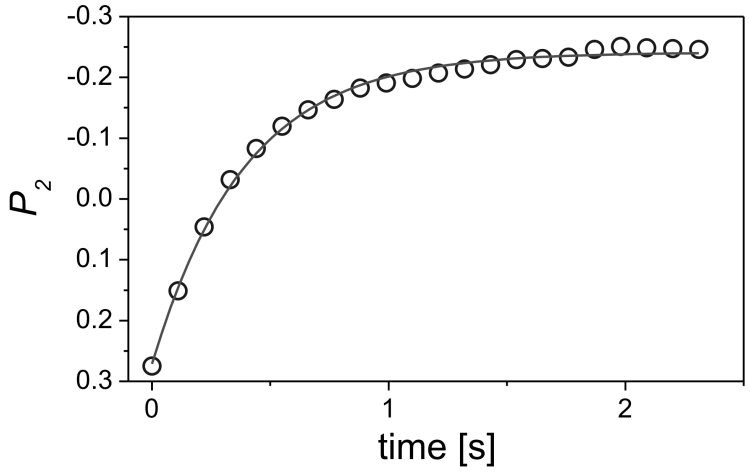

Figure 3.3: *Typical evolution of the orientational parameter P_2 for a 40 wt. % $S_{50}V_{50}$[78] solution in THF exposed to an electric field of 1.5 kV/mm. The solid line represents a least squares fit of the data according to Equation 3.2 with $P_{2,0} = 0.27$, $P_{2,\infty} = -0.24$, and $\tau = 0.39$ se.*

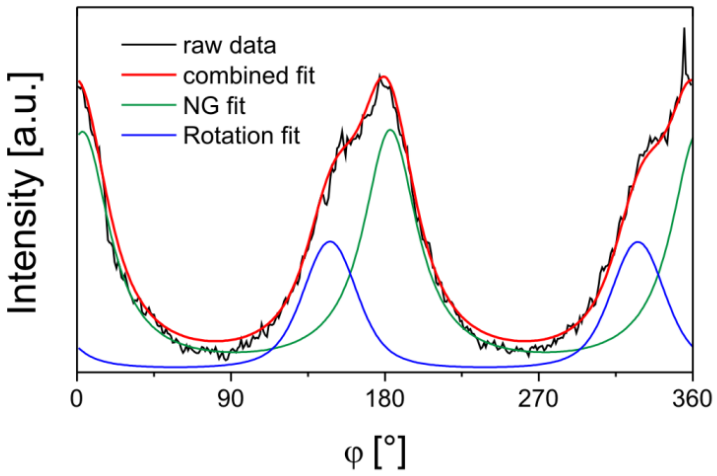

Figure 3.4: *Deconvolution of the azimuthal angular scattering intensity for the reorientation of a 35 wt. % solution of $S_{50}I_{50}{}^{100}$ in toluene at 1 kV/mm. (Black) measured data, (blue) fit of rotating peak, (green) fit to component exhibiting nucleation and growth, (red) combination of fitting results.*

convolution of Gaussian and Lorentzian peak shapes

$$I(x) = I_0^L \cdot I_0^G \int_{-\infty}^{+\infty} \frac{\omega_L^2 \cdot \mathrm{e} - (\frac{2t\sqrt{\ln 2}}{\omega_G})^2}{\omega_L^2 + 4(x - x_0 - t)^2} \mathrm{d}t$$

with ω_L is the Lorentz FWHM, and ω_G the Gauss FWHM, I_L and I_G are the corresponding intensities.

Nucleation and growth is characterized by the appearance of a new peak at the final position, which grows on expense of the initial peak as a function of time. *Grain rotation*, on the other hand, is characterized by a continuous shift of the peak position from the initial to the final orientation. The deconvoluted scattering patterns were evaluated either by using the orientational order parameter or both the peak area (*nucleation and growth*) and angular shift of the peak maxima (*rotation of grains*) (see Figure 3.4). For the fitting procedure the systems exhibiting pure *rotation* or pure *nucleation and growth* can be used to estimate the peak position and peak widths.

In order to determine the exact peak position and thus the characteristic spacings for the lamellae oriented along the field lines and for those oriented perpendicular to the field, i. e. parallel to the electrodes, the corrected two-dimensional SAXS data were averaged over a 30° opening angle in horizontal direction (perpendicular to

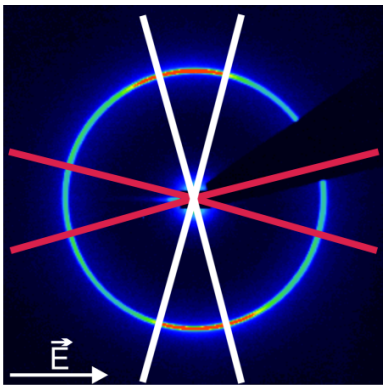

Figure 3.5: *Two-dimensional scattering pattern of a 50 wt. % solution of* $S_{55}I_{45}$[51] *dissolved in THF after applicaton of an electric field. The white and the red sector correspond to lamellae oriented along the field direction and to those oriented perpendicular to the field, respectively. The arrow indicates the direction of the electric field vector.*

the electric field lines) and vertical direction (parallel to the field lines) as shown in Figure 3.5. The peak position in q was analyzed with a Voigt based fitting model and the lamellar spacing d was then calculated according to $d = 2\pi/q$.

Influence of Initial Order on the Microscopic Mechanism of Alignment

The mechanism of microdomain orientation in concentrated block copolymer solutions exposed to a DC electric field was investigated by *in-situ* synchrotron small-angle x-ray scattering. As a model system, concentrated solutions of a lamellar polystyrene-*b*-polyisoprene block copolymer in toluene was used. It was found, that both the microscopic mechanism of reorientation and the kinetics of the process strongly depend on the initial degree of order in the system. In a highly ordered system with the lamellae being aligned perpendicular to the electric field vector, only *nucleation and growth of domains* is possible as a pathway to reorientation and the process proceeds rather slowly. In less ordered samples *grain rotation* becomes possible as an alternative pathway and the reorientation is considerably faster. The interpretation of these findings is strongly corroborated by dynamic self-consistent field simulations.

4.1 Introduction

Owing to the different dielectric properties of the two blocks, an orientation of block copolymer microdomains parallel to an external electric field is energetically favored. The orientation of block copolymer microdomains by means of an electric field has been shown to be feasible with field strengths ranging from one to several tens of volts per micron, depending on the difference in the dielectric constants. Recent experiments and computer simulations have shown that two distinctly different microscopic pathways are possible when an ordered block copolymer mesostructure of arbitrary orientation is exposed to an external electric field [Bök02b, Bök03b, Zve03]. In case of sufficiently weak segregation between the two blocks, local nuclei of the favored parallel orientation are created. Subsequently, these nuclei grow. Consequently, in a scattering experiment only the initial and the final orientations are observed while the intensity of the latter growing on expense of the former. Al-

ternatively, in the case of stronger segregation between the respective blocks, the orientation of entire grains rotates, mediated by movement of individual defects perpendicular to the microdomain structure, until the favored orientation parallel to the field is reached. In this case, a scattering experiment will detect a continuous shift of the scattering pattern from the initial to the final orientation as has been found for electric field as well as for shear alignment [Bök02b, Pol96].

While the above considerations hold for bulk samples, in thin films additional effects come into play. Both lamellar and cylindrical mesophases in block copolymers preferentially align parallel to any boundary surface as such alignment typically decreases the interfacial energy of the structure with the boundary surface. In case of a plate capacitor, these effects counteract the effect of the electric field which points perpendicular to the boundary surfaces. In consequence, a minimum electric field strength (threshold electric field strength) is required to overcome the parallel interfacial alignment [Xu03b, Xu04b, Tso02]. Moreover, it has been shown that close to the electrodes the parallel alignment may prevail even if the bulk of the film is oriented perpendicular to the interfaces, resulting in a mixed orientation of grains. This also holds for shear aligned samples where the effective forces are much larger than in the electric field case [Lau99, Win93]. While the thermodynamics of this competition is widely understood, the influence of the initial degree of order and initial orientation with respect to the boundary surfaces on the microscopic pathway leading to microdomain reorientation has barely been studied. This is even more surprising given the obvious importance of defect density and initial degree of order for the reorientation process as has been described for shear alignment experiments. *Grain rotation* relies on the movement of individual defects and therefore should strongly depend on the defect density. For the *nucleation of grains* of preferred orientation on the other hand, both structural defects as well as thermal fluctuations may serve as nuclei. Onuki and Fukuda have pointed out that undulation instabilities in lamellae in an oblique electric field will only develop if the angle between the plane of the lamellae and the electric field vector is sufficiently large [Onu95]. Therefore, not only the defect density but also the degree of orientation and the angle between the microdomains and the electric field vector should be of importance.

In the following, the influence of the degree of initial order on the microscopic route towards domain alignment is investigated in detail. In a plate capacitor arrangement the plate spacing varied between 0.3 mm and 3.8 mm. The microdomains align parallel to the capacitor plates and the degree of order improves with decreasing

capacitor spacing. At the same time the process of reorientation slows down by about an order of magnitude as the capacitor spacing is reduced. Moreover, above a certain degree of order, described by the orientational order parameter P_2, grain rotation is completely suppressed and *domain reorientation* can only be achieved via *nucleation and growth*. Dynamic self-consistent field simulations corroborate that the different behavior is due to differences in the initial degree of order, which in turn increases with decreasing spacing between the capacitor plates.

4.2 Materials

For the following studies the lamellar $S_{50}I_{50}{}^{100}$ block copolymer was used (for details see Table 3.1). Block copolymer solutions of 35, 50, and 55 wt. % in toluene were prepared. The alignment experiments were performed at room temperature with a DC voltage of 1 kV/mm.

4.3 Deconvolution of Reorientation Process

By analyzing the overall azimuthal scattering pattern with two Voigt-based fitting model described in section 3.4, the orientation process can be deconvoluted. Figure 4.1 shows the 3D representation of the azimuthal angular dependence of the scattering intensity for the reorientation of a 35 wt. % solution of $S_{50}I_{50}{}^{100}$ with an initial order parameter of $P_{2,0} = 0.66$. The measured data, the fit of both mechanisms and the fits of the single mechanisms can be compared.

The order parameter P_2 can be calculated using Equation 3.1 for every angular curve resulting from the fitting procedure. By plotting P_2 against time a characteristic time for the deconvoluted mechanisms can be determined (see Figure 4.2).

From this set of data, following conclusions can be drawn:

- At early and late stages, the two processes cannot be distinguished quantitatively as the peak intensities decrease (early stage) or grow (late stage) while the position of the peaks shift, i. e. the rotating grains grow in size and number during the orientation process.

- Comparison between the typical time constant of *rotation* and *nucleation and growth* for a certain overall process are identical within the error of the fitting procedure.

- The characteristic times from the single mechanism evaluation in (c, d, e) of Figure 4.2 cannot be taken as an absolute measure comparing the time frame of the experiment, in which both mechanisms can be distinguished clearly ($\tau = 8 - 60\,\mathrm{s}$).

- The orientation processes are interlinked with each other such that the kinetics of the governing mechanism tends to dictate the kinetics and thus the rate of the resulting overall reorientation process.

Therefore the overall process was fitted with a single time constant and the result was used as a relative measure to compare the kinetics of the observed processes in dependence on the initial orientation.

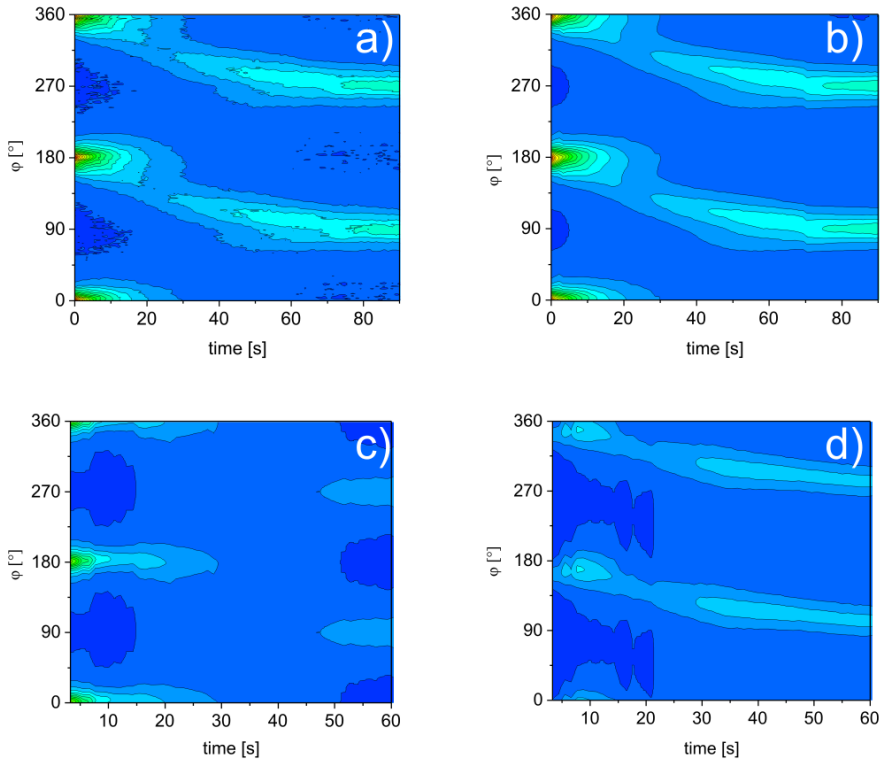

Figure 4.1: *3D representation of the azimuthal angular dependence of the scattering intensity for the reorientation of a 35 wt. % solution of $S_{50}I_{50}{}^{100}$: (a) measured data, (b) fit with both mechanistic components, (c) fit to component exhibiting nucleation and growth, (d) fit to component exhibiting grain rotation. The color code was chosen so that blue represents lowest intensity and yellow stands for the highest scattering intensity.*

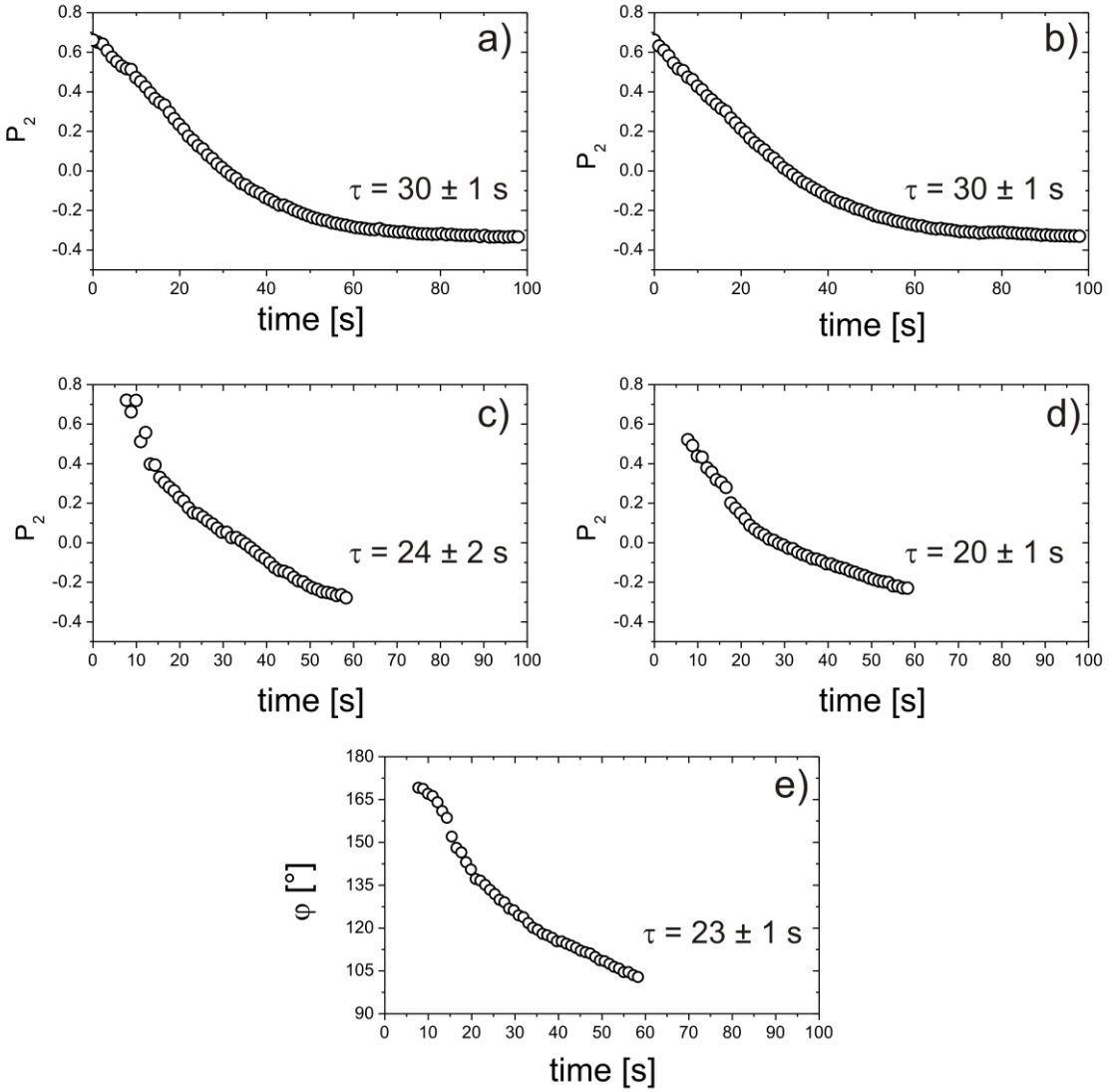

Figure 4.2: *Evolution of orientational order parameter P_2 with time for the same system as in Figure 4.1. (a) Orientational order parameter for measured data ($\tau = 30 \pm 1$ s), (b) overall fit of both mechanisms ($\tau = 30 \pm 1$ s), (c) nucleation and growth ($\tau = 24 \pm 2$ s), (d) grain rotation ($\tau = 20 \pm 1$ s), and (e) angular shift of peak maxima for rotation of grains ($\tau = 23 \pm 1$ s).*

4.4 Results and Discussion

4.4.1 Results from in-situ SAXS Measurements

Using different capacitor spacings, the initial degree of order in the microdomain structures prior to application of the electric field can be controlled. As mentioned in

section 3.2, the lamellae are exposed both to the shear fields occurring during sample preparation and to the surface fields favoring parallel alignment of the lamellae. In consequence, the initial microdomain orientation is not random, but is preferentially aligned parallel to the capacitor plates. This alignment can easily be quantified through the orientational order parameter P_2 at $t = 0$.

The discussion is started with the kinetics of microdomain reorientation as followed in the center of the capacitor filled with a polymer solution exhibiting an initial degree of orientational order of $P_{2,0} = 0.46$.

Figure 4.3 shows the 2D SAXS patterns in the absence of an external electric field (a) and after exposure to the electric field for different times (b, c). Clearly, at short times an intermediate orientation is observed pointing to grain rotation as the dominant reorientation process. This is clearly visible in the time dependent plot of the azimuthal scattering intensity (d) as well, which also shows that at least a major

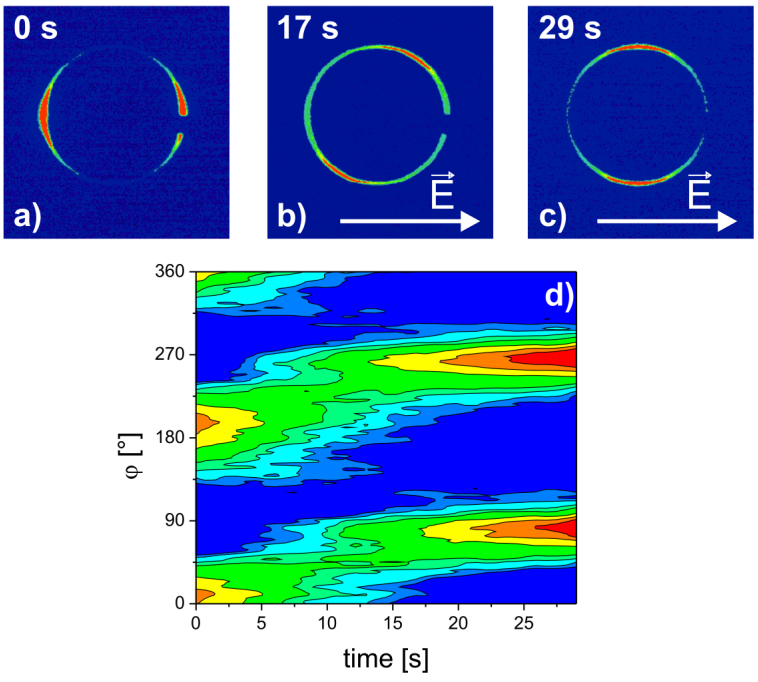

Figure 4.3: *(a-c) Scattering images of a 35 wt. % solution of $S_{50}I_{50}{}^{100}$ in toluene prior (a) and after (b, c) application of an electric field (1 kV/mm and $P_{2,0} = 0.46$). (d) 3D representation of the azimuthal angular dependence of the scattering intensity for the reorientation. The arrow indicates the direction of the electric field vector.*

part of the scattering intensity is rotated continuously from the initial orientation at $\varphi = 0°$ and 180°, respectively, to the final orientation at $\varphi = 90°$ and 270°. This situation changes significantly if a samples with higher initial alignment is examined.

In Figure 4.4 the reorientation behavior of a polymer solution with $P_{2,0} = 0.83$ is depicted. In contrast to the data shown in Figure 4.3, at any time only two distinct domain orientations are observed resulting in scattering peaks at $\varphi = 0°$ and 180° (a, initial) and at $\varphi = 90°$ and 270° (c, final). At intermediate times, both orientations coexist (b), while almost no intermediate orientations are observed and only a negligible portion of the sample rotates. The time dependent plot of the azimuthal scattering intensity (d) clearly shows the switching between the initial and the final orientation. This scattering behavior is indicative of *nucleation and growth of grains* of the final orientation. *Grain rotation* seems to be almost completely suppressed in this situation.

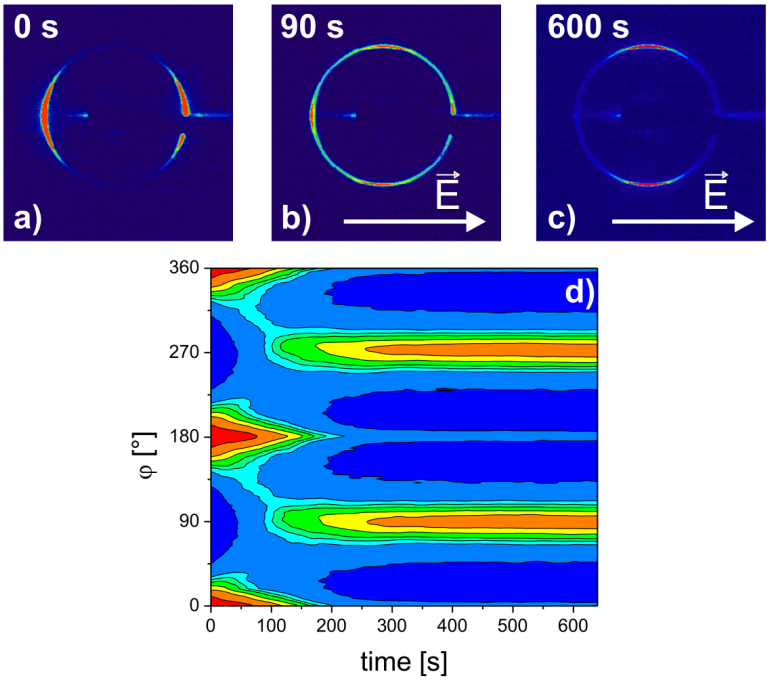

Figure 4.4: *(a-c) Scattering images of a 35 wt. % solution of $S_{50}I_{50}{}^{100}$ in toluene prior (a) and after (b, c) application of an electric field (1 kV/mm and $P_{2,0} = 0.83$). (d) 3D representation of the azimuthal angular dependence of the scattering intensity for the reorientation. The arrow indicates the direction of the electric field vector.*

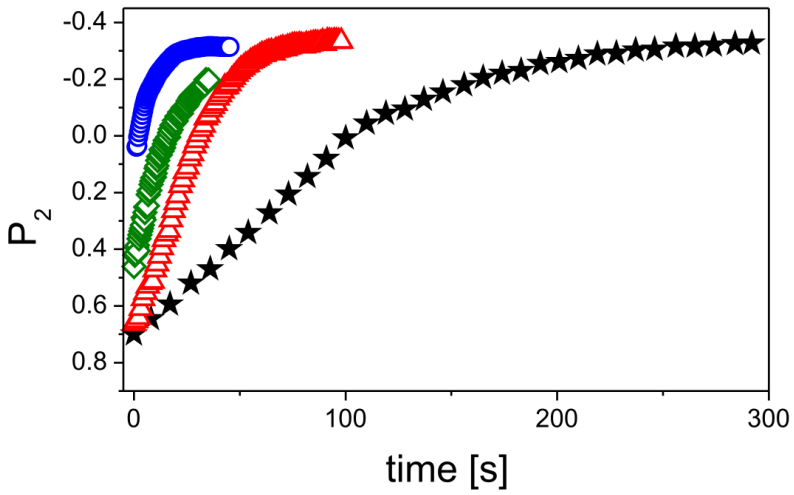

Figure 4.5: *Kinetics of a 35 wt. % solution of $S_{50}I_{50}{}^{100}$ in toluene at 1 kV/mm for different initial degrees of order. Evolution of the orientational order parameter ○: $P_{2,0} = 0.04$ (R), ◇: $P_{2,0} = 0.46$ (R), △: $P_{2,0} = 0.66$ (R), ★: $P_{2,0} = 0.83$ (NG), NG = nucleation and growth, R = rotation.*

It is interesting to quantify the kinetics of reorientation as a function of $P_{2,0}$. In Figure 4.5 the time dependence of the P_2-values calculated from the raw data according to Equation 3.1 is shown. Fitting a single exponential to the data yields time constants τ, which increase from $\tau = 7.8\,\mathrm{s}$ at $P_{2,0} = 0.04$ to as much as $\tau = 81\,\mathrm{s}$ for $P_{2,0} = 0.83$ (Table 4.1).

In Figure 4.6, the kinetic data (τ-values) as a function of the initial degree of

Table 4.1: *Time constants of the reorientation behavior at different values of $P_{2,0}$ obtained from fits using Equation 3.2 ($S_{50}I_{50}{}^{100}$: $w_P = 35$ wt.%, $E = 1$ kV/mm, NG = nucleation and growth, R = rotation).*

$P_{2,0}$	$\tau[s]$	dominating mechanism
0.83	81.0	NG
0.66	29.6	R
0.55	15.0	R
0.50	9.0	R
0.04	7.8	R

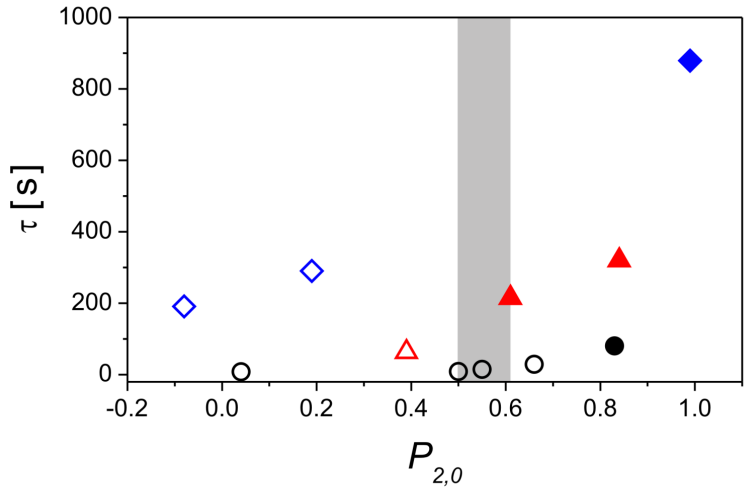

Figure 4.6: *Experimental time constants τ as a function of the initial order parameter $P_{2,0}$ for solutions of $S_{50}I_{50}{}^{100}$ in toluene at 1 kV/mm: ◇=55 wt. %, △=50 wt. %, ○=35 wt. %. Full symbols relate to nucleation and growth as the dominant mechanism, while open symbols refer to grain rotation.*

order $P_{2,0}$ of the microdomains for 3 different block copolymer solutions is plotted (see Figure caption for details). Full symbols relate to *nucleation and growth* as the dominant mechanism, while open symbols refer to *grain rotation*. Only at sufficiently low degrees of initial order *grain rotation* is observed. A minimum degree of initial order can be identified, which is characterized by a $P_{2,0}$-value between 0.6 and 0.7, at which a change from *rotation of grains* to *nucleation and growth* is observed. It therefore seems reasonable to assume that the degree of initial alignment (and in turn: the defect density) has significant influence on the microscopic pathway for microdomain reorientation in the presence of the electric field.

4.4.2 Computer Simulations

The above interpretation is strongly corroborated by analysis of the real space data provided by computer simulations. A. Zvelindovsky and A. Sevink have performed two-dimensional dynamic self-consistent field simulations on lamellar diblock copolymer melts starting from two different initial conditions. In all cases the microdomain structure was first exposed to a shear field resulting in alignment of the lamellae in a well-defined direction to the electric field vector. Different shearing times and directions (a, b: perpendicular to the electric field vector, c: parallel to the electric field

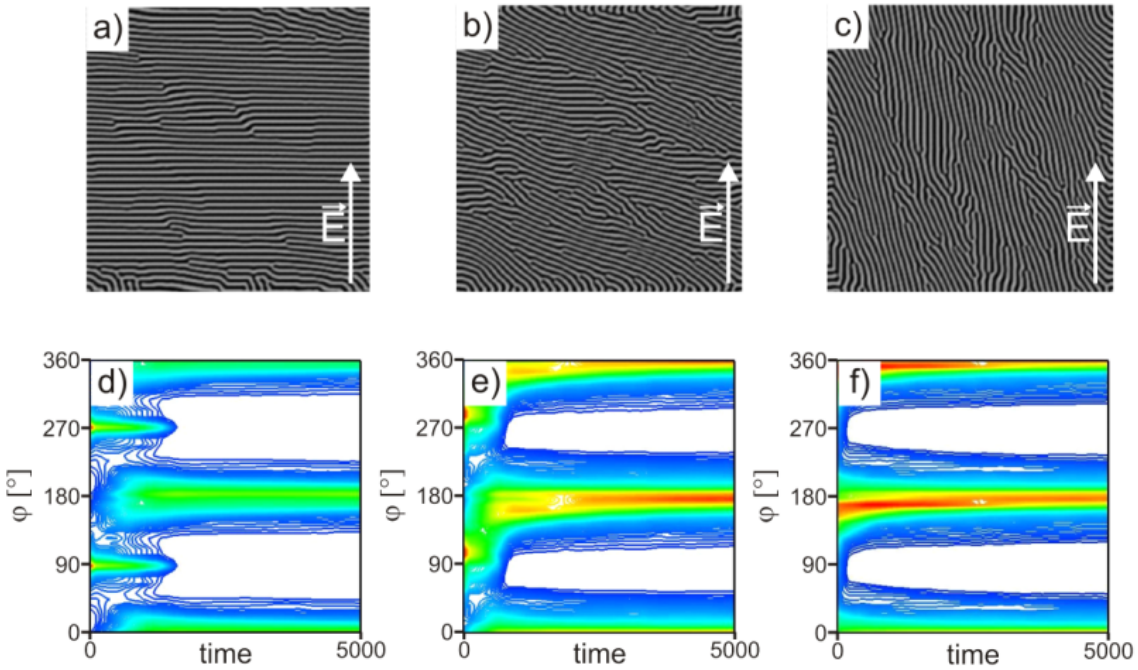

Figure 4.7: *(a, b, c) Self-consistent field theory simulations of initial microdomain structure, prealigned using shear: (a) highly aligned sample (7500 timesteps of shear perpendicular to electric field), (b) less aligned sample (2500 timesteps of shear perpendicular to electric field), (c) least aligned sample (2500 timesteps of shear parallel to electric field). (d, e, f) Squared Fourier transform of 2D simulated structures at dimensionless time t: (d) nucleation and growth mechanism for highly aligned sample, (e) combination of nucleation and growth mechanism and some grain rotation for the less aligned sample. (f) solely grain rotation mechanism for the least aligned sample. The electric field strength is $\tilde{\alpha} = 0.2$. The arrow indicates the direction of the electric field vector.*

vector) were chosen in order to produce initial states of different degrees of alignment. The first copolymer system studied has a mean field interaction of $\epsilon_{AB} = 6\,\mathrm{kJ/mol}$. It was found earlier to exhibit *nucleation and growth* as the dominant reorientation mechanism [Bök03b, Zve03]. Initial microdomain structures created this way are shown in Figure 4.7.

4.4.3 Comparison of Experiments with Computer Simulation

Indeed, as the electric field is applied, a distinctly different behavior is observed depending on the initial degree of alignment parallel to the electrodes. In the highly aligned sample with a largely dominant microdomain orientation perpendicular to the electric field vector (Figure 4.7 a), the reorientation process is rather slow and proceeds exclusively via *nucleation and growth*. The scattering functions calculated from these simulations are shown in Figure 4.7 d and exhibit the same characteristic features seen in the experimental scattering intensity in Figure 4.4.

In the less aligned sample (Figure 4.7 b) reorientation is found to proceed faster and *grain rotation* increasingly contributes to the reorientation. This is seen in the scattering functions shown in Figure 4.7 e, which resemble the experimental data

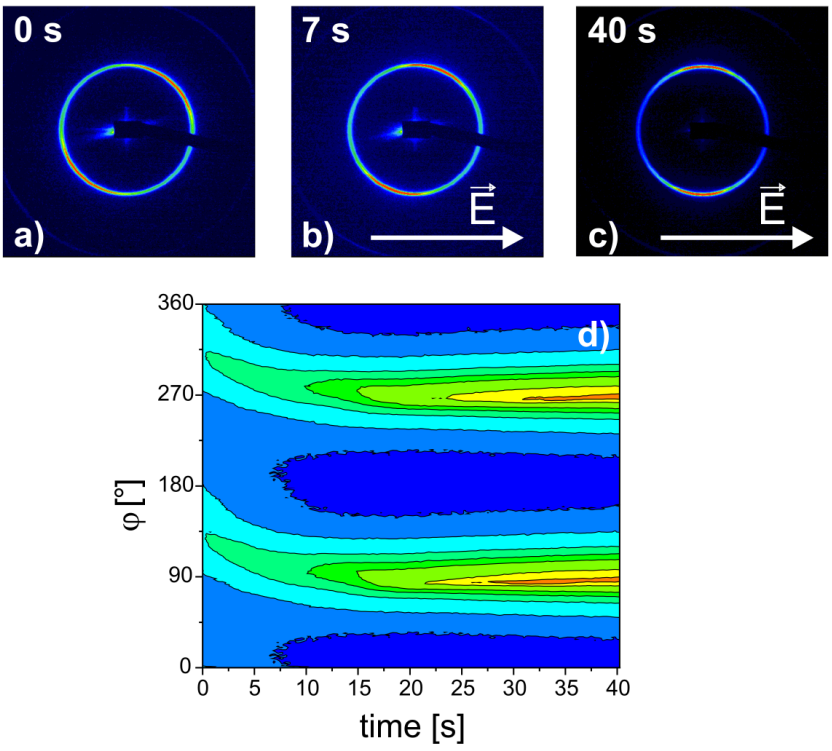

Figure 4.8: *(a-c) Scattering images of a 35 wt. % solution of $S_{50}I_{50}{}^{100}$ in toluene prior (a) and after (b, c) application of an electric field (1 kV/mm and $P_{2,0} = 0.04$). (d) 3D representation of the azimuthal angular dependence of the scattering intensity for the reorientation. The dominant mechanism here is grain rotation. The arrow indicates the direction of the electric field vector.*

found at large capacitor spacing (Figure 4.3).

In the case of a structure even less aligned parallel to the electrodes, Figure 4.7 c, the same copolymer system exhibits only *grain rotation* via movement of individual defects perpendicular to the lamellae. The scattering function in Figure 4.7 f exclusively shows a shift of the peak, with no signs of *nucleation and growth* mechanisms present. This is very similar to what was observed for $P_{2,0} = 0.04$ as depicted in Figure 4.8, showing that the lamellae are less ordered and tilted towards the electric field lines. Obviously, consistent with the theory of Onuki *et al.* [Onu95], the initial

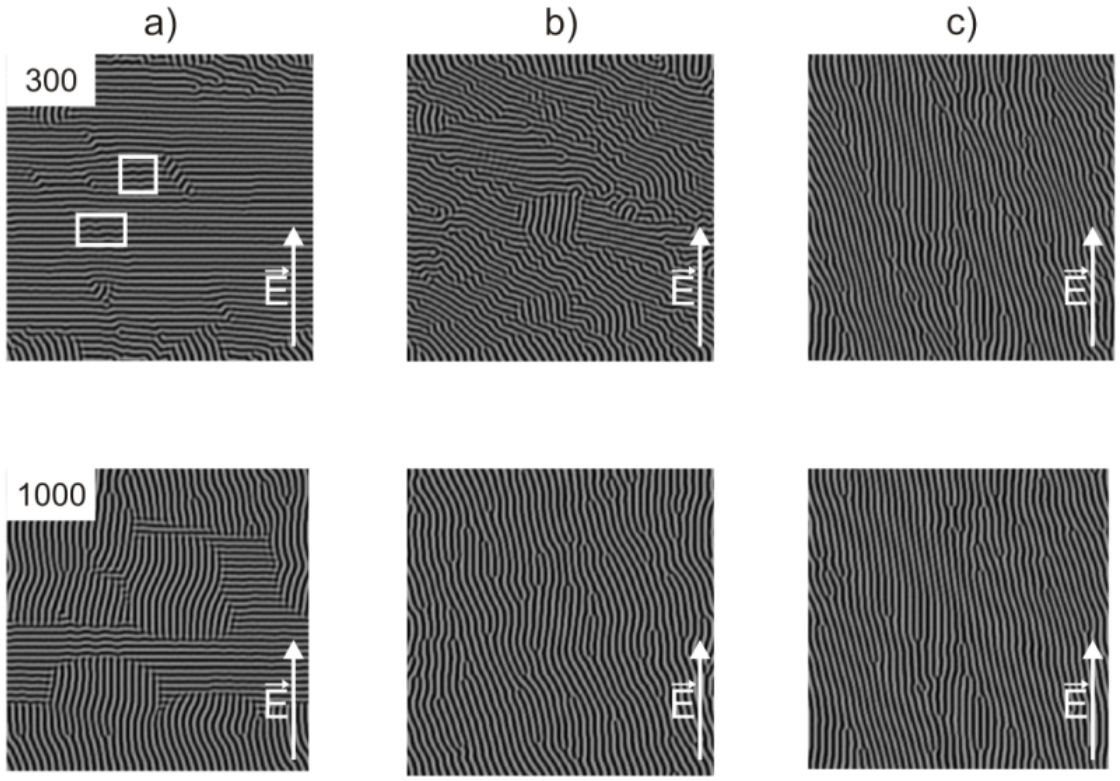

Figure 4.9: *Self-consistent field theory simulation. Real space representation of reorientation mechanisms for different pre-oriented samples in Figure 4.7: (a) nucleation and growth mechanism for highly aligned sample (white frames highlight undulation instabilities and nucleation sites), (b) combination of nucleation and growth mechanism and some grain rotation for less aligned sample (lower left corner: rotation; center: nucleation and growth), (c) solely grain rotation mechanism for the least aligned sample. Top row of snapshots is taken at the initial stages at dimensionless time $\tilde{t}$=300 bottom row at time $\tilde{t}$=1000. The arrow indicates the direction of the electric field vector.*

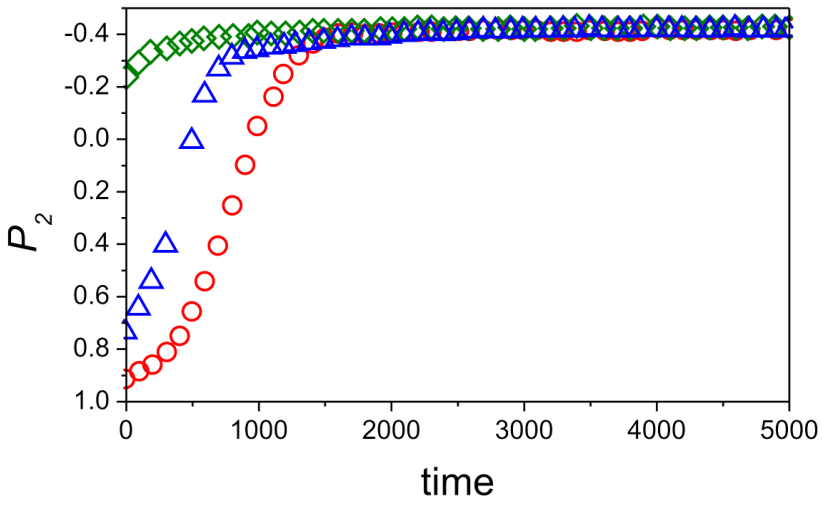

Figure 4.10: *Evolution of the order parameter for the systems in Figures 4.7 and 4.9 as a function of dimensionless time $\tilde{t}$. P_2 is calculated from the 2D simulation images analog Equation 3.1. (a = ○), (b = △), (c = ◇)as in Figure 4.7 and 4.9.*

angle between the lamella plane and the electric field vector is not sufficient for the instabilities in the structure to grow. Such instabilities are needed to nucleate grains of an orientation parallel to the external field. In this case, the only possible route to follow for the system is the *rotation of grains*, as it proceeds via individual defect movement.

Figure 4.9 provides a detailed real space view of the above described processes. It can be seen in Figure 4.9 a that even in the absence of defects in the initial structure in Figure 4.7 a, grains of the new phase nucleate due to the growth of instabilities. The number of nuclei depends on the initial defect density (see Figures 4.9 a and 4.9 b). The speed of the reorientation processes can be monitored by P_2 plots as shown in Figure 4.10, which qualitatively follow similar trends as the experimental curves, as a function of initial alignment (see Figure 4.5).

In addition, A. Zvelindovsky and A. Sevink have also performed simulations for the copolymer system with a mean field interaction of $\epsilon_{AB} = 8$ kJ/mol, which was found earlier to reorient by the *grain rotation* mechanism only [Zve03]. Figure 4.11 a shows a total suppression of the rotation in the better aligned sample compared to the one in Figure 4.11 b (the latter one is the same as in Zvelindovsky *et al.* [Zve03]). The system in Figure 4.11 a is seemingly trapped kinetically and only a few defects typical for *nucleation and growth* (white boxes) are generated slowly. This finding

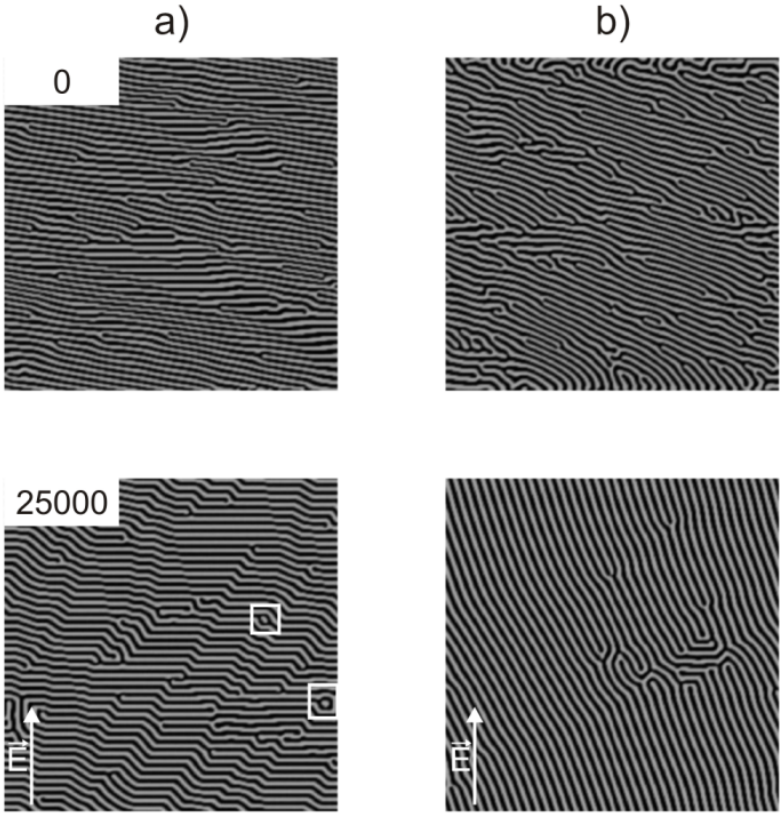

Figure 4.11: *Self-consistent field simulation of a system exhibiting only grain rotation mechanism. (a) better aligned sample, (b) less aligned sample. Top row: initial structure, bottom row: final structure at dimensionless time $\tilde{t}$=25000. The electric field strength is $\tilde{\alpha} = 0.2$. The arrow indicates the direction of the electric field vector.*

is consistent with the interpretation of the experiments mentioned earlier, that the *rotation* will be increasingly suppressed in a thinner slit, where lamellae are initially oriented more parallel to the electrodes.

Judging from the simulation results, it may indeed be assumed that the different degrees of initial order are responsible for the observed differences both in the kinetics and in the mechanism of reorientation. As can be seen from Figure 4.6, the process of reorientation becomes slower with increasing alignment and decreasing defect density. This is accompanied by a switch in mechanism from *rotation of domains* to *nucleation and growth*. Once the degree of initial order reaches a value of $P_{2,0} > 0.6$, grain rotation seems to be largely suppressed. For $P_{2,0} > 0.7$ grain rotation is no longer observed. Obviously, the number of defects in the microstructure becomes

insufficient to support grain rotation by defect movement. Here, structural defects exclusively serve as nucleation centers for new domains. Comparing the rather different time constants for the *nucleation and growth* process at the highest degrees of initial order, one is led to the assumption that at $P_{2,0} = 0.9$ the number of structural defects is too small to initiate sufficient nucleation centers. Therefore, thermal fluctuations of the lamellae amplified by the external electric field are needed for nuclei to be formed.

4.5 Conclusion

It has been found that both the reorientation pathway and the reorientation kinetics for lamellar microdomains in an external electric field strongly depend on the degree of order present prior to the application of the field. Samples of the same concentration but different initial order not only exhibit different mechanisms of orientation but also proceed at different rates. For intermediate degrees of order, where orientation proceeds via both pathways, it is found that the dominating mechanism dictates the overall rate of reorientation. It is observed consistently that for all systems *rotation* of lamellae by defect movement is faster than reorientation by *nucleation and growth* of new domains. Based on these results, one may conclude that above a certain initial orientation parallel to the electrodes the defect density is too low to allow for *rotation* of domains. In addition, the pressure on the well-aligned lamellae (as pointed out already by Onuki and Fukuda [Onu95]) is larger than for less aligned samples and therefore leads to undulation instabilities which finally serve as nucleation centers for the growth of grains oriented parallel to the external electric field. This leads to a switch in orientation mechanism with increasing initial microdomain orientation from *rotation* to *nucleation and growth*.

On the Physical Origin of Block Copolymer Alignment

Following discussions on the driving factors leading to microdomain orientation, the impact of the dielectric contrast and the incompatibility of the blocks on the kinetics of domain orientation was studied. Therefore, the reorientation kinetics of various block copolymer solutions exposed to an external DC electric field was investigated. The characteristic time constants follow a power law indicating that the reorientation is driven by a decrease in electrostatic energy. Moreover, the observed exponent suggests an activated process in line with the expectations for a *nucleation and growth* process. When properly scaled, the data collapse onto a single master curve spanning several orders of magnitude both in reduced time and in reduced energy. The power law dependence of the rate of reorientation derived from computer simulations based on dynamic density functional theory agrees well with the experimental observations. First experiments in AC electric fields at sufficiently high frequencies confirm the notion that the reorientation process is dominated by differences in the dielectric constants rather than by mobile ions.

5.1 Introduction

Both theoretical and experimental work has dealt with the mechanisms and driving force leading to microdomain alignment in block copolymer systems subjected to an external electric field. Besides the direct visualization of different microscopic mechanisms (*rotation* of the structural elements via defect movement versus *nucleation and growth* of domains initiated by electric field induced structural instabilities) with x-ray scattering methods [Bök02c, Bök03b], considerable efforts have concentrated on the relation between defects and the pathways leading the microdomains to align parallel to the electric field [Amu94, TA02]. From theoretical models, there are two possible major driving forces for the orientation to take place. First, there is the *dielectric mechanism*, which is based on the dielectric contrast between the copolymer blocks leading to a minimum in electrostatic free energy whenever the dielectric interfaces are oriented parallel to the electric field vector [Lan84]. The gain

in free energy should be proportional to $\frac{(\varepsilon_A-\varepsilon_B)^2}{\langle\varepsilon\rangle}E^2$ with $\varepsilon_{A,B}$ being the dielectric constants of the polymer blocks and $\langle\varepsilon\rangle$ being the average dielectric constant for the system. This mechanism is referred to as the *dielectric effect*. Due to the quadratic dependence on the electric field strength this effect is expected to work both in DC and AC electric fields. Recently, Wang *et al.* [Wan06] have shown that complexation of ions leads to an effective increase of the dielectric constant of one of the blocks resulting in an improved microdomain alignment in DC fields in line with the above expectation. However, a quantitative confirmation of the predicted behavior is still lacking.

Another approach recently discussed is the theoretical possibility of mobile ions contributing to the reorientation process as they may lead to an effective polarization of the anisotropic block copolymer structure thus allowing for microdomain alignment at field strengths much lower than required by the *dielectric mechanism* [Tso03a]. An electric field will then exert a torque on the microdomains until a parallel orientation of such dipoles along the field direction is established. If mobile ions are present in a certain block copolymer system, the ionic effect is expected to dominate the dielectric driving force in DC fields or at low frequency AC fields (< 50 Hz) as the effect is inversely proportional to the frequency.

In the following the issue outlined above is addressed and a first quantitative study of the reorientation kinetics in solutions of various model block copolymers exposed to an electric field is presented. The dielectric contrast is systematically varied and its influence on the reorientation rate is shown. The scaling behavior of the rate of reorientation is analyzed and compared to results of dynamic self-consistent field simulations. Furthermore, the electric threshold field for several block copolymers is estimated. Finally, first kinetic experiments in high frequency AC electric field were performed indicating that the process is indeed dominated by the dielectric contrast rather than by mobile ions.

5.2 Materials

Five different lamella forming diblock copolymers, $S_{50}V_{50}{}^{78}$, $S_{47}H_{10}M_{43}{}^{82}$, $S_{50}T_{50}{}^{100}$, $S_{50}I_{50}{}^{100}$, and $S_{49}M_{51}{}^{100}$ of comparable chain lengths, however, with different dielectric contrast were studied. Details about these systems can be found in Table 3.1. The polymers were dissolved in THF, which is a rather neutral solvent for the block copolymer systems under investigation with concentrations slightly above the order-disorder concentration. Among the five materials the dielectric contrast $(\varepsilon_A - \varepsilon_B)$

varies between 0.25 and 4.9 (see Table 5.1). The measured dielectric contrasts in THF after correction for the pure solvent are in agreement with the values in the melt. The ion content of all samples is estimated to range between 1-10 ppm. The alignment experiments were performed at room temperature in a similar capacitor ($d = 2$ mm) applying either DC (voltage between 0.25 and 3 kV/mm) or AC electric fields of around 0.4 kV/mm. The order parameter P_2 and the characteristic time τ for reorientation were calculated according to Equation 3.1 and 3.2, respectively.

Table 5.1: *Dielectric contrasts of the different diblock copolymers in THF solutions at room temperature.*

Block copolymer system	Dielectric contrast $(\varepsilon_A - \varepsilon_B)^*$
$S_{50}I_{50}{}^{100}$	0.25 ± 0.10
$S_{49}M_{51}{}^{100}$	1.20 ± 0.10
$S_{50}T_{50}{}^{100}$	1.24 ± 0.10
$S_{47}H_{10}M_{43}{}^{82}$	2.00 ± 0.25
$S_{50}V_{50}{}^{78}$	4.90 ± 0.39

5.3 Results and Discussion

5.3.1 Comparison of $S_{47}H_{10}M_{43}{}^{82}$ and $S_{49}M_{51}{}^{100}$

In previous investigations on solvent based systems [Bök02c], the interplay between viscosity (i. e. chain mobility) and dielectric contrast (i. e. electric driving force) turned out to be critical. In order to study the influence of the dielectric contrast on the reorientation, the inclusion of a short, polar middle block (PHEMA) into polystyrene-*b*-poly(methyl methacrylate) is used to tailor both the degree of incompatibility and the dielectric contrast between the two majority phases ($\Delta\varepsilon_{S_{49}M_{51}{}^{100}} = 1.2$, $\Delta\varepsilon_{S_{47}H_{10}M_{43}{}^{82}} = 2.0$). As indicated by differential scanning calorimetry (DSC), rheological and TEM experiments reported by Böker *et al.* [Bök02c], it is anticipate that PHEMA and PMMA form a mixed phase.

The lowest possible concentration and thus viscosity to give a phase separated polymer solution for the $S_{49}M_{51}{}^{100}$ diblock copolymer system was found at 53 wt. %

∗ The ε-values for PS, PI, P*t*BMA, and PMMA were measured by dielectric spectroscopy [Kre02], ε_{PHEMA} and ε_{P2VP} are taken from [Yam94] and [Neg97], respectively.

in THF. The order-disorder transition (ODT) for the $S_{47}H_{10}M_{43}{}^{82}$ triblock copolymer at room temperature is around 40 wt. %. Obviously, the presence of the PHEMA middle block leads to an increased incompatibility and thereby to a lower order-disorder concentration. Thus, the viscosity of solutions just above the order-disorder concentration is significantly lowered by the inclusion of the PHEMA middle block.

First, the reorientation of the $S_{49}M_{51}{}^{100}$ solution was investigated. Here, only slow reorientation of the microdomains could be realized at a field strength of 2 kV/mm as shown in Figure 5.1. The data shown here represent the fastest possible alignment kinetics achievable for the $S_{49}M_{51}{}^{100}$ system, as with increasing polymer concentration, the viscosity immediately dominates the process, rendering the reorientation impossible. Obviously, above the order-disorder concentration the force implied on the lamellae is not sufficient to lead to significant reorientation. In the case of the $S_{47}H_{10}M_{43}{}^{82}$ triblock copolymer a different behavior is observed. As soon as an electric field of 1 kV/mm is applied to a 40 wt. % solution, the scattering pattern changes significantly. The peaks at $\varphi = 0°$ and 180° decrease and new scattering maxima at $\varphi = 90°$ and 270° grow with time, resulting in a time constant of $\tau = 89$ s (Figure 5.2). With increasing polymer concentration and thus increasing viscosity,

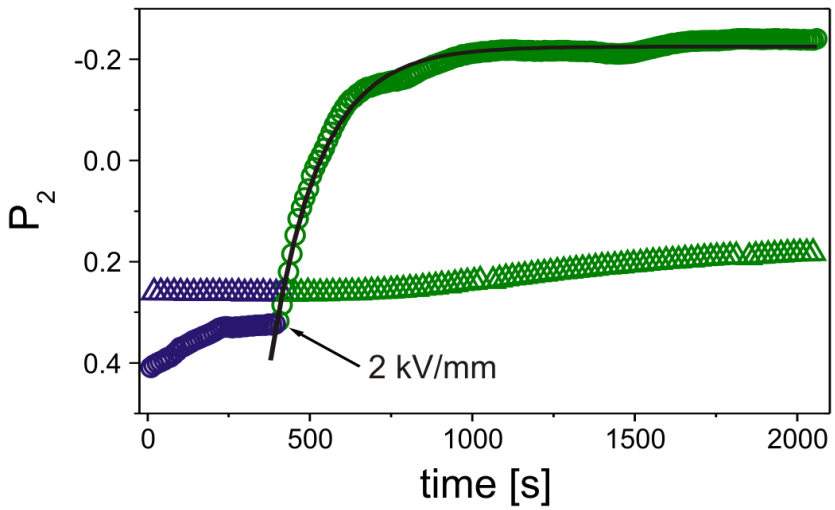

Figure 5.1: *Evolution of the order parameter P_2 with time for a 45 wt. % solution of $S_{47}H_{10}M_{43}{}^{82}$ in THF at ○ 1 kV/mm and ○ 2 kV/mm. For comparison, the data for a 53 wt. % solution of $S_{49}M_{51}{}^{100}$ in THF at △ 1 kV/mm and △ 2 kV/mm is added. The solid line represents the least squares fit to the data resulting in $\tau_{S_{47}H_{10}M_{43}{}^{82}} = 157$ s.*

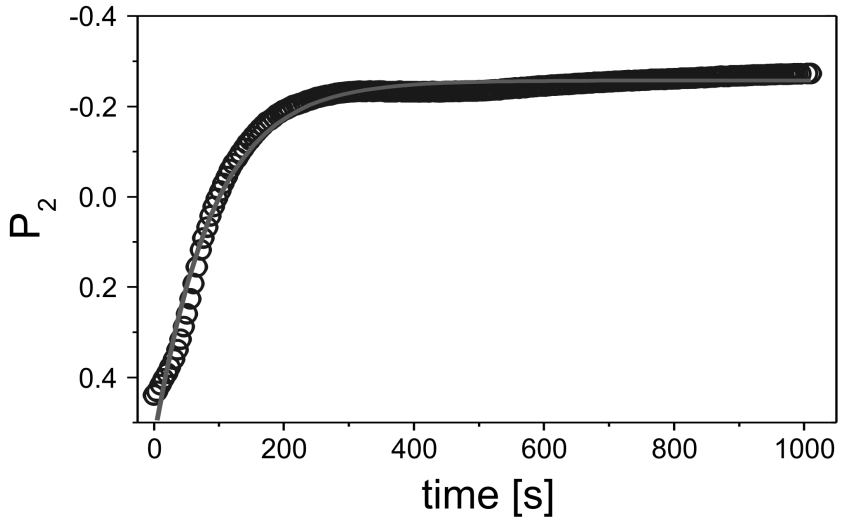

Figure 5.2: *Evolution of the order parameter for a 40 wt. % solution of $S_{47}H_{10}M_{43}^{82}$ in THF at 1 kV/mm. The solid line represents the least squares fit to the data resulting in $\tau_{S_{47}H_{10}M_{43}^{82}} = 89\ s$.*

the reorientation process is slowed down significantly (see Figure 5.1). At a polymer concentration of 45 wt. % only very slow orientation could be detected for 1 kV/mm and at a concentration of 50 wt. %, within the experimental time window of several minutes, no microdomain orientation could be achieved at field strengths as high as 6 kV/mm. This behavior results from a delicate balance between an increase of both the driving force for reorientation (i. e. a larger dielectric contrast) and the viscous retardation as the polymer concentration is increased. The exact behavior is difficult to predict, however, the data shown in Figure 5.1 indicate that in the particular system studied here the increase in viscosity dominates over the increase of the driving force.

5.3.2 Scaling Behavior

Further investigations to probe the influence of the dielectric contrast were performed. The reorientation for the $S_{47}H_{10}M_{43}^{82}$, $S_{50}V_{50}^{78}$, $S_{50}T_{50}^{100}$ and $S_{50}I_{50}^{100}$ copolymer systems were studied depending on the dielectric contrast and electric field strength. It is expected that the rate of alignment $1/\tau$ is proportional to the driving force for reorientation. Therefore, the discussion is started with the rate dependence on the electric field strength E and on the dielectric contrast ($\Delta\varepsilon = \varepsilon_A - \varepsilon_B$). In Figure 5.3 the alignment rate as a function of the electric

field strength for the four different block copolymer systems is shown. Systematically, a power-law dependence with a nearly identical exponent of around 2.7 for all four systems is observed. As outlined above, a simple theoretical consideration leads to an exponent of 2 for the dielectric effect. The fact that consistently an exponent significantly larger than two is observed is in accordance with earlier predictions by Amundson *et al.* [Amu93]. The authors pointed out that an exponent larger than 2 is to be expected if the alignment process is characterized by an activation step involving an energy barrier. Such an activation energy is anticipated, e. g. for the creation of undulations serving as nuclei for domains aligned in the preferred direction [Fuk95, Mat05]. Indeed, under the experimental conditions chosen throughout the present study, the block copolymer solutions are only weakly phase-separated and microdomain reorientation is dominated by *nucleation and growth* [Bök02c].

Aside from the power law itself the data in Figure 5.3 also indicate the relevance of the dielectric contrast. The system with the largest dielectric contrast ($S_{50}V_{50}^{78}$,$\Delta\varepsilon = 4.9$) exhibits the fastest reorientation kinetics while the two systems with the smallest dielectric contrast ($S_{50}T_{50}^{100}$, $\Delta\varepsilon = 1.24$; $S_{50}I_{50}^{100}$, $\Delta\varepsilon = 0.25$) exhibit the slowest reorientation behavior. For a quantitative comparison between

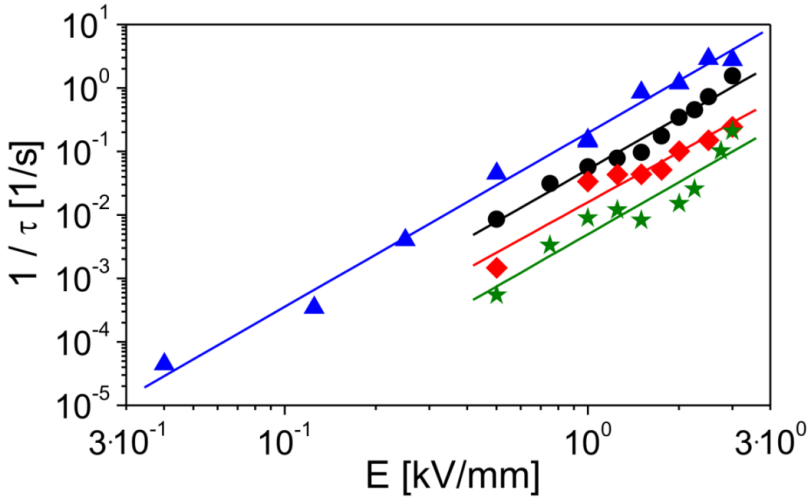

Figure 5.3: *DC electric field dependence of the rate of alignment $1/\tau$ for ▲ 40 wt. % $S_{50}V_{50}^{78}$, ● 40 wt. % $S_{47}H_{10}M_{43}^{82}$, ♦ 40 wt. % $S_{50}I_{50}^{100}$, and ★ 50 wt. % $S_{50}T_{50}^{100}$ in THF. The solid lines represent least squares fits of the power law $1/\tau = a \cdot E^x$ to the data points yielding $x_{S_{50}V_{50}^{78}} = 2.73$, $x_{S_{47}H_{10}M_{43}^{82}} = 2.73$, $x_{S_{50}I_{50}^{100}} = 2.63$, and $x_{S_{50}T_{50}^{100}} = 2.73$.*

the different block copolymers the viscosities of the respective solutions need to be taken into account. Therefore, the shear viscosities η at 1 rad/s of the samples were determined. Assuming furthermore the predicted dependence of $1/\tau$ on the dielectric properties one can try to create a master curve by plotting the data of Figure 5.3 as $\frac{\eta}{\tau}$ versus $\frac{(\varepsilon_A-\varepsilon_B)^2}{\langle\varepsilon\rangle}E^2$. The result of this procedure is shown in Figure 5.4. Three of the four block copolymers fall onto a single curve, covering three orders of magnitude in field energy and five orders of magnitude in $\frac{\eta}{\tau}$. This scaling behavior is a strong indication that the dielectric contrast of the pure block copolymers constitutes the major driving force for the reorientation process in electric fields. Interestingly, the most polar system ($S_{50}V_{50}{}^{78}$) deviates towards smaller values. It is assumed that this deviation is due to an electrorheological effect [Pri95] leading to a larger viscosity under electric field influence. This effect is expected to be more pronounced for polar materials.

5.3.3 Computer Simulations

The results outlined above are strongly corroborated by analysis of the real space data provided by numerical calculations. H. Schoberth used the dynamic self-consistent field (DSCF) theory to calculate the structure evolution in a lamella forming diblock copolymer melt with parameters chosen to yield a reorientation

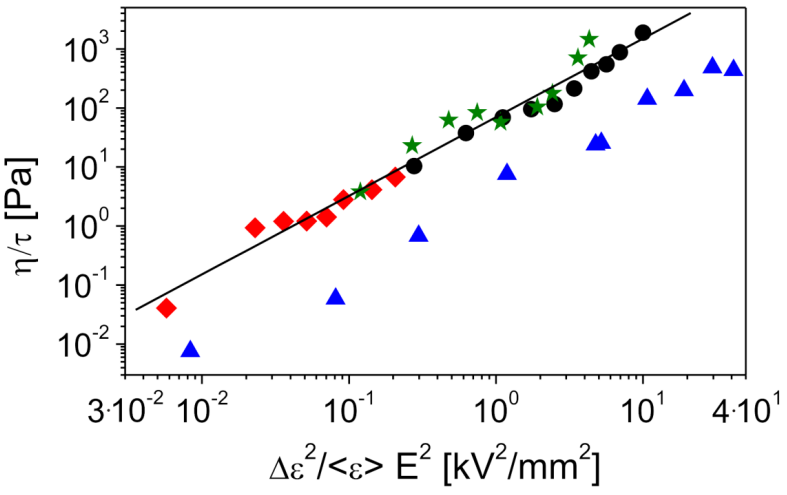

Figure 5.4: *Same data as in Figure 5.3 with the x- and y-axis scaled by* $\frac{(\varepsilon_A-\varepsilon_B)^2}{\langle\varepsilon\rangle}E^2$ *and* η*, respectively for* ▲ *40 wt. %* $S_{50}V_{50}{}^{78}$ *,* ● *40 wt. %* $S_{47}H_{10}M_{43}{}^{82}$ *,* ♦ *40 wt. %* $S_{50}I_{50}{}^{100}$ *, and* ★ *50 wt. %* $S_{50}T_{50}{}^{100}$ *in THF.*

mechanism similar to the one observed in the experiments [Bök03a, Bök03b].

From the simulation the order parameter P_2 can be calculated. By analyzing P_2 with a single-exponential fit the rate of reorientation can be extracted. In Figure 5.5 the rate dependence on the parameter $\tilde{\alpha}$ is shown for small and large simulation boxes. The parameter $\tilde{\alpha}$ is quadratic in the electric field and the dielectric contrast and hyperbolic in the average dielectric constant. Thus, Figure 5.5 can be compared with Figure 5.4. Again a power law dependence of the reorientation rate is observed. The power law dependence of $\tilde{\alpha}$ to the power of 1.45 corresponds to an exponent of 2.9 for E. For the given governing mechanism of *nucleation and growth*, this exponent is independent of the size of the simulation box as well as the initial orientational order of the system, e. g. initial lamellar tilt, as can be seen from the different initial states of alignment in Figure 5.6 (a-d). Large differences in initial alignment after shear influence the mechanism of the process (see chapter 4), however, as long as an activation step is involved, the scaling of $1/\tau$ versus E is not affected. Therefore, one may regard this behavior as an universal property of the specific reorientation process. As mentioned above an exponent larger than 2 indicates an activated state. Indeed, if the results of the simulations in real space

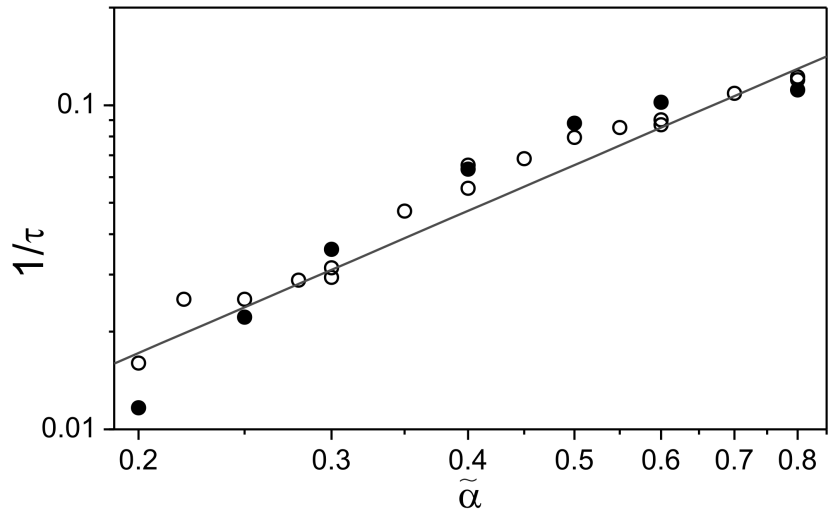

Figure 5.5: *Dependence of the rate of reorientation on the parameter $\tilde{\alpha}$ ($\tilde{\alpha} \propto E^2 \frac{\Delta\varepsilon^2}{\langle\varepsilon\rangle}$) calculated from dynamic self consistent field simulations for a ○ 32 x 32 x 32 and a ● 64 x 64 x 64 grid points box. The solid line represents a least squares fit of the power law $1/\tau = a \cdot \tilde{\alpha}^x$ to the data points yielding $x = 1.45$, i. e. $1/\tau \approx E^{2.9}$*

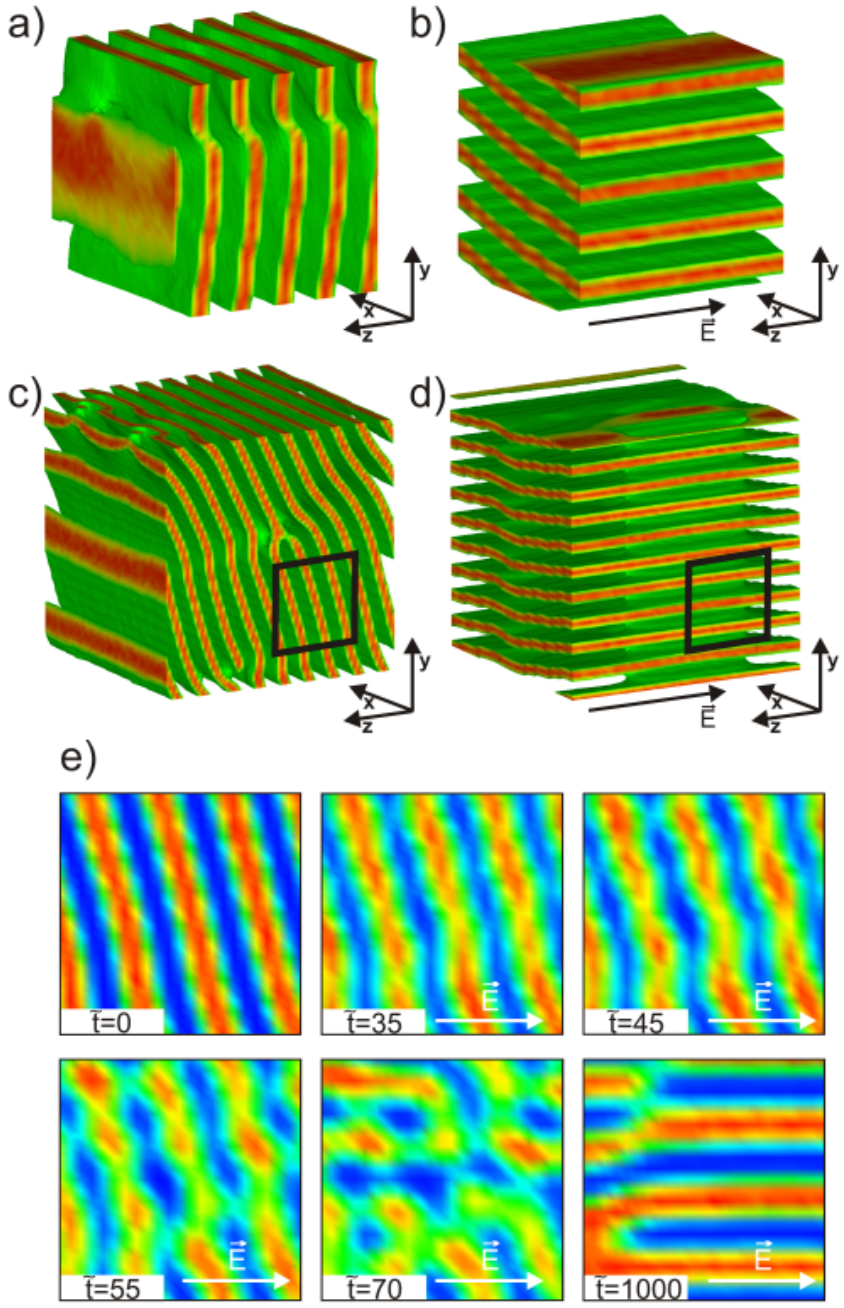

Figure 5.6: *Initial (a, c) and final (b, d) three dimensional structure of the* $32 \times 32 \times 32$ *(a, b) and* $64 \times 64 \times 64$ *(c, d) grid points boxes. The black retangle indicates the detailed representation in (e). The snapshots are taken at the dimensionless times* $\tilde{t} = 0, 35, 45, 55, 70, 1000$*. The arrows indicate the direction of the electric field vector.*

(shown in Figure 5.6) were followed an activated step is observed. As soon as the electric field is applied the lamellae start to undulate and eventually disrupt. These undulations serve as nuclei which merge in the electric field direction as has been shown earlier [Bök03b]. This nucleation process is rather fast. However, the achievement of perfect long ranged order requires the successive annihilation of low energy defects, which requires much longer times.

5.3.4 Estimation of the Threshold Electric Fields

While the above considerations were solely concerned with the field dependence of the reorientation rate, it is interesting to examine the energy gain in the capacitor once alignment parallel to the electric field has been achieved. It was pointed out earlier that the effect of an electric field will compete with the influence of the boundary surfaces (i. e. the capacitor plates), which are known to induce an alignment of lamellar microdomains parallel to the boundary surfaces due to reduction in interfacial energy. This interplay leads to a threshold field strength (E_t) below which no reorientation can be achieved [TA00]. Above this threshold the gain in electrostatic energy after reorientation is sufficient to compensate for the energetic penalty associated with the formation of T-junctions [Tso02].

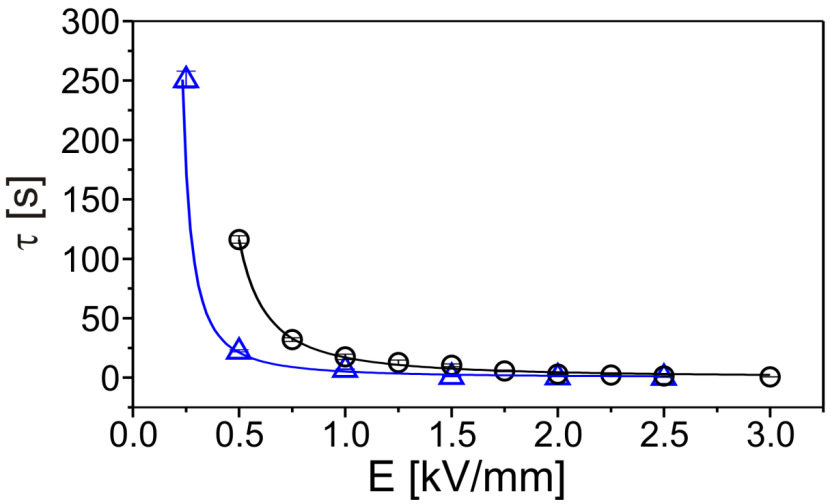

Figure 5.7: *Electric field dependence of the time constant τ for △ 40 wt. % $S_{50}V_{50}{}^{78}$ and ○ 40 wt. % $S_{47}H_{10}M_{43}{}^{82}$ in THF. The solid lines represent least squares fits of the power law $\tau = \alpha(E - E_t)^a$ to the data points yielding the treshold fields $E_{t(S_{50}V_{50}{}^{78})} = 0.185\ kV/mm$ and $E_{t(S_{47}H_{10}M_{43}{}^{82})} = 0.315\ kV/mm$.*

Table 5.2: *Threshold fields and dielectric contrast for the different diblock copolymers in THF solutions at room temperature.*

Block copolymer system	Threshold field E_t [V/mm]	Dielectric contrast $(\varepsilon_A - \varepsilon_B)^{\dagger}$
$S_{50}I_{50}{}^{100}$	487 ± 9	0.25 ± 0.10
$S_{50}T_{50}{}^{100}$	434 ± 29	1.24 ± 0.10
$S_{47}H_{10}M_{43}{}^{82}$	315 ± 45	2.00 ± 0.25
$S_{50}V_{50}{}^{78}$	185 ± 23	4.90 ± 0.39

If the field strength is reduced below a critical value of E, no reorientation is observed on the time scale of the experiment (ca. 3600 s). The threshold field E_t can be approximated by fitting a hyperbolic dependence $\tau = \alpha(E - E_t)^a$ to the data in Figure 5.3 (see Figure 5.7 for $S_{50}V_{50}{}^{78}$ and $S_{47}H_{10}M_{43}{}^{82}$). By this, E_t for the four block copolymer systems is obtained (Table 5.2).

Qualitatively, a clear correlation between E_t and $\Delta\varepsilon$ is found: The larger the dielectric contrast the smaller the threshold field needed to overcome the defect energy described above. This result seems reasonable assuming that the defect energy will be of the same order of magnitude for all four block copolymers studied. Since in the framework of the dielectric effect the energy gain is expected to increase with the dielectric contrast, this finding, again, indicates the importance of dielectric contributions to the overall process.

5.3.5 Kinetics in AC Electric Fields

While the results discussed so far are in line with the predictions for a dielectrically driven microdomain orientation one shall now turn to a critical experimental test of possible contributions of mobile ions. An experiment allowing AC electric fields to be applied to the sample *in-situ* at the X-ray beamline was set-up. According to the considerations by Tsori *et al.* [Tso03a] ionic contributions should no longer play a role once the frequency of the AC electric field is considerably higher than the inverse time needed by the ions to move to the domain boundaries. First this

† The ε-values for PS, PI, P*t*BMA, and PMMA were measured by dielectric spectroscopy [Kre02], $\varepsilon_{\mathrm{PHEMA}}$ and $\varepsilon_{\mathrm{P2VP}}$ are taken from [Yam94] and [Neg97], respectively.

characteristic frequency for a 40 wt. % solution of $S_{50}V_{50}{}^{78}$ in THF is estimated. The drift velocity s of an ion carrying a charge Ze in an electric field of strength E is given by

$$s = \frac{Ze}{6\pi\eta a}E$$

where η is the viscosity of the solution and a is the radius of the ion. Since Li^+ ions are expected to be the main contamination due to the ionic polymerization procedure, a quantitative estimate for this ionic species is carried out. With $Z_{Li^+} = 1$, $a_{Li^+} = 59$ pm [Lid96], $\eta_{40\,\text{wt.\%}\ S_{50}V_{50}{}^{78}} = 170$ Pa s and $E \approx 0.7$ kV/mm a drift velocity of $s \approx 0.6$ μm/s is obtained. For an estimate of the characteristic time the smallest characteristic distance of the system, i. e. the lamellar spacing of $d = 32$ nm was used. Given the above drift velocity the ion needs at least 53 ms to travel this distance. Hence, a characteristic frequency of around 20 Hz is found for this system. Considerably larger distances will be involved for the ion to travel to the outer limits of the grains, which would translate into considerably lower frequencies. Yet, in order to ensure that the system is in the high frequency regime, the frequency was increased by more than two orders of magnitude above this estimate and measurements at 5 kHz with an effective electric field strength of around 0.4 kV/mm were performed.

In Figure 5.8 a the time evolution of the azimuthal angular dependence of the scattering intensity during the reorientation of a $S_{50}V_{50}{}^{78}$ solution in the presence of an AC electric field is shown. The reorientation process is dominated by *nucleation and growth of domains*: The initial peaks at $\varphi = 0°$ and 180° decrease and grow at the final position at $\varphi = 90°$ and 270°. This finding is in line with earlier observations in DC electric fields (see chapter 4). From a single-exponential fit to P_2 the time constant of $\tau = 75$ s for the reorientation process is extracted (see Figure 5.8 b). The fact that reorientation in AC electric fields at a frequency considerably above what is expected to be the high frequency limit [Tso03a] is observed points to the fact that for the system under study any contribution from mobile ions on the microdomain reorientation can be excluded. A quantitative comparison of the time constant with the corresponding DC value is barely possible as the exact field strength acting on the sample is difficult to assess due to unknown AC resistance of other parts of the set-up.

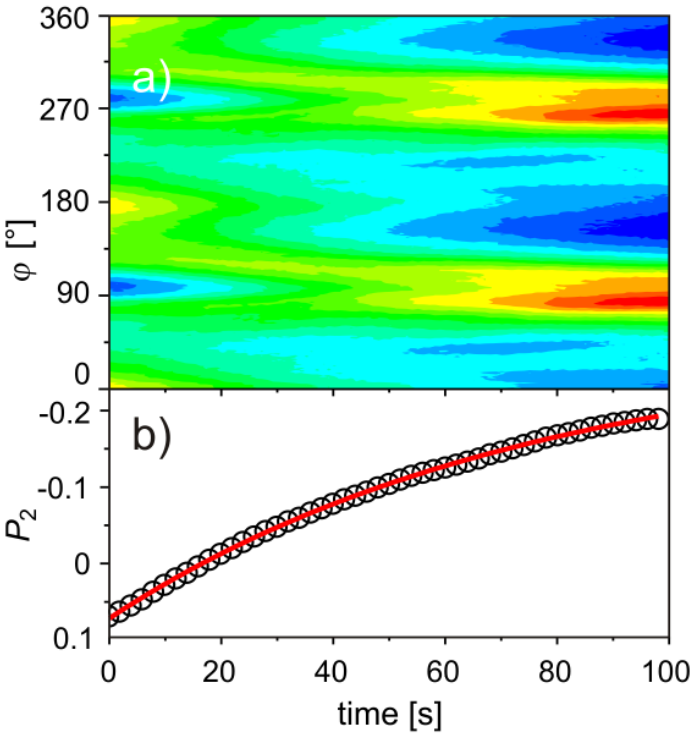

Figure 5.8: *(a) Time evolution of the azimuthal angular dependence of the scattering intensity for a 40 wt. % solution of* $S_{50}V_{50}$[78] *in THF exposed to an AC electric field with* $E \approx 0.4\ kV/mm$ *and* $f = 5\ kHz$*. (b) Evolution of the orientational order parameter* P_2 *for the measurement in (a). The solid line represents a least squares fit of an exponential to the data yielding a time constant* τ *of 75 s.*

5.4 Conclusion

In summary it was found that the interplay of enhanced microphase separation and contribution to a higher dielectric contrast between the phases by incorporation of the PHEMA middle block in PS-*b*-PMMA results in an improved electric field induced alignment. Furthermore, the experimental data strongly indicate that the *dielectric effect* plays the major role as the driving force for block copolymer reorientation in electric fields. When properly scaled, the data for different block copolymer systems collapse onto a single master curve spanning several orders of magnitude both in reduced time and in reduced energy. The observed exponent suggests an activated process in line with the expectations for a *nucleation and growth* process. These observations are corroborated by dynamic self-consistent simulations. In ad-

dition, the threshold field for each system was calculated and a dependence on the dielectric contrast was found. Furthermore, measurements with AC electric fields with high frequencies well above the high frequency limit were performed. Reorientation of the system with same characteristics as the reorientation in DC electric fields is observed.

Electric Field Induced Order-Order-Transitions

The influence of an electric field on various microdomain structures was investigated. As model systems, concentrated solutions of different polystyrene-*b*-polyisoprene block copolymers in toluene were used. Different electric field induced order-order-transitions can be identified for higher field strengths depending on the original microdomain structure. An electric field induced alignment can be achieved for the anisotropic microdomain structures, such as lamellae, hexagonally perforated lamellae and cylinders. For the cubic gyroid phase an alignment does not occur but a order-order-transition to aligned cylinders is induced by the electric field. In addition, the hexagonally perforated lamellae undergoes a phase transition to the lamellar phase under stronger electric fields. Some of these order-order-transitions were theoretically predicted based on computer simulations using the dynamic self-consistent field theory but not observed experimentally yet.

6.1 Introduction

Block copolymers show typical well-known microdomain structures, such as the body-centered cubic crystal of spherical domains (S), hexagonally packed cylinders (C), bicontinuous gyroid (G), and lamellar domains (L). In predicting the equilibrium phase diagram the mean-field theories, such as the Ginzburg-Landau type model with the random phase approximation (RPA) and the self-consistent field theory (SCFT), are quite useful. Both experiments and theory have shown that the fifth ordered phase, the hexagonally perforated lamellae (HPL), is not thermodynamically stable and therefore has to be considered as a metastable phase [Haj95, Vig98].

Despite the limited accessibility, the HPL phase has drawn much attention due to its fascinating structural characteristics. The HPL structure consists of alternating minority and majority component layers in which hexagonally packed channels of the majority component extend through the minority component. The stacking sequence of HPL channels can be modeled as both ABAB... and ABCABC...

patterns. The ABC stacking has a rhombohedral (trigonal) symmetry (space group $R\bar{3}m$) whereas the AB stacking has a hexagonal symmetry (space group $P6_3/mmc$). The free energy calculations for the two HPL structures showed that the two states are metastable in the intermediate segregation limit with nearly degenerated free energy [För94, Mat97a]. From the geometrical point of view, the HPL structure consists of planar tripods and the gyroid structure can be generated from the HPL phase by rotating the dihedral angle of the connecting tripods to 70.53° [För94, Zhu03].

The gyroid morphology ($Ia\bar{3}d$ symmetry) is of great interest due to its bicontinuous nature of two mutually interpenetrating labyrinth networks. Taking advantage of its complex domain structure, the G structure is expected to have a wide applicability to various techniques, for example, three dimensional photonic crystals, microporous systems, nanoreactors, etc. [Edr01, Has97, Zha98].

Among the equilibrium ordered phases, a rich variety of reversible order-order phase transitions (OOTs), such as C↔S [Kim00, Kri00, Lee02], L↔C [Haj94], L↔G [Vig98, Sch94], and C↔G [Sch02, Sak98, Ham99, Haj98], have been observed experimentally. These OOTs can be induced by changing the temperature, addition of homopolymers or selective solvents, or by imposing an external field such as flow field or an electric field. The kinetic pathways from the L→G transition as well as the C→G transition induced by either a change in temperature or by addition of selective solvents, was investigated experimentally [Esk05, Par05, Ham04, Wan02] and theoretically [Yu05, Hon06, Zve00, Ima01, Ly07]. The HPL phase has been observed as a transient structure for both transitions [Ham04, Wan02, Ima01].

The driving force for the reorientation of microdomain structures under an electric field is the electrostatic free energy penalty associated with the dielectric interfaces which are not parallel to the electric field lines. While the free energy penalty can be eliminated by reorientation of lamellae and cylinders, it cannot be eliminated in cubic phases, such as the gyroid or spherical phase. However, it can be reduced by distorting the phase. When a field is applied on lamellar or hexagonal phases, it exerts torque which causes grain rotation. The torque is zero, and the energy lowest, when the lamellae or cylinders are oriented parallel to the field. The S, G, and HPL phases, on the other hand, always have dielectric interfaces that are not parallel to the field, and their free energy under the influence of an electric field is higher than without field. Hence, the structures elongate in the applied field direction, to an extent which is a balance between electrostatic and elastic forces. Thus, the free energy of this distorted phase, whose symmetry is reduced, increases

with respect to the other phases, a circumstance which can bring about a phase transition [Tso06]. For instance, Xu investigated experimentally and theoretically the S→C transition in a diblock copolymer under an applied electric field [Xu04c]. The C→G transition, the L→G transition, as well as the G→C transition under an electric field was investigated using the dynamical self-consistent field theory (SCFT) [Lya06b, Ly07]. These types of transformation have not been studied experimentally.

6.2 Materials

In order to investigate possible order-order-transitions under an electric field, a series of polystyrene-*b*-polyisoprene block copolymers, $S_{64}I_{36}{}^{78}$, $S_{67}I_{33}{}^{75}$, $S_{69}I_{31}{}^{72}$, $S_{72}I_{28}{}^{69}$, and $S_{76}I_{24}{}^{76}$, was synthesized. The block copolymers cover a composition range from $\phi_S = 61$ % to $\phi_S = 73$ % with a molecular weight of $M_n \approx 74\,\mathrm{kg/mol}$. Details on the polymers can be found in Table 3.1. The polymers were dissolved in toluene leading to a concentration of 45 wt. %. All experiments were performed at room temperature in a capacitor with an electrode spacing of 1 mm and a DC voltage up to 11 kV/mm.

6.3 Results and Discussion

6.3.1 Phase Diagram without Electric Field

First, the phase diagram without an electric field was determined. The Figures 6.1 to 6.4 illustrate the scattering pattern for four different polystyrene-*b*-polyisoprene block copolymer solutions in toluene. Clearly, different microdomain structures can be identified.

For $S_{64}I_{36}{}^{78}$ (see Figure 6.1), the block copolymer with the highest polyisoprene fraction, the pattern exhibits four strong reflections at relative spacings 1 : 2 :3 : 4 which can be attributed to a lamellar structure. The strong reflections at 0° indicate an alignment of the lamellae parallel to the electrode surfaces.

A more complex scattering pattern was found for $S_{67}I_{33}{}^{75}$ (see Figure 6.2), exhibiting more reflections as listed in Table 6.1. Three strong reflections at ratios of 1 : 2 : 3 can be identified indicating a layer structure. The azimuthal position at 0° and 90° reveal an alignment both parallel and perpendicular to the electrode surface. In the inner and outer lowest reflections, 6-fold spots are visible. This indicates hexagonal in-layer perforations. Along with the layer structure this pat-

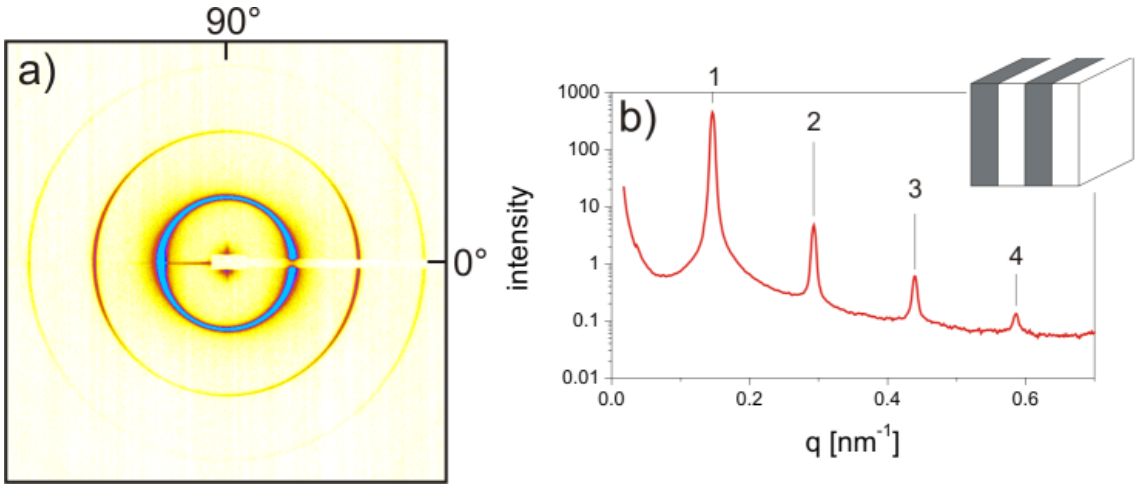

Figure 6.1: *(a) Two-dimensional scattering pattern of a 45 wt. % solution of $S_{64}I_{36}{}^{78}$ in toluene. (b) Scattering profile of this solution. The inset shows the expected lamellar structure according to the observed reflections.*

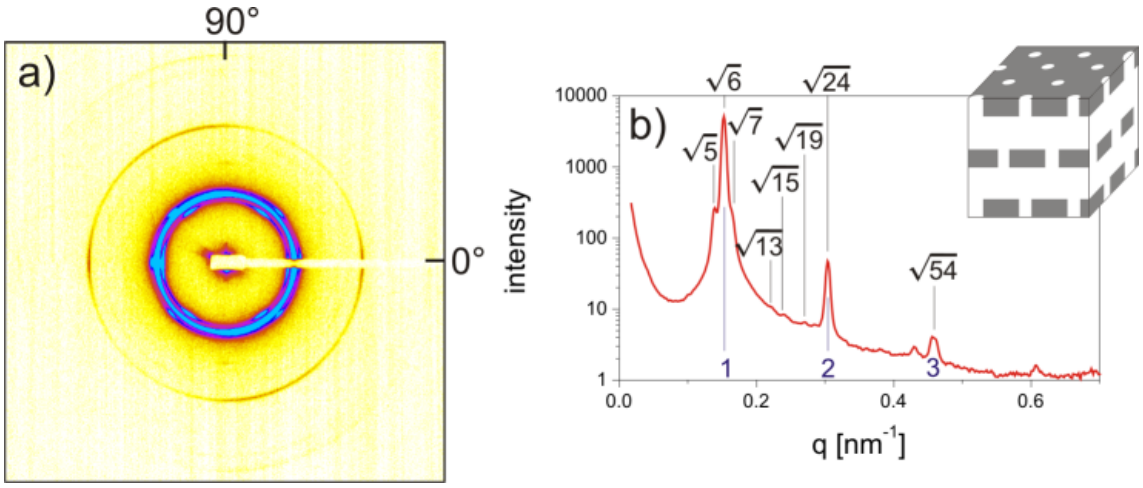

Figure 6.2: *(a) Two-dimensional scattering pattern of a 45 wt. % solution of $S_{67}I_{33}{}^{75}$ in toluene. (b) Scattering profile of this solution. The blue indexed reflections indicate the layer structure while the other indicate the hexagonal perforations. The inset shows the expected hexagonally perforated lamella structure according to the observed reflections.*

tern identifies the microdomain structure as a hexagonally perforated lamellae. The HPL can exhibit possible stacking sequences, i. e. ABAB..., ABCABC... or the combination of the two. Considering the periodicity and the symmetry of these stacking sequences the position in the scattering pattern can be calculated [Ahn00]. Table 6.1 shows the calculated reflections for a ABCABC... stacking. When these are compared with the data for $S_{67}I_{33}$[75] , within the limits of experimental accuracy, good agreement is observed between experimentally measured and claculated pattern. Thus, the perforations of the HPL structure are stacked in the ABCABC... pattern. As mentioned above, the HPL structure is not thermodynamically stable but can be found as an intermediate metastable structure between L and G.

Decreasing of the polyisoprene fraction ($S_{69}I_{31}$[72] , see Figure 6.3) produces a scattering pattern which can be attributed to the G phase. Nine reflections can be detected. The relative positions of these reflections belong to the series $\sqrt{n}q$ where n =3, 4, 7, 10, 11, 12, 19, 21, and 25. This sequence of observed reflections can be indexed as indicated in Table 6.2. The 10-to-1 intensity ratio between the first and

Table 6.1: *Comparison of observed peak positions and azimuthal angles for $S_{67}I_{33}$[75] with those predicted for ABCABC... stacking of a HPL structure [Ahn00].*

predicted			observed	
relative peak position	azimuthal angle ($\pm\varphi°$)	(hkl)	relative peak position	azimuthal angle ($\pm\varphi°$)
$\sqrt{5}$	68.3	(101)	$\sqrt{5}$	54 ± 1
$\sqrt{6}$	0.0	(003)	$\sqrt{6}$	0
$\sqrt{7}$	51.7	(102)	$\sqrt{7}$	43 ± 1
$\sqrt{13}$	90.0	(110)	$\sqrt{13}$	90
$\sqrt{15}$	32.9	(104)	$\sqrt{15}$	*
$\sqrt{18}$	79.1	(201)		
$\sqrt{19}$	55.9	(113)	$\sqrt{19}$	*
$\sqrt{20}$	68.9	(202)		
$\sqrt{24}$	0.0	(006)	$\sqrt{24}$	0
$\sqrt{54}$	0.0	(009)	$\sqrt{54}$	*

* The peak intensity is too weak to found a significant azimuthal angular dependence

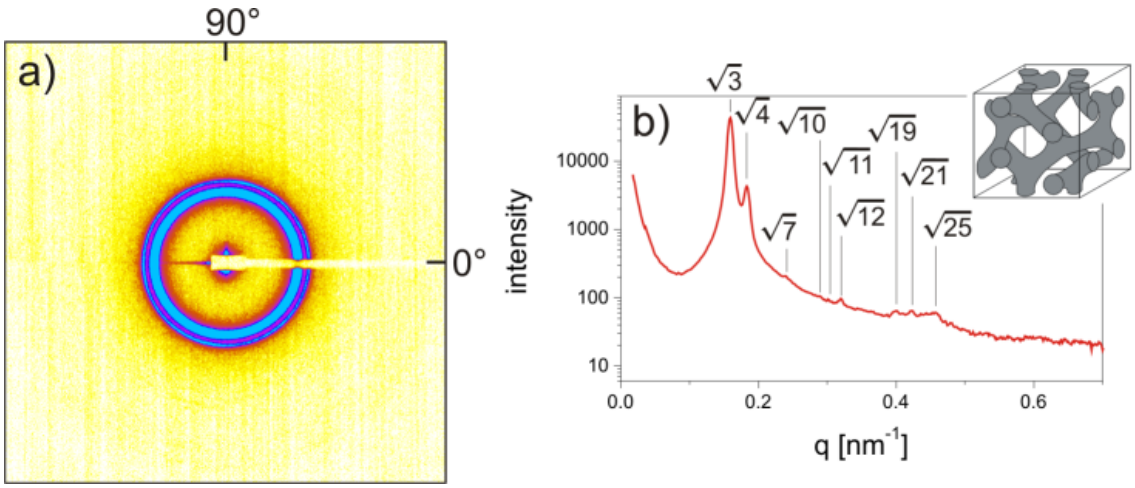

Figure 6.3: *(a) Two-dimensional scattering pattern of a 45 wt. % solution of $S_{69}I_{31}{}^{72}$ in toluene. (b) Scattering profile of this solution. The inset shows the expected gyroid structure according to the observed reflections.*

second peak is consistent with that calculated and observed for the bicontinuous $Ia\bar{3}d$ morphology [Luz67].

With further decrease of the polyisoprene fraction ($S_{72}I_{28}{}^{69}$, see Figure 6.4) the scattering pattern shows reflections at ratios of $1:\sqrt{3}:2:\sqrt{4}$ typical for hexagonally

Table 6.2: *Comparison of observed peak positions for $S_{69}I_{31}{}^{72}$ with those predicted for a gyroid structure [För94].*

predicted		observed	predicted		observed
relative peak position	(hkl)	relative peak position	relative peak position	(hkl)	relative peak position
$\sqrt{3}$	(211)	$\sqrt{3}$	$\sqrt{15}$	(521)	
$\sqrt{4}$	(220)	$\sqrt{4}$	$\sqrt{16}$	(440)	
$\sqrt{7}$	(321)	$\sqrt{7}$	$\sqrt{19}$	(611)	$\sqrt{19}$
$\sqrt{8}$	(400)		$\sqrt{20}$	(620)	
$\sqrt{10}$	(420)	$\sqrt{10}$	$\sqrt{21}$	(541)	$\sqrt{21}$
$\sqrt{11}$	(332)	$\sqrt{11}$	$\sqrt{23}$	(631)	
$\sqrt{12}$	(422)	$\sqrt{12}$	$\sqrt{24}$	(444)	
$\sqrt{13}$	(431)		$\sqrt{25}$	(543)	$\sqrt{25}$

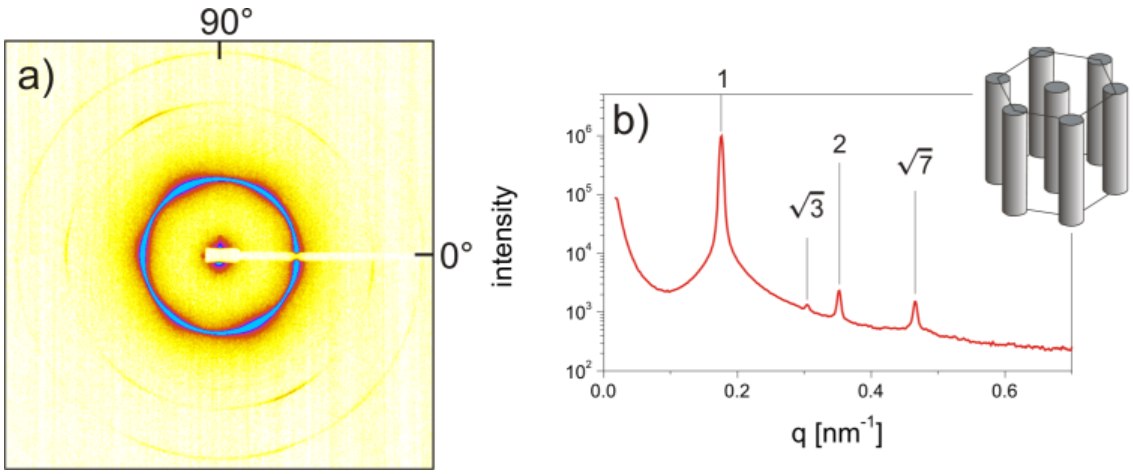

Figure 6.4: *(a)Two-dimensional scattering pattern of a 45 wt. % solution of $S_{72}I_{28}$[69] in toluene. (b) Scattering profile of this solution. The inset shows the expected cylindrical structure according to the observed reflections.*

arranged cylinders. The 6-fold spots indicate that the cylinders are aligned in the direction of the x-ray beam. For the $S_{76}I_{24}$[76] system also a cylindrical structure was identified.

6.3.2 Alignment of Lamellae

The mechanism of electric field induced alignment of lamellar forming block copolymer solutions is well documented by Böker *et al.* [Bök02b, Bök03b]. The alignment of the lamellar $S_{64}I_{36}$[78] system proceeds via the *nucleation and growth* mechanism as expected for a weakly segregated polymer solution. In Figure 6.5 a the evolution of the azimuthal angular dependence of the first order Bragg peak is shown. As soon as an electric field of 1 kV/mm is applied the scattering pattern changes significantly. The peak maxima at $\varphi = 0°$ and 180° decrease, and new maxima at $\varphi = 90°$ and 270° grow with time. This behavior can be explained by the creation of nucleation centers due to undulations of the lamellar structure. These nucleation centers are oriented parallel to the electric field and they grow in the direction of the electric field at the expense of lamellae aligned perpendicular to the field. However, a microdomain structure other than lamellae, i. e. an order-order-transition, was not observed during the course of the experiment. In Figure 6.5 b the evolution of the scattering profile during the alignment process is shown. Clearly, no transient structure occurs during the reorientation. This holds even true if the electric field strength is increased.

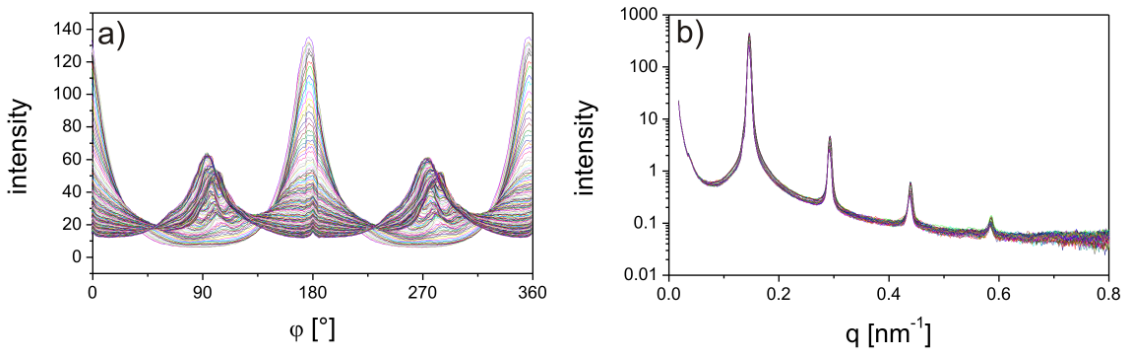

Figure 6.5: *(a) Evolution of the azimuthal angular dependence of the first order Bragg peak during electric field alignment ($E = 1\ kV/mm$) for a 45 wt. % solution of $S_{64}I_{36}$[78] in toluene. (b) Scattering profile of this solution.*

6.3.3 Effect of the Electric Field on the HPL Phase

In the case of the hexagonally perforated lamellar structure of $S_{67}I_{33}$[75] no alignment could be achieved for electric field strengths below 3 kV/mm. As soon as an electric field of 3 kV/mm is applied the lamellae reorient in the electric field direction via the *rotation* mechanism. For this mechanism the reorientation proceeds by the movement of defects. In Figure 6.6 a the evolution of the azimuthal angular dependence of the first order Bragg peak of the layer structure is shown. A distinctly different behavior compared to the lamellar system is found. The initial peaks continuously shift from their original positions at $\varphi = 0°$ and 180° to their final positions at

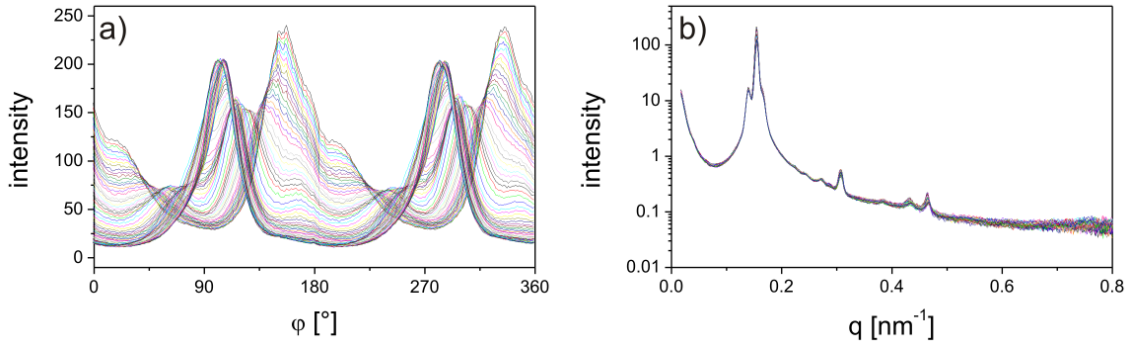

Figure 6.6: *(a) Evolution of the azimuthal angular dependence of the second order Bragg peak, i. e. the first order peak of the layer structure, during electric field alignment ($E = 3\ kV/mm$) for a 45 wt. % solution of $S_{67}I_{33}$[75] in toluene. (b) Scattering profile of this solution.*

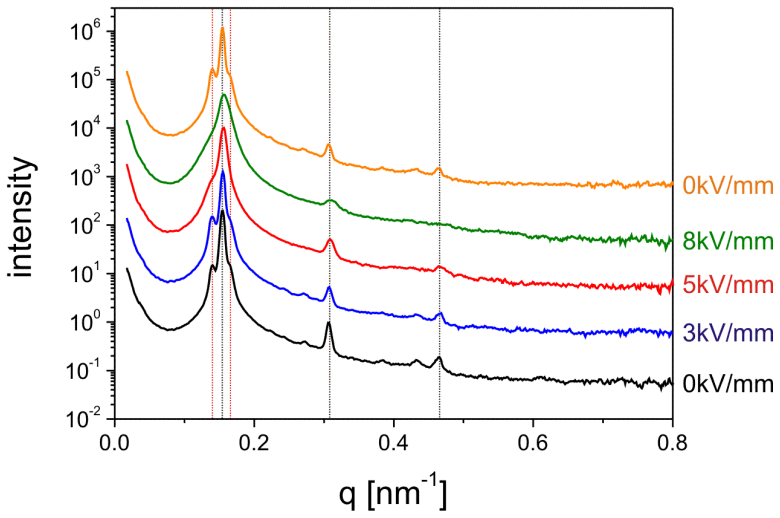

Figure 6.7: *Scattering profiles for a 45 wt. % solution of $S_{67}I_{33}^{75}$ in toluene for (black) E=0 kV/mm, (blue) E=3 kV/mm, (red) E=5 kV/mm, (green) E=8 kV/mm, and (orange) E=0 kV/mm. The black dashed lines point to the Bragg peaks attributed to the layer structure while the red dashed lines indicate the first two peaks arise from the perforations.*

φ = 90° and 270°, respectively. One may conclude from this behavior that the energy penalty for undulations in a hexagonally perforated lamellae is higher as for lamellar structures. Therefore, higher electric field strengths are required to reorient the structure and the alignment proceeds rather via the movement of defects than by the creation of nucleation centers due to undulations. As can be seen from the evolution of the scattering profile during the reorientation process (Figure 6.6 b) the HPL structure remains intact during the alignment process.

If the electric field strength is increased to 4-5 kV/mm the typical reflections of the perforations start to vanish and finally disappear with further increase to 7-8 kV/mm whereas the reflections of the layer structures remain unchanged. Figure 6.7 illustrates the evolution of the scattering profile depending on the electric field strength. As soon as the electric field is switched off the characteristic perforation peaks start to grow again (see Figure 6.8).

This behavior indicates an order-order-transition from hexagonally perforated lamellae to lamellae under the influence of an electric field. As mentioned above there is an electrostatic energy penalty when the electric field lines cross the dielectric interfaces causing the reorientation of the microdomain structure. The HPL phase can decrease this penalty to some extent by reorientation of the lamellar lay-

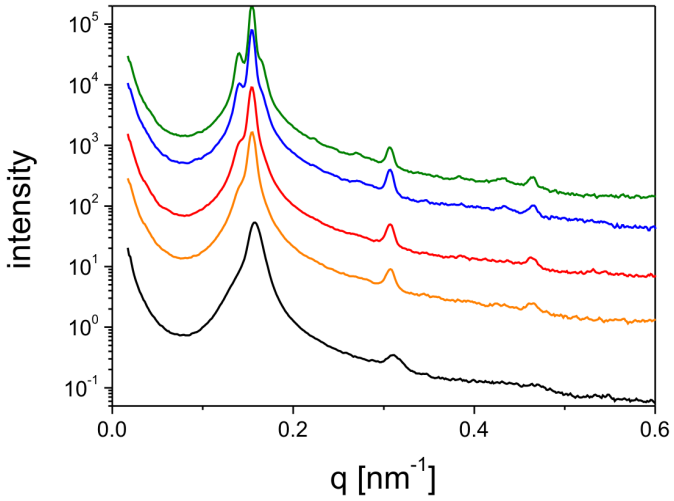

Figure 6.8: *Time evolution of the scattering profile for a 45 wt. % solution of $S_{67}I_{33}$[75] in toluene when the electric field is switched off after (black) 0 s, (orange) 5 s, (red) 15 s, (blue) 95 s, and (green) 285 s.*

ers in the field direction. However, even when all lamellar layers are aligned parallel to the field lines, the interface of the perforations is still aligned perpendicular to the field. With increasing electric field strength the energy penalty also increases resulting in a distortion of the HPL phase leading to a higher free energy of this phase. At some point the free energy of the L phase is lower and a phase transition to the L phase occurs. If the electric field is decreased the energy penalty decreases and the free energy of the HPL phase becomes again lower than the free energy of the L phase for this block copolymer composition. Thus, a phase transition from L→HPL occurs without field.

6.3.4 Effect of the Electric Field on the Gyroid Phase

The electrostatic energy penalty associated with the dielectric interfaces which are oriented perpendicular to the electric field lines cannot be eliminated in cubic phases, such as the gyroid phase. The energy penalty can only be reduced by distorting the phase but still there are interfaces which are crossed by the field lines. The structure will be elongated until the electrostatic forces overcome the elastic forces and a phase transition will occur [Tso06].

In Figure 6.9 the scattering profile for the gyroid phase of $S_{69}I_{31}$[72] depending on the applied electric field strength is shown. Until an electric field strength of

5 kV/mm the scattering pattern does not change. At a field strength of 6 kV/mm the characteristic gyroid reflections slight shift to lower q-values and at a field strength of 7 kV/mm a new reflection appears in the inner circle of the first order Bragg peak which may indicate a HPL structure as has been observed by Imai *et al.* [Ima01, Ima05]. With further increase of the electric field strength to 9 kV/mm the inner and outer reflections of the first order Bragg peak start to vanish and at a field

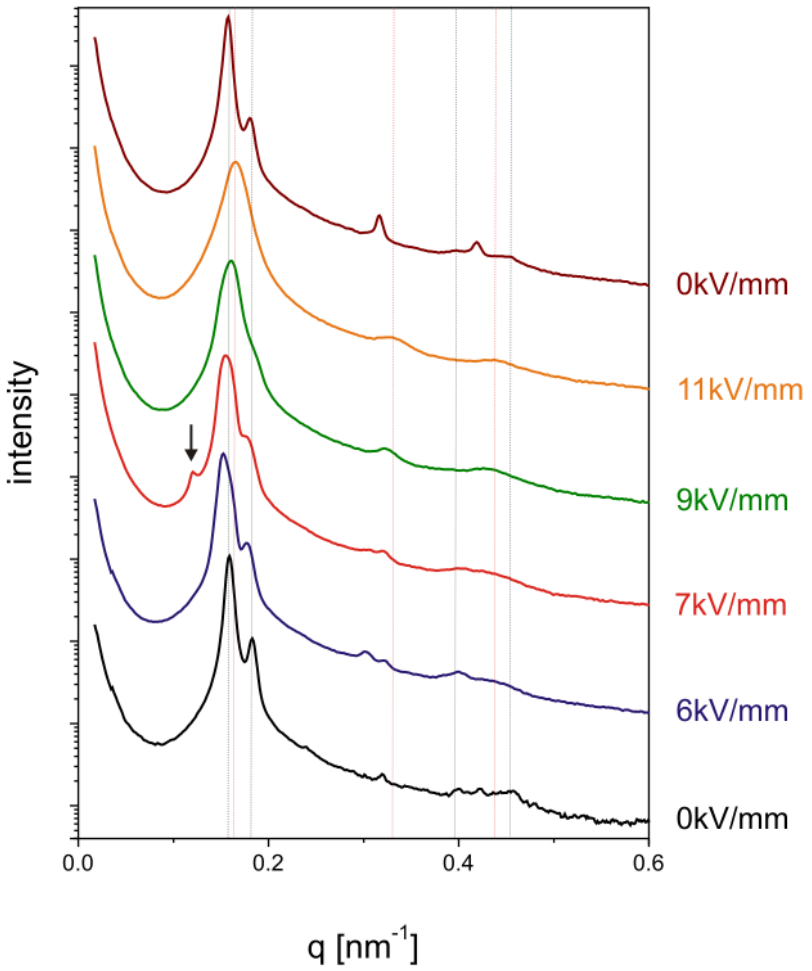

Figure 6.9: *Scattering profile for a 45 wt. % solution of $S_{69}I_{31}{}^{72}$ in toluene for (black) E=0 kV/mm, (blue) E=6 kV/mm, (red) E=7 kV/mm, (green) E=9 kV/mm, (orange) E=11 kV/mm, and (brown) E=0 kV/mm. The black dashed lines point to the Bragg peaks typical for the gyroid phase ($\sqrt{3}:\sqrt{4}:\sqrt{19}:\sqrt{25}$), the red dashed lines indicate the cylindrical structure with peak ratios of $1:2:\sqrt{7}$ and the arrow indicate the peak attributed to the transient HPL structure [Ima01, Ima05].*

strength of 11 kV/mm only peaks in the ratio of $1:2:\sqrt{7}$ can be identified which are characteristic for a cylindrical structure. Once the field is switched off, the original gyroid peaks appear again. During this transition no further transient peaks, i. e. transient structures, were observed.

For the gyroid phase it is not possible to reduce the electrostatic energy penalty by reorientation. If the electric field strength is high enough the gyroid phase undergoes a phase transition to the cylindrical phase which can be aligned parallel to the field lines and thus decrease the electrostatic energy. Matsen proposed that the temperature induced G→C transition is initiated by the formation of a 5-fold junction from one 3-fold junction of the gyroid phase. Next its original three connections rupture leaving a cylindrical unit connecting two distant 4-fold junctions. These transform into 5-fold junctions, and then their original connections break increasing the length of the cylinder. Repeating this process causes the lattice of G to unzip into cylinders [Mat98]. The G→C transition under an electric field was investigated by Zvelindovsky *et al.* using the dynamical self-consistent field theory (SCFT) [Lya06b, Ly07]. The same pathway as proposed by Matsen was found. On the other hand, the HPL phase is a common transient structure in the pathway of G→L transition and was also observed experimentally in the C→G transition [Ham04, Wan02, Ima01]. The HPL phase consists of planar tripods and can be generated from the G phase by rotating the dihedral angle of the connecting tripods [För94, Zhu03]. According to the observed scattering profiles one may conclude that in this case the G→C transition under an electric field proceeds via the HPL structure.

If the electric field is decreased the free energy of the gyroid phase becomes again lower than the free energy of the cylindrical phase. Thus, a C→G transition occurs. In this case a transient HPL phase could not be detected. For the C→G transition Matsen proposed the formation of one 5-fold junction connecting four neighboring cylinders, which pinches off, breaking the center cylinder and leaving the 3-fold junction required by the gyroid structure. The two free ends of the broken cylinder are highly unfavorable and should quickly form two 4-fold junctions. Again the 4-fold junction breaks off and produces a 3-fold junction as well as a free end. The formation and disruption of 4-fold junctions continues and hence the gyroid structure grows along the cylinder direction [Mat98]. Figure 6.10 illustrates the proposed mechanism. Clearly, this mechanism is favored in the case of aligned cylinder. In the investigated transition here, the cylinders are strongly aligned due

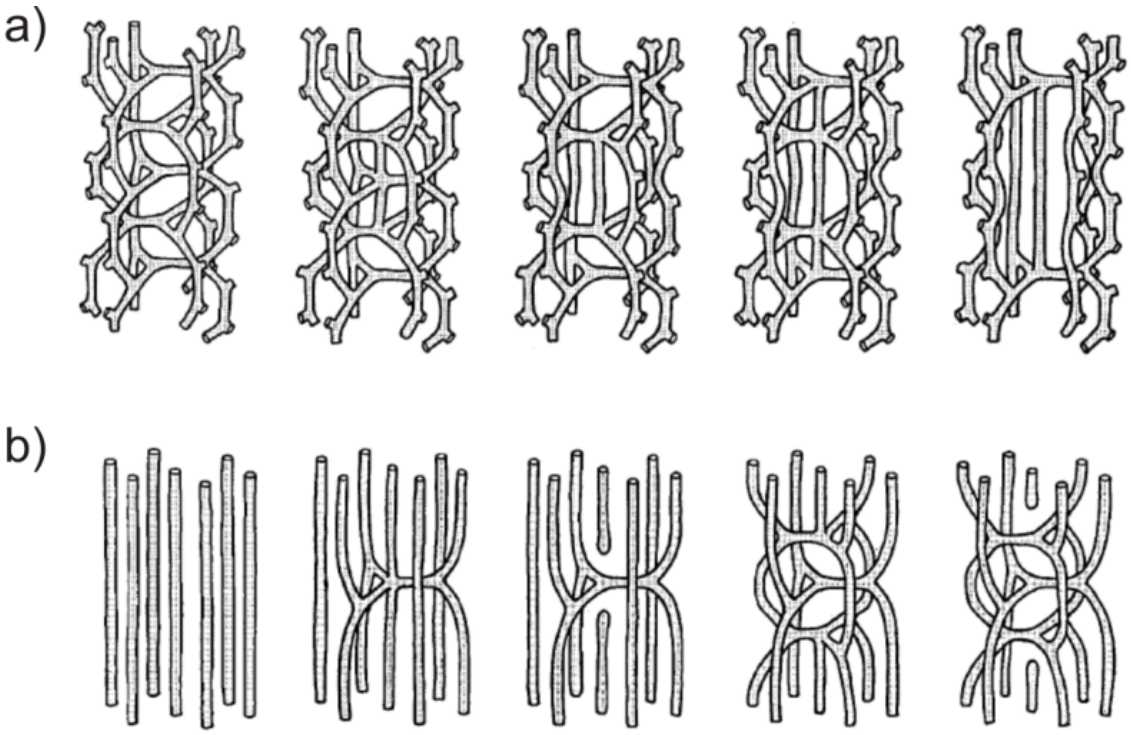

Figure 6.10: *Schematic illustration of the (a) G→C and (b) C→G transition as proposed by Matsen [Mat98].*

to the applied electric field ($P_2 = -0.29$) and therefore the C→G transition may proceed rather by the mechanism proposed by Matsen than via the HPL transient structure.

6.3.5 Alignment of Cylinders

Since the cylindrical structure is an anisotropic structure it can be aligned by an electric field. In Figure 6.11 a typical evolution of the scattering pattern and the azimuthal angular dependence of the first order Bragg peak is shown for the alignment of $S_{76}I_{24}$[76] with an electric field of $E = 2$ kV/mm. The cylinders rotate from the initial orientation parallel to the electrodes, i. e. perpendicular to the electric field lines (signals at $\varphi = 0°$ and 180°) to the orientation parallel to the electric field vector (signals at $\varphi = 90°$ and 270°). In contrast to the lamellar system, this is not a cooperative process where the dielectric bodies rotate along a common direction. The cylinders seem to break up and one fraction rotates clockwise and the other one counterclockwise. The cylindrical structure remains intact during the reorientation and a transient structure is not observed.

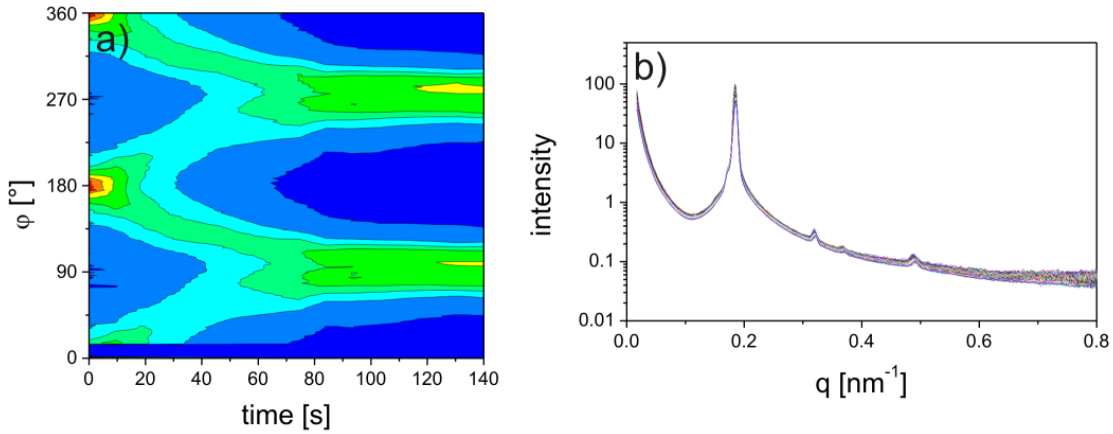

Figure 6.11: *(a) Evolution of the azimuthal angular dependence of the first order Bragg peak during electric field alignment ($E = 2\ kV/mm$) for a 45 wt. % solution of $S_{76}I_{24}$[76] in toluene. (b) Scattering profile of this solution.*

Mostly, even for higher electric field strengths the scattering pattern remains unchanged but in some cases of the cylinder reorientation a new peak in the inner circle of the first order Bragg peak grows with higher electric field strengths. Figure 6.12 shows the scattering profile for the reorientation of $S_{76}I_{24}$[76] depending on the electric field strength. Clearly, at field strengths of $E = 3\,\mathrm{kV/mm}$ a new reflection appears and vanishes again at field strengths of $E = 5\,\mathrm{kV/mm}$. This behavior may be explained by an insufficient alignment of the cylinders via the *rotation* mechanism. Most of the cylinders are rotating in the final orientation. If there are some small grains with perpendicular aligned cylinders remaining, they are trapped in this orientation. For higher electric field strengths the electrostatic energy increases for these cylinders and the reorientation may proceed via a transient state. One may identify this transient state again as a HPL phase since the additional peak can be indexed for a HPL structure as described by Imai *et al.* [Ima01, Ima05]. Indeed, a lower degree of alignment ($P_2 > -0.20$) after the application of a moderate electric field strength ($E = 1-2\,\mathrm{kV/mm}$) can be found for systems exhibiting this transient structure. With increasing electric field strength a transient structure can be found and the systems achieve a higher degree of alignment ($P_2 \approx -0.3$). For systems achieving a high degree of alignment ($P_2 < -0.30$) after the application of moderate field strengths, a transient structure cannot be observed during the course of the experiment.

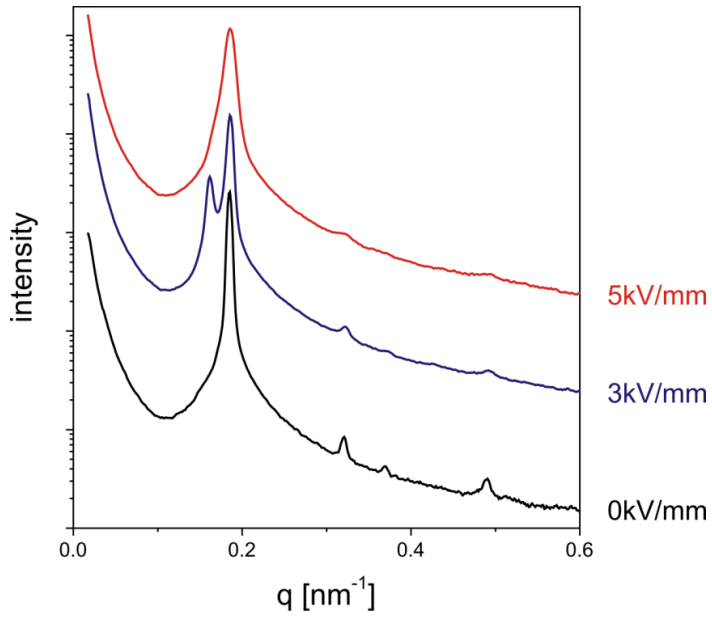

Figure 6.12: *Scattering profile for a 45 wt. % solution of $S_{76}I_{24}{}^{76}$ in toluene for (black) E=0 kV/mm, (blue) E=3 kV/mm, and (red) E=5 kV/mm.*

6.4 Conclusion

In summary, different order-order transitions in block copolymers of various compositions induced by an electric field were found. Order-order-transitions were identified for microdomain structures which cannot be aligned in the electric field direction in such a way that all dielectric interfaces are parallel to the field lines. Thus, the electrostatic energy penalty increases with increasing electric field strength until the free energy of aligned lamellae and cylinders is lower than the original structures, respectively. In the case of the metastable hexagonally perforated lamellae the layers can be aligned in the field direction but not the perforation. Here, a transition to the lamellar phase was observed. Since the gyroid phase is a cubic phase it cannot be aligned at all and thus a transition to the cylinder phase occurs in order to eliminate the electrostatic energy penalty. This transition proceeds via a HPL phase in the direction from G→C and via 3-, 4- and 5-fold reconnections of cylinders to form a bicontinous network from C→G.

In the case of cylindrical microstructures the energy penalty can be eliminated by reorientation of the cylinders in the electric field direction. Most of the cylinders are rotating directly in the corresponding direction. But if there are cylinders trapped perpendicular to the field the reorientation proceeds via a transient state.

Electric Field Induced Changes in the Periodicity of Block Copolymer Microdomains

Block copolymers self-assemble into microphase separated domains yielding highly regular structures with length scales of the order of several tens of nanometers. However, the characteristic size of the resulting structures is usually determined by molecular parameters of the constituent polymer molecules and cannot easily be adjusted on demand. Here, the influence of an electric field on the characteristic domain spacing of block copolymer microdomains was investigated. A change of the domain spacing by as much as six percent depending on the electric field strength was found. This change is fully reversible and proceeds on a time scale of several milliseconds. The influence of the electric field strength on several block copolymers with lamellar and cylindrical microstructure is discussed. Furthermore, the dependence on the phase separation, on the polarity of the solvent, on the composition and on the existence of ions was studied. A tentative explanation of the observed effect is given based on the anisotropic polarizabilities of the monomeric constituents.

7.1 Introduction

In the past, electric fields have successfully been used to achieve long-ranged order in block copolymer nanostructures (see section 1.2.2). For many potential applications, however, the dimensions of the nanostructures need to be tuned precisely as well. Therefore tools for the systematic variation of the characteristic spacing of the nanostructures in a predictable and simple manner are indispensable. For microphase separated copolymers, tuning of the morphology and size of the nanoscopic patterns formed is typically achieved by changing the molecular weights or the block ratio of the polymers used. However, this approach only allows control of the characteristic spacing on coarse scales, while precise adjustment of the spacing is impossible. The addition of a homopolymer corresponding to one or both of the polymer blocks or the addition of a non-selective solvent has successfully been used

to fine-tune block copolymer nanostructures [Win91b, Win91a, Tan91]. However, an exact adjustment to within a percent of the characteristic spacing seems barely possible. Moreover, this approach is not reversible.

The equilibrium domain spacing results from a competition between entropic and enthalpic contributions to the free energy. The former accounts for the entropic losses due to stretching or compression of the polymer chains and the latter for the interfacial energy (for details see section 1.1). Gurovich has developed a microscopic self-consistent mean-field theory of copolymer melts in an electric field (see section 1.2.1 and [Gur94b, Gur94a, Gur95]). He predicts changes of the characteristic spacings due to anisotropic deformation of the chain conformation resulting in an effective composition ϕ^* which is different from the actual chemical composition ϕ.

In the following, first experimental results strongly supporting the theoretical predictions outlined above are presented. The reversible tuning of the block copolymer microdomain spacing over a relative range of 6 percent without changing the molecular weight or the block ratio, and without chemically modifying the polymer or including any additives is shown. The effect on a lamellar polystyrene-*b*-polyisoprene diblock copolymer was studied in detail. A significant decrease (slight increase) of the lamellar distance was found for lamellae oriented along (perpendicular to) the electric field direction. The influence of the effective segregation power, the overall molecular weight, the chemical composition, the polarity of the solvent and the effect of ions was investigated. Furthermore, the kinetics of the lamellar deformation and the relaxation process was monitored. Moreover, the effect was also found for cylindrical polystyrene-*b*-polyisoprene diblock copolymers as well as for methacrylate based system. For polystyrene-*b*-poly(2-vinylpyridine) a different behavior was found indicating an effect of the electric field on the Flory-Huggins parameter for the respective system.

7.2 Materials

For the detailed study five different lamella forming PS-*b*-PI diblock copolymers, $S_{46}I_{54}{}^{108}$, $S_{50}I_{50}{}^{100}$, $S_{55}I_{45}{}^{51}$, $S_{58}I_{42}{}^{48}$, and $S_{64}I_{36}{}^{47}$, with compositions varying from $\phi_S = 43$ % to 61 % and molecular weights between $M_n = 47$ kg/mol and 108 kg/mol were investigated. The polymers were dissolved in toluene or tetrahydrofurane (THF) with concentrations ranging from 50 to 57 wt. %. In order to study a possible effect of ions, LiCl was dissolved in THF which was then used to

prepare polymer solutions resulting in an ion content of 7600 ppm. Moreover the effect on a cylinder forming PS-*b*-PI diblock copolymer, $S_{75}I_{25}{}^{66}$, lamella forming methacrylate based systems, $S_{46}H_4M_{50}{}^{134}$ and $S_{49}M_{51}{}^{100}$, and a lamella forming PS-*b*-PVP diblock copolymer, $S_{54}V_{46}{}^{99}$, dissolved in toluene or THF, respectively, was investigated. Details about the polymer systems can be found in Table 3.1.

All experiments were performed at room temperature in a capacitor with an electrode spacing of 1 mm. In order to exclude effects which may arise from the reorientation process itself, all samples were prealigned in an electric field of 2 kV/mm until the orientational order parameter was constant. Due to this prealignment, most of the microstructures are oriented along the electric field lines. In order to study the effect of different field strengths, a DC voltage up to 13 kV/mm was kept constant for 5 minutes before taking the data to ensure that the block copolymer solution is in its equilibrium state. For the static measurements the highest lateral resolution (2048 x 2048 pixels) of the CCD detector was chosen. For the kinetic studies the highest time resolution, i. e. the lowest lateral resolution (1024 x 256 pixels) was taken allowing a readout rate of 20 frames per second. To determine the exact peak position for the microstructure oriented along the field lines and for the microstructure oriented perpendicular to the field, the corrected two-dimensional SAXS data were averaged over a 30° opening angle in horizontal and vertical direction as described in section 3.4.

7.3 Results and Discussion

7.3.1 Effect of an Electric Field on the Polymer Chains

For the first investigation of the general effect of an electric field on the microphase separation a 50 wt % solution of $S_{55}I_{45}{}^{51}$ in THF was studied. A strongly anisotropic scattering pattern as shown in Figure 7.1 is observed for high electric fields. The position of the first order Bragg peak is different for lamellae which are aligned in the field direction and those which are aligned perpendicular to the field direction.

Figure 7.2 shows the effect of the electric field strength on the lamellar spacing for the lamellae aligned in field direction and the lamellae aligned perpendicular, respectively. The lamellar distance for the lamellae oriented along the field lines decreases rapidly with increasing electric field strength, while the lamellar distance for the lamellae oriented perpendicular to the field only slightly increases. This behavior can be explained by a significant stretching of the polymer chains due

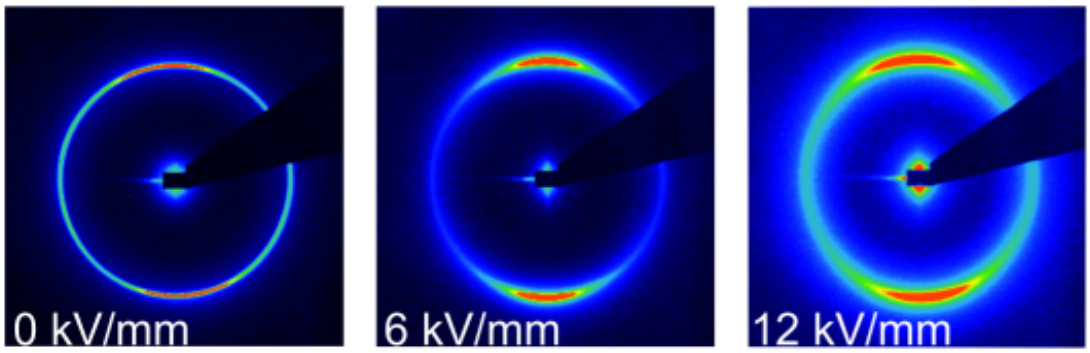

Figure 7.1: *Two-dimensional scattering patterns of a 50 wt. % solution of* $S_{55}I_{45}{}^{51}$ *in THF for different electric field strengths.*

to different polarizabilities of the segments. Due to the benzene side group in the polystyrene, the PS chains will be elongated slightly perpendicular to the field lines, while the PI chains will be stretched significantly parallel to the field lines due to the C=C double bonds in the backbone [Den40].

Microphase separation leads to a stretching of the chains perpendicular to the lamellar interfaces. If such a lamella is aligned parallel to the field direction (Figure 7.3), the following effect is expected: The PI chains are more affected by the

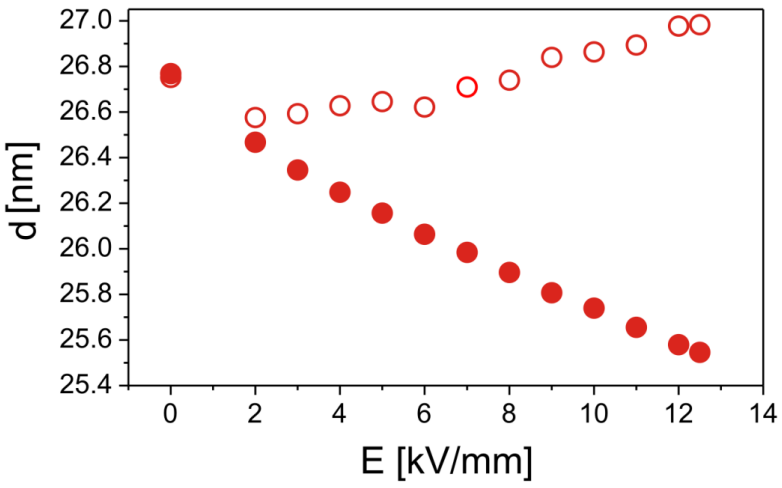

Figure 7.2: *Dependence of the lamellar distance d of (●) parallel and (○) perpendicular to the electric field lines aligned lamellae on the electric field strength for a 50 wt. % solution of* $S_{55}I_{45}{}^{51}$ *in THF.*

electric field than the PS chains because of the higher polarizability of the isoprene monomers. The chains will be stretched along the field direction, i. e. parallel to the phase boundary. Therefore, to some extent, the electric field counteracts the stretching induced by the microphase separation. Thus, the overall conformation of the chains approaches a Gaussian shape and the entropy increases. In consequence, the lamellar distance decreases. On the other hand, if the lamellae are oriented perpendicular to the electric field direction, the chain stretching induced by the electric field acts perpendicular to the lamellar plane and therefore adds to the stretching already induced by the microphase separation. In consequence the lamellar spacing is increasing and the conformational entropy further decreases. Due to the quadratic dependence of the entropic energy on the degree of stretching as explained in section 1.1 this effect is indeed expected to be weaker than in the other direction in agreement with the experimental observation (Figure 7.2).

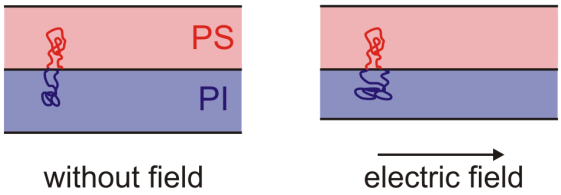

Figure 7.3: *Schematic illustration of the proposed chain stretching effect for aligned lamellae.*

7.3.2 Influence of Different Physical Parameters

In order to assess the influence of several physical parameters the relative change in the lamellar distance was quantified as

$$\Delta d = \frac{d_\perp - d_\parallel}{d_0}$$

where $d_\perp$ and $d_\parallel$ are the lamellar distances of lamellae aligned perpendicular and parallel to the electric field lines, respectively. For all solutions a linear dependence of Δd on the electric field strength was found. However, a different behavior was observed for different degrees of phase separation, different compositions, and different solvents.

Influence of the Degree of Phase Separation

As mentioned in section 1.1.3 a common approach for block copolymer solutions is to adopt the dilution approximation, which states that the phase diagram of a copolymer solution can be obtained from the corresponding melt phase diagram by replacing χ_{AB} with $\phi_P\chi_{AB}$, where ϕ_P is the polymer volume fraction in the solution. Thus, the degree of phase separation can be changed by varying the polymer concentration. Comparing a 50 wt. % $S_{55}I_{45}{}^{51}$ and a 57 wt. % solution of $S_{55}I_{45}{}^{51}$ in THF (Figure 7.4) the chain stretching effect is stronger for systems with a lower concentration, i. e. a lower degree of phase separation. As discussed in section 1.1 the lamellar distance is determined by the balancing of the interfacial energy and the entropic energy. The degree of phase separation only influences the interfacial energy, i. e. a lower degree of phase separation leads to a lower interfacial energy because $\mathcal{F}_{interfacial} \propto \chi_{eff}^{1/2} \propto (\phi_P\chi_{AB})^{1/2}$. Thus the entropic energy has a stronger influence at lower concentrations and the chain stretching effect is more pronounced. Although the degree of polymerization also influences the degree of phase separation, it has no influence on the interfacial energy, because $\mathcal{F}_{interfacial} \propto \sqrt{\chi N}\left(\frac{d}{\sqrt{N}}\right)^{-1} \propto N^0$. Thus, an effect of the molecular weight is not expected.

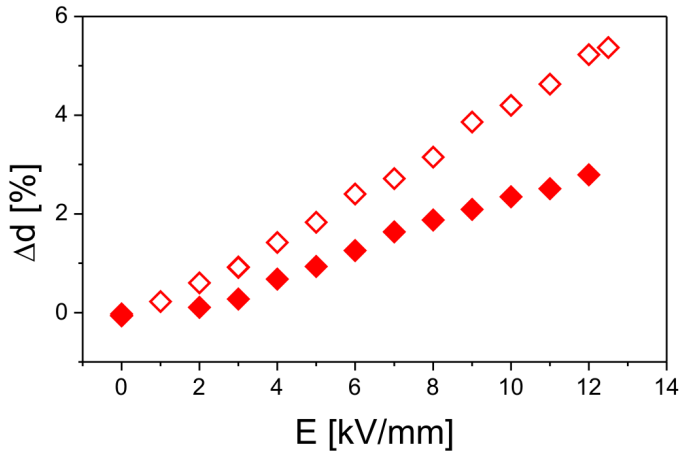

Figure 7.4: *Dependence of the relative change in the lamellar distance Δd on the electric field strength E for a (◊) 50 wt. % and a (♦) 57 wt. % solution of $S_{55}I_{45}{}^{51}$ in THF.*

Influence of the Polarity of the Solvent

Furthermore, an influence of the solvent polarity by comparing the copolymer $S_{55}I_{45}$[51] dissolved in toluene and in THF (see Figure 7.5) was found. The THF solution is more strongly influenced by the electric field than the toluene solution. Both THF and toluene are good, non-selective solvents for PS-*b*-PI, as $\chi_{toluene-PS} = 0.44$, $\chi_{toluene-PI} = 0.40$, $\chi_{THF-PS} = 0.32$, and $\chi_{THF-PI} = 0.40$ [Hua98]. The major difference, however, is that THF ($\varepsilon = 7.8$) is more polar than toluene ($\varepsilon = 2.6$). The electric field induced polarization of the chains is more effectively stabilized by solvation of the monomeric units by the polar THF than the non-polar toluene molecules [Sun99]. As a result, the polarizability of the chains is higher in THF than in toluene. Consequently, the chains are more stretched by the electric field in polar solvents.

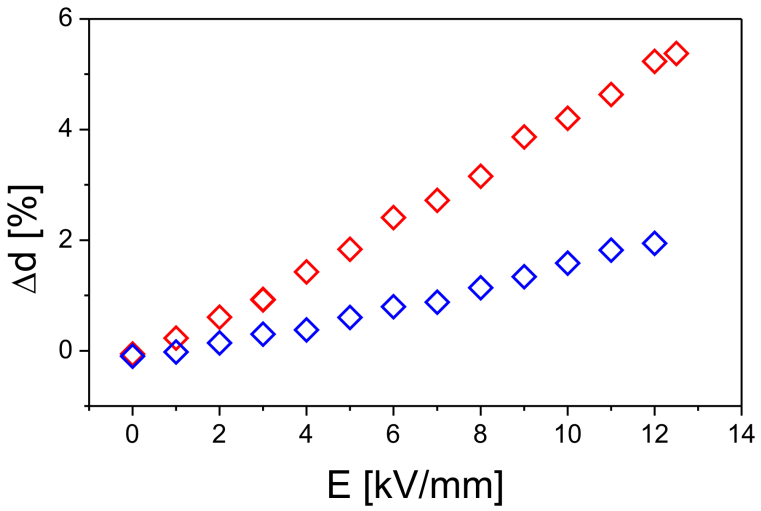

Figure 7.5: *Dependence of the relative change in the lamellar distance Δd on the electric field strength E for a 50 wt. % solution of $S_{55}I_{45}$[51] in (◇) THF and (◇) in toluene.*

Influence of Ions

In this context it is interesting to investigate the influence of ions. Since ions can form complexes with the monomers and thus increase the dielectric constant of the respective block, an increasing chain stretching effect is possible. However, a complexation of the ions with either polystyrene or polyisoprene is not expected. Indeed by comparing an ion free solution of $S_{55}I_{45}$[51] in THF and an ion contaminated solution, no significant difference can be observed (Figure 7.6).

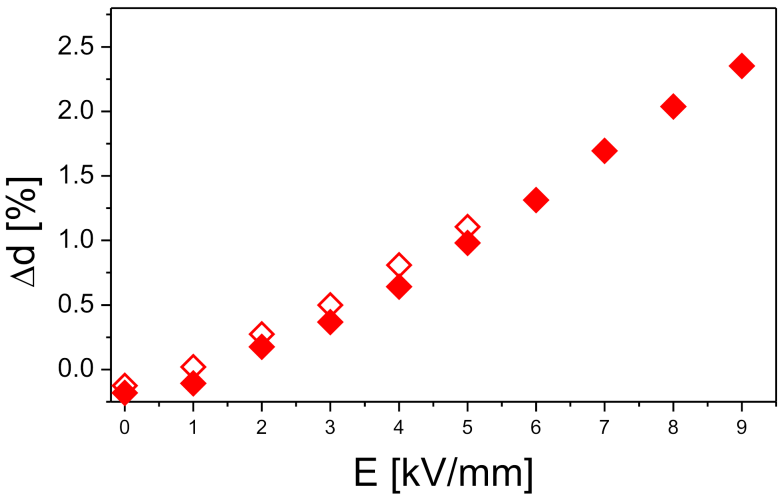

Figure 7.6: *Dependence of the relative change in the lamellar distance Δd on the electric field strength E for a 50 wt. % of $S_{58}I_{42}{}^{48}$ in THF (◊) with and (♦) without ions.*

Influence of Composition

In addition, a significant influence of the block copolymer composition on the magnitude of the chain stretching effect is found. This is illustrated in Figure 7.7, where five different block copolymers with varying PS content (all 50 wt. % solutions in THF) are compared by calculating the slope of the Δd versus E curves. As the composition determines the entropic energy, a symmetric copolymer is expected to exhibit a lower entropic energy than an asymmetric one. Hence, the increase of the entropic energy by electric field induced chain stretching is more efficient for a symmetric copolymer, leading to a more pronounced effect for the symmetric block copolymer in this study ($\phi_{PS} \approx 0.5$).

In summary, a stronger chain stretching effect is found for lower incompatibility, higher symmetry of the block ratio, and higher polarity of the solvent. The molecular weight as well as possible ions have no influence on this effect.

7.3.3 Kinetic Measurements

Since the change in the periodicity of the microdomain structure can be useful with respect to possible technological applications, it is of great interest to quantify the kinetics and the reversibility of this process. Therefore, the time evolution of the lamellar distance upon application of the electric field was followed. In Figure 7.8 a

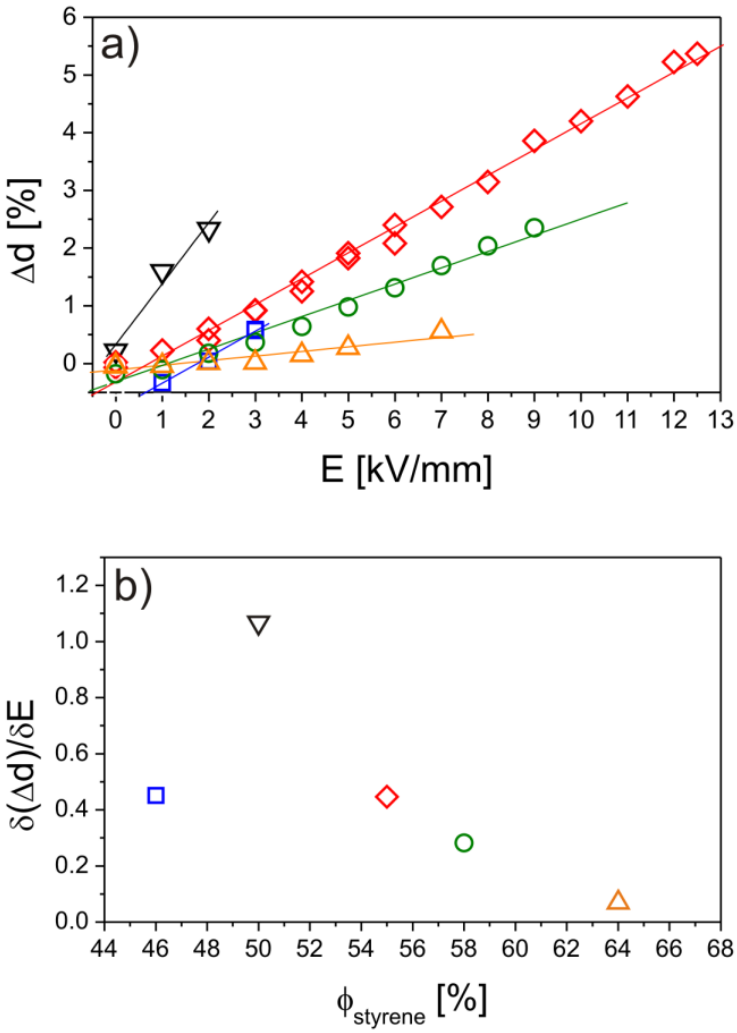

Figure 7.7: *(a) Dependence of the relative change in the lamellar distance* Δd *on the electric field strength E for different block copolymer compositions:* □ $S_{46}I_{54}{}^{108}$, ▽ $S_{50}I_{50}{}^{100}$, ◇ $S_{55}I_{45}{}^{51}$, ○ $S_{58}I_{42}{}^{48}$, *and* △ $S_{64}I_{36}{}^{47}$, *all 50 wt. % solutions in THF. (b) Dependence of the strength of the chain stretching effect* $\frac{\delta\Delta d}{\delta E}$ *on the styrene volume fraction* ϕ_S *for the same solutions.*

the time dependence of the lamellar distance for lamellae oriented in the field direction is shown when the electric field is switched on for a 50 wt. % solution of $S_{55}I_{45}{}^{51}$ in toluene. As soon as the electric field is applied, the copolymer structure responds and the periodicity of the lamellae is decreased immediately. This process is faster than the time resolution of the detector, i. e. the process has a time constant considerably smaller than 45 ms. To assure that the process is reversible, the relaxation of

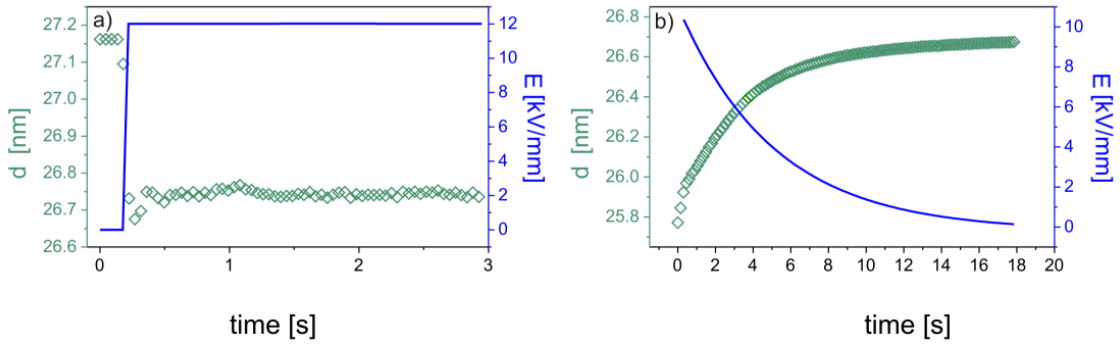

Figure 7.8: *(a) Time dependence of the lamellar distance of aligned lamellae with increasing electric field strength for a 50 wt. % solution of* $S_{55}I_{45}{}^{51}$ *in toluene. (b) Time dependence of the lamellar distance of aligned lamellae with decreasing electric field strength for the same solution.*

the domain spacing after the applied field was switched off was followed. Figure 7.8 b shows the time evolution of the lamellar distance of the aligned lamellae when the field strength is decreased. Due to the high voltage applied, it takes several seconds for the capacitor to unload. The domain size closely follows the decreasing electric field strength.

7.3.4 Influence on a Cylindrical Block Copolymer

If a cylinder forming system is considered, the same effect as found for lamellae is observed. For cylinders lying in the field direction the distance between the cylinders is strongly decreasing whereas the distance for cylinders aligned perpendicular to the electric field is slightly increasing on application of an electric field. This behavior as well as the difference in the cylinder distance ΔL is illustrated in Figure 7.9. This effect can be explained again by a stretching of the polymer chains. In this case the cylinder forming component is polyisoprene embedded in a matrix of polystyrene. The PI chains will be stretched parallel to the field lines, i. e. the cylinders lying in the field direction become thinner while the matrix does not change because of the low polarizability of the PS chains. Since the PI chains are covalently attached to the PS chains not only the cylinder diameter is decreasing but also the distance between the cylinders. The influence of the physical parameters described above is expected to be the same as in the lamellar case and was not investigated.

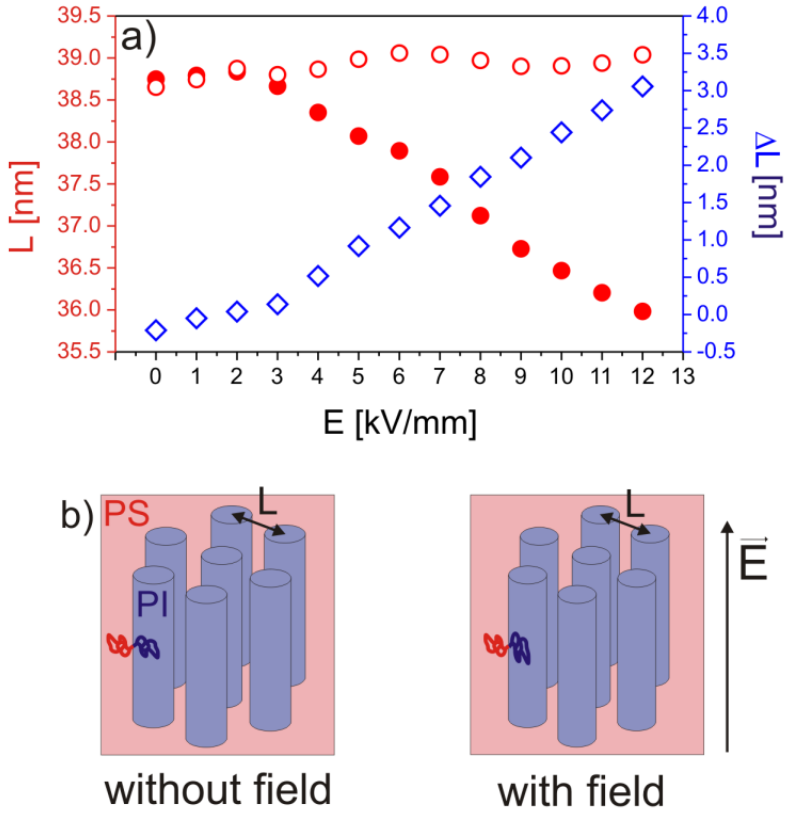

Figure 7.9: *(a) Dependence of the cylinder distance L of aligned (●) and non-aligned (○) cylinders and of the difference (◇) $\Delta L = L_{\perp} - L_{\parallel}$ on the electric field strength for a 45 wt. % solution of $S_{75}I_{25}$[66] dissolved in toluene. (b) Sketch of the chain stretching effect for aligned cylinders.*

7.3.5 Methacrylate Based Systems

In order to investigate the effect on methacrylate based polymer systems two lamella forming diblock copolymers, $S_{46}H_4M_{50}$[134] and $S_{49}M_{51}$[100] were studied. As mentioned in chapter 5 the inclusion of the polar PHEMA middle block leads to an increased incompatibility and thereby to a lower order-disorder concentration. The solutions studied here were both slightly above the order-disorder concentration. After applying the electric field again a decrease in the lamellar spacing of the in field aligned lamellae is found for both systems while the lamellar distance for the lamellae aligned perpendicular to the field does not change significantly (see Figure 7.10). This behavior can be explained by a stretching of the PMMA chain due to different polarizabilities of the backbone and the methyl methacrylate side chain.

By comparison of the $S_{46}H_4M_{50}$[134] and $S_{49}M_{51}$[100] solutions a stronger response of

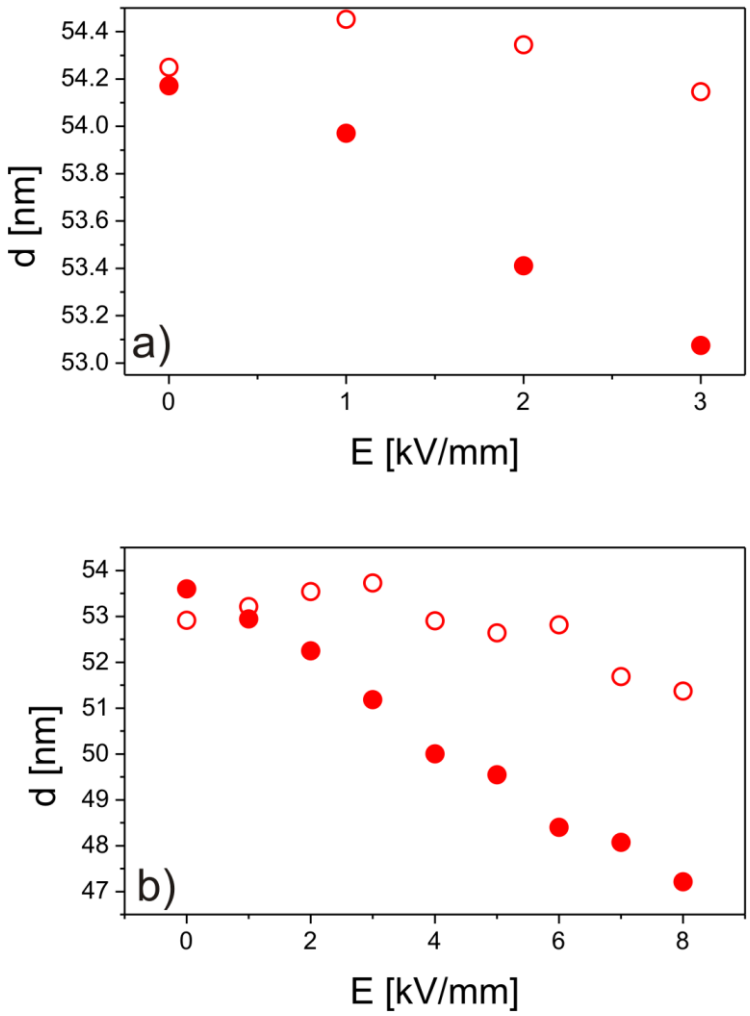

Figure 7.10: *Dependence of the lamellar distance d of parallel (●) and perpendicular to the field lines aligned (○) lamellae on the electric field strength for a (a) 40 wt. % solution of* $S_{46}H_4M_{50}{}^{134}$ *and a (b) 55 wt. % solution of* $S_{49}M_{51}{}^{100}$ *in THF.*

the PS-*b*-PMMA system on the electric field is observed. The chain stretching effect depends also on the Flory-Huggins parameter χ_{AB}. this parameter only influences the interfacial energy, i. e. a lower χ_{AB} parameter leads to a lower interfacial energy. Thus, the entropic energy has a stronger influence and the chain stretching effect is more pronounced for lower χ_{AB} ($\chi_{SHM} > \chi_{SM}$).

7.3.6 Effect on PS-b-PVP

A different effect of the electric field on the characteristic microdomain spacing is observed in the case of the lamellar polystyrene-*b*-poly(2-vinyl pyridine). As illustrated in Figure 7.11 both the lamellar distance of lamellae aligned in field direction and those aligned perpendicular to the field decrease. This behavior cannot be explained by a stretching effect of the polymer chain in the electric field direction since both orientations show the same behavior. Due to the high χ_{AB} parameter for PS-*b*-PVP only a weak chain stretching effect is expected.

The lamellar distance results of a balance between the entropic and enthalpic energy. Since the electric field has no or only a weak effect on the entropic energy in this case it seems that the electric field influences the enthalpic energy, i. e. the interfacial energy between the two blocks. The observed behavior indicates a decrease of the interaction parameter χ_{AB} between polystyrene and poly(2-vinyl pyridine) due to the electric field which may lead to a phase transition of the diblock in the disorder regime with further increase of the electric field. This effect on the interaction parameter can also occur in the other polymer systems but it may be superposed due to the chain stretching effect.

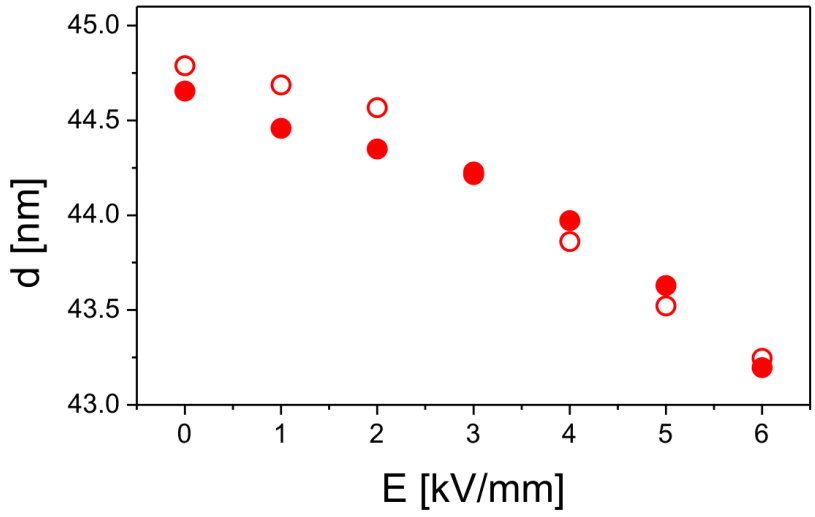

Figure 7.11: *Dependence of the lamellar distance d of parallel (●) and perpendicular to the field lines aligned (○) lamellae on the electric field strength for a 40 wt. % solution of* $S_{54}V_{46}{}^{99}$ *in THF.*

7.4 Conclusion

In summary, a strong response of the characteristic spacing of the lamellar and cylindrical structure of block copolymer solutions exposed to an external electric field was found. If one block has different polarizabilities along the backbone and along the side chain the following effect is observed: When the lamellae are aligned in the field direction, the lamellar distance decreases with increasing electric field strength. On the other hand, the lamellae which are oriented perpendicular to the field show a slightly increasing domain spacing. This behavior can be explained by a chain stretching effect due to coupling of the induced monomeric dipoles to the electric field. The change in the periodicity becomes more pronounced with increasing electric field strength, decreasing segregation power, increasing symmetry of the block ratio, and increasing polarity of the solvent. Furthermore, the observed effect is fully reversible and exhibits an extremely fast kinetics, which makes it a very promising candidate in view of possible applications in switchable nanostructures.

Summary

The influence of external electric fields on the microdomain structure of block copolymers has been studied. The results range from an analysis of the mechanism and kinetics of the reorientation process, via the discussion of the driving force, to first investigations on the influence of an electric field on the phase behavior. The electric field induced effects on concentrated block copolymer solutions were investigated by *in-situ* synchrotron small-angle x-ray scattering.

The first part concerns the analysis of the mechanism and kinetics of the alignment of lamellar forming diblock copolymer solutions as well as a quantitative study of the reorientation kinetics of various block copolymers in order to clarify the driving force of reorientation in a DC electric field.

It is shown that both the reorientation pathway and kinetics strongly depend on the degree of order present prior to the application of the electric field. In a highly ordered system with the lamellae being aligned perpendicular to the electric field vector, only *nucleation and growth* is possible as a pathway and the process is rather slow. In less ordered samples *grain rotation* becomes possible as an alternative pathway and the reorientation is considerably faster. For intermediate degrees of order, where the reorientation proceeds via both mechanisms, it is found that the dominating mechanism dictates the overall rate of reorientation. Based on these results, it is concluded that above a certain initial orientation parallel to the electrodes, i. e. perpendicular to the field lines, the defect density is too low to allow for *rotation* of domains. In addition, the pressure on well-aligned lamellae is larger than for less aligned lamellae leading to undulation instabilities which serve as nucleation centers for the growth of lamellae oriented parallel to the electric field lines. The interpretation of these findings is strongly corroborated by dynamic self-consistent field simulations.

Furthermore, following discussions on the driving force leading to microdomain orientation, the impact of the dielectric contrast on the reorientation kinetics is demonstrated. The reorientation kinetics of various block copolymer solutions ex-

posed to a DC electric field was studied. The characteristic times for the alignment process follow a power law indicating that the reorientation is driven by a decrease in electrostatic energy. Moreover, when properly scaled, the data collapse onto a single master curve spanning several orders of magnitude both in reduced time and in reduced energy. The observed exponent suggest an activated process in line with the expectations for a *nucleation and growth* process. These observations are corroborated by dynamic self-consistent simulations. In addition, the threshold field for each system was estimated and a dependence on the dielectric contrast is found. These experimental data strongly indicate that the reorientation process is dominated by differences in the dielectric constant rather than by possible mobile ions. Furthermore, first experiments in AC electric fields at sufficiently high frequencies confirm this notion.

The second part of this thesis describes the influence of an electric field on the phase behavior of block copolymers. It is shown that a gyroid phase (G) as well as a hexagonally perforated lamella phase (HPL) exposed to an electric field undergo a phase transition to cylinders (C) and lamellae (L), respectively. Furthermore, an anisotropic deformation of the chain conformation in various lamellar and cylindrical block copolymer solutions via electric fields is demonstrated.

In order to study possible phase transitions under the influence of an electric field various microdomain structures were investigated. Different order-order-transitions (OOTs) and reorientation mechanisms can be identified for higher electric field strengths depending on the original microdomain structure. An electric field induced alignment can be achieved for the anisotropic microdomain structures, such as lamellae, hexagonally perforated lamellae and cylinders. For the cubic gyroid phase an alignment does not occur. OOTs are found for microdomain structures which cannot be aligned in the electric field direction in a way that all dielectric interfaces are parallel to the field lines. In the case of the metastable HPL phase the layers can be aligned in the field direction but not the perforation. Here, a transition to the lamellar phase was observed. The gyroid phase cannot be aligned at all and thus a transition to the cylinder phase occurs. This transition proceeds via an HPL phase in the direction from G→C and via 3-, 4- and 5-fold reconnections of cylinders to form a bicontinous network from C→G. The driving force for these OOTs is the electrostatic energy penalty associated with the dielectric interfaces which are not parallel to the electric field lines. Some of these OOTs were theoretically predicted based on computer simulations using the dynamic self-consistent field theory but

were not observed experimentally yet.

In addition, a strong response of the characteristic spacing of lamellar and cylindrical microdomain structures of block copolymers exposed to an electric field is found. If one block has different polarizabilities along the backbone and along the side chain the following effect is observed: When the lamellae are aligned in the field direction, the lamellar distance decreases with increasing electric field strength. On the other hand, the lamellae which are oriented perpendicular to the field show a slightly increasing domain spacing. This behavior can be explained by a chain stretching effect due to coupling of the induced monomeric dipoles to the electric field. The change in the periodicity becomes more pronounced with increasing electric field strength, decreasing segregation power, increasing symmetry of the block ratio, and increasing polarity of the solvent. Furthermore, the observed effect is fully reversible and proceeds on a time scale of several milliseconds making it a very promising candidate in view of possible applications in switchable nanostructures. The characteristic spacing of a microdomain structure is usually determined by molecular parameters of the constituent polymer molecules and cannot easily be adjusted on demand. Here, the domain spacing can be changed by as much as six percent depending on the electric field strength without changing the molecular weight or the block ratio, and without chemically modifying the polymer or including any additives.

In summary, the driving force of the electric field induced alignment of block copolymer structures as well as the microscopic mechanism and kinetics were clarified. In addition, it was demonstrated that the application of an electric field not only reorients anisotropic microdomain structures but also induces order-order transitions for microdomain structures which cannot be aligned in the electric field direction in a way that all dielectric interfaces are parallel to the field lines. Furthermore, an effect of the electric field on chain conformation was found leading to a reversible change in the characteristic spacing of the respective microdomain structure.

Zusammenfassung

In der vorliegenden Arbeit wurde der Einfluss von äußeren elektrischen Feldern auf die Mikrodomänenstruktur von Blockcopolymeren untersucht. Die Resultate reichen von einer Analyse der Mechanismen und Kinetik des Reorientierungsprozesses, über eine Diskussion der treibenden Kraft für diesen Prozess, bis hin zu ersten Untersuchungen des Einflusses eines elektrischen Feldes auf das Phasenverhalten von Blockcopolymeren. Die durch das elektrische Feld hervorgerufenen Effekte auf konzentrierte Blockcopolymerlösungen wurden mittels *in-situ* Röntgenkleinwinkelstreuung (SAXS) untersucht.

Im ersten Teil dieser Arbeit wurden die Mechanismen und die Kinetik der Reorientierung von Diblockcopolymeren unterschiedlicher Zusammensetzung in Lösung analysiert, um die treibende Kraft dieses Prozesses aufzuklären.

Die Mechanismen der Mikrodomänenorientierung von konzentrierten Lösungen eines lamellaren Blockcopolymers wurden unter Einfluss eines elektrischen Gleichstromfeldes untersucht. Es konnte gezeigt werden, dass sowohl der Mechanismus als auch die Kinetik der Reorientierung stark von dem Ordnungsgrad vor dem Anlegen des elektrischen Feldes abhängt. In einem hoch geordneten System, bei dem die Lamellen senkrecht zu dem elektrischen Feldvektor ausgerichtet sind, ist der einzig mögliche Weg für die Reorientierung der *Nukleierungs- und Wachstumsprozess*, welcher relativ langsam verläuft. In schwach geordneten Systemen wird die *Rotation von Domänen* als alternativer Mechanismus möglich und die Reorientierung verläuft deutlich schneller. Für dazwischen liegende Ordnungsgrade verläuft die Reorientierung über beide Mechanismen. Es konnte dabei gezeigt werden, dass der vorherrschende Mechanismus die Geschwindigkeit der Ausrichtung bestimmt. Aufgrund dieser Resultate kann gefolgert werden, dass bei einem bestimmten Grad der Vororientierung parallel zu den Elektroden, und somit senkrecht zum elektrischen Feldvektor, die Defektdichte zu niedrig für den *Rotationprozess* ist. Außerdem ist die Kraft auf gut ausgerichtete Lamellen größer als auf schwach ausgerichtete Lamellen,

dies führt zu Undulationen, welche als Nukleierungszentren für Lamellen, die parallel zu den elektrischen Feldlinien wachsen, dienen können. Die Interpretation dieser Ergebnisse wird durch Simulationen gestützt, die dynamischen selbstkonsistenten Feldtheorie beruhen.

Weiterhin wurde aufgrund von Diskussionen über die treibende Kraft, die zur Reorientierung von Mikrodomänen führt, der Einfluss des dielektrischen Kontrastes auf die Reorientierungskinetik untersucht. Dafür wurde die Reorientierungskinetik von einer Vielzahl von Blockcopolymerlösungen unter Einfluss eines elektrischen Gleichstromfeldes studiert. Die charakteristischen Zeitkonstanten für den Ausrichtungsprozess folgen einem Potenzgesetz, welches auf eine Reorientierung durch eine Abnahme der elektrostatischen Energie hinweist. Darüber hinaus fallen die Daten, wenn sie entsprechend skaliert werden, auf eine Masterkurve, die sich über mehrere Größenordnungen in sowohl in der reduzierten Zeit als auch in der reduzierten Energie erstreckt. Der resultierende Exponent deutet einen aktivierten Prozess hin, wie er auch für den *Nukleierungs- und Wachstumsprozess* erwartet wird. Diese Beobachtungen werden auch durch Simulationen, basierend auf der dynamischen selbstkonsistenten Feldtheorie, gestützt. Zusätzlich wurde der elektrische Schwellenwert für die Reorientierung bestimmt und es wurde eine Abhängigkeit von dem dielektrischen Kontrast gefunden. Diese experimentellen Daten weisen stark darauf hin, dass der Reorientierungsprozess eher durch den dielektrischen Kontrast als durch mögliche bewegliche Ionen hervorgerufen wird. Weiterhin wurden erste Experimente mit elektrischen Wechselfeldern bei genügend hohen Frequenzen durchgeführt, die ebenfalls diese Annahme bestätigen.

Der zweite Teil dieser Arbeit beschreibt den Einfluss eines elektrischen Feldes auf das Phasenverhalten von Blockcopolymeren. Es konnte gezeigt werden, dass sowohl die Gyroid-Phase (G) als auch die hexagonal perforierte lamellare Phase (HPL) einer Phasenumwandlung zu Zylindern (C) bzw. Lamellen (L) unter dem Einfluss eines elektrischen Feldes unterliegen. Weiterhin wurde eine durch elektrische Felder hervorgerufene anisotrope Deformation der Kettenkonformation in verschiedenen lamellaren und zylindrischen Blockcopolymerlösungen gefunden.

Um mögliche Phasenübergänge unter Einfluss eines elektrischen Feldes zu untersuchen, wurden unterschiedliche Mikrodomänenstrukturen studiert. Verschiedene Ordnungs-Ordnungs-Übergänge und Reorientierungsmechanismen wurden in Abhängigkeit von der anfänglichen Mikrodomänenstruktur für hohe Feldstärken gefunden. Eine Ausrichtung durch das elektrische Feld konnte für anisotrope Struk-

turen wie Lamellen, hexagonal perforierte Lamellen und Zylinder erreicht werden. Für die kubische Gyroid-Phase tritt keine Ausrichtung auf. Ordnungs-Ordnungs-Übergänge wurden für Strukturen gefunden, bei denen nicht alle dielektrischen Grenzflächen parallel zu den Feldlinien ausgerichtet werden können. Im Fall der HPL-Phase können zwar die Schichten ausgerichtet werden, jedoch nicht die hexagonalen Perforationen. Hier wurde ein Übergang zur lamellaren Phase beobachtet. Die Gyroid-Phase kann überhaupt nicht ausgerichtet werden. Daher erfolgt ein Übergang in die zylindrische Phase. Dieser Übergang vollzieht sich über die HPL-Phase in Richtung G→C und unter vielfacher Verknüpfung der Zylinder von C→G. Die treibende Kraft für diese Ordnungs-Ordnungs-Übergänge ist die höhere freie Energie, die von der elektrostatischen Energie der nicht ausgerichteten dielektrischen Grenzflächen im elektrischen Feld herrührt. Einige dieser Ordnungs-Ordnungs-Übergänge wurden aufgrund von Simulationen theoretisch vorhergesagt, aber bisher noch nicht experimentell beobachtet.

Weiterhin wurde eine starke Abhängigkeit der charakteristischen Abstände von lamellaren und zylindrischen Blockcopolymermikrostrukturen abhängig von der elektrischen Feldstärke gefunden. Wenn ein Block unterschiedliche Polarisierbarkeiten entlang des Rückgrats und entlang der Seitenkette aufweist wird folgender Effekt beobachtet: Für die Lamelle, die in Feldrichtung ausgerichtet ist, nimmt der Lamellenabstand mit steigender Feldstärke ab. Andererseits nimmt der Lamellenabstand leicht zu, wenn die Lamelle senkrecht zum Feld ausgerichtet ist. Dieses Verhalten kann durch einen Kettenstreckungseffekt erklärt werden, der durch die Ausrichtung der induzierten Dipole in den Monomeren durch das elektrische Feld hervorgerufen wird. Die Änderung in der Periodizität ist stärker ausgeprägt mit steigender Feldstärke, abnehmender Phasenseparation, zunehmender Symmetrie der Blockverhältnisse und zunehmender Polarität des Lösungsmittels. Weiterhin ist dieser Effekt vollständig reversibel und vollzieht sich innerhalb von Millisekunden. Dies macht den Effekt viel versprechend im Hinblick auf mögliche Anwendungen von schaltbaren Nanostrukturen. Die charakteristischen Abstände in Mikrodomänstrukturen werden normalerweise durch molekulare Parameter des entsprechenden Polymers bestimmt und können nicht einfach nach Wunsch geändert werden. Hier können die Domänenabstände in Abhängigkeit von der elektrischen Feldstärke ohne Änderung des Molekulargewichtes, der Blockverhältnisse, ohne chemische Modifikation des Polymers oder durch irgendwelche niedermolekularen Zusätze um bis zu 6% geändert werden.

Zusammenfassend wurden die sowohl die treibende Kraft als auch die mikroskopischen Mechanismen und die Kinetik für die Ausrichtung von Blockcopolymerstrukturen mittels elektrischer Felder aufgeklärt. Weiterhin wurde gezeigt, dass das Anlegen eines elektrischen Feldes nicht nur anisotrope Strukturen ausrichtet, sondern auch Ordnungs-Ordnungs-Übergänge in Strukturen hervorruft, deren dielektrische Grenzflächen nicht komplett ausgerichtet werden können. Außerdem wurde ein Effekt des elektrischen Feldes auf die Kettenkonformation gefunden, so dass eine reversible Änderung der charakteristischen Abstände der entsprechenden Mikrodomänenstruktur erfolgt.

Bibliography

[Abe00] V. Abetz and T. Goldacker. "Formation of superlattices via blending of block copolymers". *Macromol Rapid Comm*, **21** (1), 16–34 (2000)

[Ahn00] J. H. Ahn and W. C. Zin. "Structure of shear-induced perforated layer phase in styrene-isoprene diblock copolymer melts". *Macromolecules*, **33** (2), 641–644 (2000)

[Alb94] R. J. Albalak and E. L. Thomas. "Roll-Casting of Block-Copolymers and of Block Copolymer-Homopolymer Blends". *Journal of Polymer Science Part B-Polymer Physics*, **32** (2), 341–350 (1994)

[Alm90] K. Almdal, J. H. Rosedale, F. S. Bates, G. D. Wignall, and G. H. Fredrickson. "Gaussian-Coil to Stretched-Coil Transition in Block Copolymer Melts". *Phys. Rev. Lett.*, **65** (9), 1112–1115 (1990)

[Amu91] K. Amundson, E. Helfand, D. D. Davis, X. Quan, S. S. Patel, and S. D. Smith. "Effect of an Electric-Field on Block Copolymer Microstructure". *Macromolecules*, **24** (24), 6546–6548 (1991)

[Amu93] K. Amundson, E. Helfand, X. Quan, and S. D. Smith. "Alignment of Lamellar Block-Copolymer Microstructure in an Electric-Field .1. Alignment Kinetics". *Macromolecules*, **26** (11), 2698–2703 (1993)

[Amu94] K. Amundson, E. Helfand, X. N. Quan, S. D. Hudson, and S. D. Smith. "Alignment of Lamellar Block-Copolymer Microstructure in an Electric-Field .2. Mechanisms of Alignment". *Macromolecules*, **27** (22), 6559–6570 (1994)

[Bat90a] F. S. Bates and G. H. Fredrickson. "Block Copolymer Thermodynamics - Theory and Experiment". *Annu. Rev. Phys. Chem.*, **41**, 525–557 (1990)

[Bat90b] F. S. Bates, J. H. Rosedale, and G. H. Fredrickson. "Fluctuation Effects in a Symmetric Diblock Copolymer near the Order-Disorder Transition". *J. Chem. Phys.*, **92** (10), 6255–6270 (1990)

[Bat99] F. S. Bates and G. H. Fredrickson. "Block copolymers - Designer soft materials". *Phys Today*, **52** (2), 32–38 (1999)

[Bök02a] A. Böker. *Self-Assembly of Block Copolymers in External Fields.* Ph.d., Universität Bayreuth (2002)

[Bök02b] A. Böker, H. Elbs, H. Hänsel, A. Knoll, S. Ludwigs, H. Zettl, V. Urban, V. Abetz, A. H. E. Müller, and G. Krausch. "Microscopic mechanisms of electric-field-induced alignment of block copolymer microdomains". *Phys. Rev. Lett.*, **89** (13), 135502 (2002)

[Bök02c] A. Böker, A. Knoll, H. Elbs, V. Abetz, A. H. E. Müller, and G. Krausch. "Large scale domain alignment of a block copolymer from solution using electric fields". *Macromolecules*, **35** (4), 1319–1325 (2002)

[Bök03a] A. Böker, V. Abetz, and G. Krausch. "Comment on "Microscopic mechanisms of electric-field-induced alignment of block copolymer microdomains" - Reply". *Phys. Rev. Lett.*, **90** (4), 049602 (2003)

[Bök03b] A. Böker, H. Elbs, H. Hänsel, A. Knoll, S. Ludwigs, H. Zettl, A. V. Zvelindovsky, G. J. A. Sevink, V. Urban, V. Abetz, A. H. E. Müller, and G. Krausch. "Electric field induced alignment of concentrated block copolymer solutions". *Macromolecules*, **36** (21), 8078–8087 (2003)

[Can05] G. Cantea. *Shear-induced alignment in block copolymer solutions.* Ph.d., Universität Bayreuth (2005)

[Che97] Z. R. Chen, J. A. Kornfield, S. D. Smith, J. T. Grothaus, and M. M. Satkowski. "Pathways to macroscale order in nanostructured block copolymers". *Science*, **277** (5330), 1248–1253 (1997)

[Den40] K. Denbigh. "The polarisabilities of bonds". *Trans Faraday Soc*, **36**, 936 (1940)

[DeR04] J. DeRouchey, T. Thurn-Albrecht, T. P. Russell, and R. Kolb. "Block copolymer domain reorientation in an electric field: An in-situ small-angle X-ray scattering study". *Macromolecules*, **37** (7), 2538–2543 (2004)

[Edr01] A. C. Edrington, A. M. Urbas, P. DeRege, C. X. Chen, T. M. Swager, N. Hadjichristidis, M. Xenidou, L. J. Fetters, J. D. Joannopoulos, Y. Fink, and E. L. Thomas. "Polymer-based photonic crystals". *Adv. Mater.*, **13** (6), 421–425 (2001)

[Esk05] R. Eskimergen, K. Mortensen, and M. E. Vigild. "Shear instability of a gyroid diblock copolymer". *Macromolecules*, **38** (4), 1286–1291 (2005)

[Eur06] European Synchrotron Radiation Facility. "ID2 High Brilliance Beamline". http://www.esrf.eu/UsersAndScience/Experiments/SCMatter/ID02/BeamlineLayout
(Date: September 13, 2006)

[Fen04] J. Feng and E. Ruckenstein. "Long-range ordered structures in diblock copolymer melts induced by combined external fields". *Journal of Chemical Physics*, **121** (3), 1609–1625 (2004)

[För94] S. Förster, A. K. Khandpur, J. Zhao, F. S. Bates, I. W. Hamley, A. J. Ryan, and W. Bras. "Complex Phase-Behavior of Polyisoprene-Polystyrene Diblock Copolymers near the Order-Disorder Transition". *Macromolecules*, **27** (23), 6922–6935 (1994)

[Fra93] J. G. E. M. Fraaije. "Dynamic Density-Functional Theory for Microphase Separation Kinetics of Block-Copolymer Melts". *J. Chem. Phys.*, **99** (11), 9202–9212 (1993)

[Fra97] J. G. E. M. Fraaije, B. A. C. vanVlimmeren, N. M. Maurits, M. Postma, O. A. Evers, C. Hoffmann, P. Altevogt, and G. Goldbeck-Wood. "The dynamic mean-field density functional method and its application to the mesoscopic dynamics of quenched block copolymer melts". *J. Chem. Phys.*, **106** (10), 4260–4269 (1997)

[Fre87] G. H. Fredrickson and E. Helfand. "Fluctuation Effects in the Theory of Microphase Separation in Block Copolymers". *J. Chem. Phys.*, **87** (1), 697–705 (1987)

[Fre89] G. H. Fredrickson and L. Leibler. "Theory of Block Copolymer Solutions - Nonselective Good Solvents". *Macromolecules*, **22** (3), 1238–1250 (1989)

[Fre96] D. Frenkel and B. Smit. *Understand Molecular Simulations* (Academic Press, San Diego, 1996)

[Fri91] H. Fried and K. Binder. "The Microphase Separation Transition in Symmetrical Diblock Copolymer Melts - a Monte-Carlo Study". *J. Chem. Phys.*, **94** (12), 8349–8366 (1991)

[Fuk95] J. Fukuda and A. Onuki. "Dynamics of Undulation Instability in Lamellar Systems". *Journal De Physique II*, **5** (8), 1107–1113 (1995)

[Gar90] C. Gardiner. *Handbook of Stochastic Methods* (Springer, Berlin, 1990)

[Gol99] T. Goldacker. *Überstrukturen in Mischungen aus Blockcopolymeren*. Ph.d., Universität Bayreuth (1999)

[Gun07] I. Gunkel, S. Stepanow, T. Thurn-Albrecht, and S. Trimper. "Fluctuation effects in the theory of microphase separation of diblock copolymers in the presence of an electric field". *Macromolecules*, **40** (6), 2186–2191 (2007)

[Gur94a] E. Gurovich. "Copolymers under a Monomer Orienting Field". *Macromolecules*, **27** (24), 7063–7066 (1994)

[Gur94b] E. Gurovich. "On Microphase Separation of Block-Copolymers in an Electric-Field - 4 Universal Classes". *Macromolecules*, **27** (25), 7339–7362 (1994)

[Gur95] E. Gurovich. "Why Does an Electric-Field Align Structures in Copolymers". *Physical Review Letters*, **74** (3), 482–485 (1995)

[Hah87] T. Hahn. *International Table for Crystallography*, volume A (Kluwer Academic Publishing, Dordrecht, 1987), 2nd edition

[Haj94] D. A. Hajduk, P. E. Harper, S. M. Gruner, C. C. Honeker, G. Kim, E. L. Thomas, and L. J. Fetters. "The Gyroid - a New Equilibrium Morphology in Weakly Segregated Diblock Copolymers". *Macromolecules*, **27** (15), 4063–4075 (1994)

[Haj95] D. A. Hajduk, P. E. Harper, S. M. Gruner, C. C. Honeker, E. L. Thomas, and L. J. Fetters. "A Reevaluation of Bicontinuous Cubic Phases in Starblock Copolymers". *Macromolecules*, **28** (7), 2570–2573 (1995)

[Haj98] D. A. Hajduk, R. M. Ho, M. A. Hillmyer, F. S. Bates, and K. Almdal. "Transition mechanisms for complex ordered phases in block copolymer melts". *J. Phys. Chem. B*, **102** (8), 1356–1363 (1998)

[Ham99] I. W. Hamley, J. P. A. Fairclough, A. J. Ryan, S. M. Mai, and C. Booth. "Lamellar-to-gyroid transition in a poly(oxyethylene)-poly(oxybutylene) diblock copolymer melt". *PCCP Phys. Chem. Chem. Phys.*, **1** (9), 2097–2101 (1999)

[Ham04] I. W. Hamley, V. Castelletto, O. O. Mykhaylyk, Z. Yang, R. P. May, K. S. Lyakhova, G. J. A. Sevink, and A. V. Zvelindovsky. "Mechanism of the transition between lamellar and gyroid phases formed by a diblock copolymer in aqueous solution". *Langmuir*, **20** (25), 10785–10790 (2004)

[Han98] K. J. Hanley and T. P. Lodge. "Effect of dilution on a block copolymer in the complex phase window". *J Polym Sci Pol Phys*, **36** (17), 3101–3113 (1998)

[Han00] K. J. Hanley, T. P. Lodge, and C. I. Huang. "Phase behavior of a block copolymer in solvents of varying selectivity". *Macromolecules*, **33** (16), 5918–5931 (2000)

[Has97] T. Hashimoto, K. Tsutsumi, and Y. Funaki. "Nanoprocessing based on bicontinuous microdomains of block copolymers: Nanochannels coated with metals". *Langmuir*, **13** (26), 6869–6872 (1997)

[Has99] T. Hashimoto, J. Bodycomb, Y. Funaki, and K. Kimishima. "The effect of temperature gradient on the microdomain orientation of diblock copolymers undergoing an order-disorder transition". *Macromolecules*, **32** (3), 952–954 (1999)

[Hel72] E. Helfand and Y. Tagami. "Theory of Interface between Immiscible Polymers .2." *J. Chem. Phys.*, **56** (7), 3592 (1972)

[Hel76] E. Helfand and Z. R. Wasserman. "Block Copolymer Theory .4. Narrow Interphase Approximation". *Macromolecules*, **9** (6), 879–888 (1976)

[Hel80] E. Helfand and Z. R. Wasserman. "Block Co-Polymer Theory .6. Cylindrical Domains". *Macromolecules*, **13** (4), 994–998 (1980)

[Her39] P. Hermans and P. Platzek. "New data on the relationship between swelling anisotropy and deformation mechanism of hydrated cellulose gels". *Kolloid-Zeitschrift*, **87**, 296–308 (1939)

[Hon83] K. M. Hong and J. Noolandi. "Theory of Phase-Equilibria in Systems Containing Block Co-Polymers". *Macromolecules*, **16** (7), 1083–1093 (1983)

[Hon06] T. Honda and T. Kawakatsu. "Epitaxial transition from gyroid to cylinder in a diblock copolymer melt". *Macromolecules*, **39** (6), 2340–2349 (2006)

[Hua98] C. I. Huang, B. R. Chapman, T. P. Lodge, and N. P. Balsara. "Quantifying the "neutrality" of good solvents for block copolymers: Poly(styrene-b-isoprene) in toluene, benzene, and THF". *Macromolecules*, **31** (26), 9384–9386 (1998)

[Ima01] M. Imai, A. Saeki, T. Teramoto, A. Kawaguchi, K. Nakaya, T. Kato, and K. Ito. "Kinetic pathway of lamellar -¿ gyroid transition: Pretransition and transient states". *J. Chem. Phys.*, **115** (22), 10525–10531 (2001)

[Ima05] M. Imai, K. Sakai, M. Kikuchi, K. Nakaya, A. Saeki, and T. Teramoto. "Kinetic pathway to double-gyroid structure". *J. Chem. Phys.*, **122** (21), 214906 (2005)

[Kel70] A. Keller, E. Pedemonte, and F. M. Willmouth. "Macro-lattice from segregated amorphous phases of a three block copolymer". *Nature*, **225** (5232), 538–9 (1970)

[Kha95] A. K. Khandpur, S. Forster, F. S. Bates, I. W. Hamley, A. J. Ryan, W. Bras, K. Almdal, and K. Mortensen. "Polyisoprene-polystyrene diblock copolymer phase diagram near the order-disorder transition". *Macromolecules*, **28** (26), 8796–8806 (1995)

[Kim00] K. Kimishima, T. Koga, and T. Hashimoto. "Order-order phase transition between spherical and cylindrical microdomain structures of block copolymer. I. Mechanism of the transition". *Macromolecules*, **33** (3), 968–977 (2000)

[Kre02] F. Kremer and A. Schönhals. *Broadband Dielectric Spectroscopy* (Springer, Berlin, 2002)

[Kri00] R. Krishnamoorti, A. S. Silva, M. A. Modi, and B. Hammouda. "Small-angle neutron scattering study of a cylinder-to-sphere order-order transition in block copolymers". *Macromolecules*, **33** (10), 3803–3809 (2000)

[Kyr02] A. V. Kyrylyuk, A. V. Zvelindovsky, G. J. A. Sevink, and J. G. E. M. Fraaije. "Lamellar alignment of diblock copolymers in an electric field". *Macromolecules*, **35** (4), 1473–1476 (2002)

[Lan84] L. Landau, E. Lifshitz, and L. Pitaevskii. *Landau and Lifshitz Course of Theoretical Physics: Electrodynamics of Continuous Media*, volume Vol 8 (Pergamon Press, New York, 1984), 2nd edition

[Lau99] J. H. Laurer, B. S. Pinheiro, D. L. Polis, and K. I. Winey. "Persistence of surface-induced alignment in block copolymers upon large-amplitude oscillatory shear processing". *Macromolecules*, **32** (15), 4999–5003 (1999)

[Lee02] H. H. Lee, W. Y. Jeong, J. K. Kim, K. J. Ihn, J. A. Kornfield, Z. G. Wang, and S. Y. Qi. "Orientational proliferation and successive twinning from thermoreversible hexagonal-body-centered cubic transitions". *Macromolecules*, **35** (3), 785–794 (2002)

[Lei80] L. Leibler. "Theory of Microphase Separation in Block Copolymers". *Macromolecules*, **13** (6), 1602–1617 (1980)

[Lid96] D. R. Lide. *Handbook of Chemistry and Physics* (CRC Press, 1996)

[Lin05] C. Y. Lin, M. Schick, and D. Andelman. "Structural changes of diblock copolymer melts due to an external electric field: A self-consistent-field theory study". *Macromolecules*, **38** (13), 5766–5773 (2005)

[Lod95] T. P. Lodge, C. Pan, X. Jin, Z. Liu, J. Zhao, W. W. Maurer, and F. S. Bates. "Failure of the Dilution Approximation in Block-Copolymer Solutions". *J Polym Sci Pol Phys*, **33** (16), 2289–2293 (1995)

[Lod03] T. P. Lodge, K. J. Hanley, B. Pudil, and V. Alahapperuma. "Phase behavior of block copolymers in a neutral solvent". *Macromolecules*, **36** (3), 816–822 (2003)

[Luz67] V. Luzzati and P. A. Spegt. "Polymorphism of Lipids". *Nature*, **215** (5102), 701 (1967)

[Ly07] D. Q. Ly, T. Honda, T. Kawakatsu, and A. V. Zvelindovsky. "Kinetic pathway of gyroid-to-cylinder transition in diblock copolymer melt under an electric field". *Macromolecules*, **40** (8), 2928–2935 (2007)

[Lya06a] K. S. Lyakhova, A. Horvat, A. V. Zvelindovsky, and G. J. A. Sevink. "Dynamics of terrace formation in a nanostructured thin block copolymer film". *Langmuir*, **22** (13), 5848–5855 (2006)

[Lya06b] K. S. Lyakhova, A. V. Zvelindovsky, and G. J. A. Sevink. "Kinetic pathways of order-to-order phase transitions in block copolymer films under an electric field". *Macromolecules*, **39** (8), 3024–3037 (2006)

[Mat94] M. W. Matsen and M. Schick. "Stable and Unstable Phases of a Diblock Copolymer Melt". *Phys. Rev. Lett.*, **72** (16), 2660–2663 (1994)

[Mat96] M. W. Matsen and F. S. Bates. "Unifying weak- and strong-segregation block copolymer theories". *Macromolecules*, **29** (4), 1091–1098 (1996)

[Mat97a] M. W. Matsen and F. S. Bates. "Block copolymer microstructures in the intermediate-segregation regime". *J. Chem. Phys.*, **106** (6), 2436–2448 (1997)

[Mat97b] M. W. Matsen and F. S. Bates. "Conformationally asymmetric block copolymers". *J Polym Sci Pol Phys*, **35** (6), 945–952 (1997)

[Mat98] M. W. Matsen. "Cylinder ¡-¿ gyroid epitaxial transitions in complex polymeric liquids". *Phys. Rev. Lett.*, **80** (20), 4470–4473 (1998)

[Mat05] M. W. Matsen. "Stability of a Block-Copolymer Lamella in a strong Electric Field". *Physical Review Letters*, **95**, 258302 (2005)

[Nar07] T. Narayanan. "Synchrotron small-angle X-ray scattering". In R. Borsali and R. Pecora (Editors), "Soft Matter: Scattering, Imaging and Manipulation, Vol III", (Springer, 2007)

[Neg97] S. Negi, J. Li, S. M. Khan, and I. M. Khan. "High dielectric constant (microwave frequencies) polymer composites." *Abstracts of Papers of the American Chemical Society*, **214**, 223–Poly (1997)

[Oht86] T. Ohta and K. Kawasaki. "Equilibrium Morphology of Block Copolymer Melts". *Macromolecules*, **19** (10), 2621–2632 (1986)

[Ols06] V. Olszowka, M. Hund, V. Kuntermann, S. Scherdel, L. Tsarkova, A. Böker, and G. Krausch. "Large scale alignment of a lamellar block copolymer thin film via electric fields: a time-resolved SFM study". *Soft Matter*, **2**, 1089–1094 (2006)

[Onu95] A. Onuki and J. Fukuda. "Electric field effects and form birefringence in diblock copolymers". *Macromolecules*, **28** (26), 8788–8795 (1995)

[Oxf07] Oxford Danfysik Synchroton Beamline Engineering. "Synchrotron Setup". http://www.oxford-danfysik.com/media/news/Australian_Synchrotron_Ring.jpg
(Date: May 16, 2007)

[Par05] I. Park, B. Lee, J. Ryu, K. Im, J. Yoon, M. Ree, and T. Chang. "Epitaxial phase transition of polystyrene-b-polyisoprene from hexagonally perforated layer to gyroid phase in thin film". *Macromolecules*, **38** (25), 10532–10536 (2005)

[Per99] G. G. Pereira and D. R. M. Williams. "Diblock copolymer melts in electric fields: The transition from parallel to perpendicular alignment using a capacitor analogy". *Macromolecules*, **32** (24), 8115–8120 (1999)

[Pin06] M. Pinna, A. V. Zvelindovsky, S. Todd, and G. Goldbeck-Wood. "Cubic phases of block copolymers under shear and electric fields by cell dynamics simulation. I. Spherical phase". *Journal of Chemical Physics*, **125** (15), 154905 (2006)

[Pol96] D. L. Polis and K. I. Winey. "Kink bands in a lamellar diblock copolymer induced by large amplitude oscillatory shear". *Macromolecules*, **29** (25), 8180–8187 (1996)

[Pri95] C. Price, N. Deng, F. R. Lloyd, H. Li, and C. Booth. "Studies of poly(styrene) solutions in an electric field: viscosity and dynamic light scattering". *Journal of the Chemical Society, Faraday Transactions*, **91** (9), 1357–62 (1995)

[Roe00] R. J. Roe. *Methods of X-Ray and Neutron Scattering in Polymer Science* (Oxford University Press, 2000)

[Ros95] J. Rosedale, F. S. Bates, K. Almdal, K. Mortensen, and G. D. Wignall. "Order and Disorder in Symmetrical Diblock Copolymer Melts". *Macromolecules*, **28** (5), 1429–1443 (1995)

[Sak98] S. Sakurai, H. Umeda, C. Furukawa, H. Irie, S. Nomura, H. H. Lee, and J. K. Kim. "Thermally induced morphological transition from lamella to gyroid in a binary blend of diblock copolymers". *J. Chem. Phys.*, **108** (10), 4333–4339 (1998)

[Sch94] M. F. Schulz, F. S. Bates, K. Almdal, and K. Mortensen. "Epitaxial Relationship for Hexagonal-to-Cubic Phase-Transition in a Block-Copolymer Mixture". *Phys. Rev. Lett.*, **73** (1), 86–89 (1994)

[Sch02] S. C. Schmidt and M. A. Hillmyer. "Morphological behavior of model poly(ethylene-alt-propylene)-b-polylactide diblock copolymers". *J Polym Sci Pol Phys*, **40** (20), 2364–2376 (2002)

[Sem93] A. N. Semenov. "Theory of Block-Copolymer Interfaces in the Strong Segregation Limit". *Macromolecules*, **26** (24), 6617–6621 (1993)

[Sev99] G. J. A. Sevink, A. V. Zvelindovsky, B. A. C. van Vlimmeren, N. M. Maurits, and J. G. E. M. Fraaije. "Dynamics of surface directed mesophase formation in block copolymer melts". *J. Chem. Phys.*, **110** (4), 2250–2256 (1999)

[Spr05] Spring 8. "Synchrotron Setup".
http://www.spring8.or.jp/s8studycase/en/users/current_user/bl/source/en/users/current_user/bl/source/publicfolder.2005-09-27.1881239888/undprinciple.png
(Date: September 19, 2005)

[Sun99] Z. Sun and C. H. Wang. "Dynamics of polymer chains in solution subject to an electric field probed by quasielastic light scattering". *Macromolecules*, **32** (8), 2605–2609 (1999)

[Szw56] M. Szwarc. "Living Polymers". *Nature*, **178** (4543), 1168–1169 (1956)

[TA00] T. Thurn-Albrecht, J. DeRouchey, T. P. Russell, and H. M. Jaeger. "Overcoming interfacial interactions with electric fields". *Macromolecules*, **33** (9), 3250–3253 (2000)

[TA02] T. Thurn-Albrecht, J. DeRouchey, T. P. Russell, and R. Kolb. "Pathways toward electric field induced alignment of block copolymers". *Macromolecules*, **35** (21), 8106–8110 (2002)

[Tan91] H. Tanaka, H. Hasegawa, and T. Hashimoto. "Ordered Structure in Mixtures of a Block Copolymer and Homopolymers .1. Solubilization of Low-Molecular-Weight Homopolymers". *Macromolecules*, **24** (1), 240–251 (1991)

[Tso02] Y. Tsori and D. Andelman. "Thin film diblock copolymers in electric field: Transition from perpendicular to parallel lamellae". *Macromolecules*, **35** (13), 5161–5170 (2002)

[Tso03a] Y. Tsori, F. Tournilhac, D. Andelman, and L. Leibler. "Structural changes in block copolymers: Coupling of electric field and mobile ions". *Physical Review Letters*, **90** (14), 145504/145501–145504/145504 (2003)

[Tso03b] Y. Tsori, F. Tournilhac, and L. Leibler. "Orienting ion-containing block copolymers using ac electric fields". *Macromolecules*, **36** (15), 5873–5877 (2003)

[Tso06] Y. Tsori, D. Andelman, C. Y. Lin, and M. Schick. "Block copolymers in electric fields: A comparison of single-mode and self-consistent-field approximations". *Macromolecules*, **39** (1), 289–293 (2006)

[Urb00] A. Urbas, R. Sharp, Y. Fink, E. L. Thomas, M. Xenidou, and L. J. Fetters. "Tunable block copolymer/homopolymer photonic crystals". *Advanced Materials*, **12** (11), 812–814 (2000)

[Vig98] M. E. Vigild, K. Almdal, K. Mortensen, I. W. Hamley, J. P. A. Fairclough, and A. J. Ryan. "Transformations to and from the gyroid phase in a diblock copolymer". *Macromolecules*, **31** (17), 5702–5716 (1998)

[Wan02] C. Y. Wang and T. P. Lodge. "Kinetics and mechanisms for the cylinder-to-gyroid transition in a block copolymer solution". *Macromolecules*, **35** (18), 6997–7006 (2002)

[Wan06] J. Y. Wang, T. Xu, J. M. Leiston-Belanger, S. Gupta, and T. P. Russell. "Ion Complexation: A Route to Enhanced Block Copolymer Alignment with Electric Fields". *Physical Review Letters*, **96**, 128301 (2006)

[Whi90] M. D. Whitmore and J. Noolandi. "Self-Consistent Theory of Block Copolymer Blends - Neutral Solvent". *J. Chem. Phys.*, **93** (4), 2946–2955 (1990)

[Whi92] M. D. Whitmore and J. D. Vavasour. "Self-Consistent Mean Field-Theory of the Microphase Diagram of Block Copolymer Neutral Solvent Blends". *Macromolecules*, **25** (7), 2041–2045 (1992)

[Win91a] K. I. Winey, E. L. Thomas, and L. J. Fetters. "Ordered Morphologies in Binary Blends of Diblock Copolymer and Homopolymer and Characterization of Their Intermaterial Dividing Surfaces". *Journal of Chemical Physics*, **95** (12), 9367–9375 (1991)

[Win91b] K. I. Winey, E. L. Thomas, and L. J. Fetters. "Swelling a Lamellar Diblock Copolymer with Homopolymer - Influences of Homopolymer Concentration and Molecular-Weight". *Macromolecules*, **24** (23), 6182–6188 (1991)

[Win93] K. I. Winey, S. S. Patel, R. G. Larson, and H. Watanabe. "Morphology of a Lamellar Diblock Copolymer Aligned Perpendicular to the Sample Plane - Transmission Electron-Microscopy and Small-Angle X-Ray-Scattering". *Macromolecules*, **26** (16), 4373–4375 (1993)

[Xu03a] T. Xu, J. T. Goldbach, and T. P. Russell. "Sequential, orthogonal fields: A path to long-range, 3-D order in block copolymer thin films". *Macromolecules*, **36** (19), 7296–7300 (2003)

[Xu03b] T. Xu, C. J. Hawker, and T. P. Russell. "Interfacial energy effects on the electric field alignment of symmetric diblock copolymers". *Macromolecules*, **36** (16), 6178–6182 (2003)

[Xu04a] T. Xu, J. T. Goldbach, J. Leiston-Belanger, and T. P. Russell. "Effect of ionic impurities on the electric field alignment of diblock copolymer thin films". *Colloid and Polymer Science*, **282** (8), 927–931 (2004)

[Xu04b] T. Xu, Y. Q. Zhu, S. P. Gido, and T. P. Russell. "Electric field alignment of symmetric diblock copolymer thin films". *Macromolecules*, **37** (7), 2625–2629 (2004)

[Xu04c] T. Xu, A. V. Zvelindovsky, G. J. A. Sevink, O. Gang, B. Ocko, Y. Q. Zhu, S. P. Gido, and T. P. Russell. "Electric field induced sphere-to-cylinder

transition in diblock copolymer thin films". *Macromolecules*, **37** (18), 6980–6984 (2004)

[Xu05a] T. Xu, C. J. Hawker, and T. P. Russell. "Interfacial interaction dependence of microdomain orientation in diblock copolymer thin films". *Macromolecules*, **38** (7), 2802–2805 (2005)

[Xu05b] T. Xu, A. V. Zvelindovsky, G. J. A. Sevink, K. S. Lyakhova, H. Jinnai, and T. P. Russell. "Electric field alignment of asymmetric diblock copolymer thin films". *Macromolecules*, **38** (26), 10788–10798 (2005)

[Yam94] R. Yamaguchi and S. Sato. "Relationship between Film Thickness and Electro-Optical Properties in Polymer Dispersed Liquid Crystal Films". *Japanese Journal of Applied Physics Part 2: Letters*, **33**, 4007 (1994)

[Yu05] B. Yu, B. H. Li, P. C. Sun, T. H. Chen, Q. H. Jin, D. T. Ding, and A. C. Shi. "Cylinder-gyroid-lamella transitions in diblock copolymer solutions: A simulated annealing study". *J. Chem. Phys.*, **123** (23), – (2005)

[Zha98] D. Y. Zhao, J. L. Feng, Q. S. Huo, N. Melosh, G. H. Fredrickson, B. F. Chmelka, and G. D. Stucky. "Triblock copolymer syntheses of mesoporous silica with periodic 50 to 300 angstrom pores". *Science*, **279** (5350), 548–552 (1998)

[Zhu03] L. Zhu, P. Huang, W. Y. Chen, X. Weng, S. Z. D. Cheng, Q. Ge, R. P. Quirk, T. Senador, M. T. Shaw, E. L. Thomas, B. Lotz, B. S. Hsiao, F. J. Yeh, and L. Z. Liu. ""Plastic deformation" mechanism and phase transformation in a shear-induced metastable hexagonally perforated layer phase of a polystyrene-b-poly(ethylene oxide) diblock copolymer". *Macromolecules*, **36** (9), 3180–3188 (2003)

[Zve98] A. V. Zvelindovsky, G. J. A. Sevink, B. A. C. van Vlimmeren, N. M. Maurits, and J. G. E. M. Fraaije. "Three-dimensional mesoscale dynamics of block copolymers under shear: The dynamic density-functional approach". *Phys. Rev. E*, **57** (5), R4879–R4882 (1998)

[Zve00] A. V. Zvelindovsky, G. J. A. Sevink, and J. G. E. M. Fraaije. "Shear-induced transitions in a ternary polymeric system". *Phys. Rev. E*, **62** (3), R3063–R3066 (2000)

[Zve03] A. V. Zvelindovsky and G. J. A. Sevink. "Comment on Microscopic mechanisms of electric-field-induced alignment of block copolymer microdomains". *Physical Review Letters*, **90** (4), 049601 (2003)

[Zve05] A. V. Zvelindovsky and G. J. A. Sevink. "Orthogonal fields: A path to long-range three-dimensional order in block copolymers". *Journal of Chemical Physics*, **123** (7), 074903 (2005)

List of Publications

During the course of this thesis the following papers have been published:

- K. Schmidt, A. Böker, H. Zettl, F. Schubert, H. Hänsel, F. Fischer, T. M. Weiss, V. Abetz, A. V. Zvelindovsky, G. Sevink, and G. Krausch, "Influence of Initial Order on the Microscopic Mechanism of Electric Field Induced Alignment of Block Copolymer Microdomains." *Langmuir* **21**, 11974 (2005)

- A. Böker, K. Schmidt, A. Knoll, H. Zettl, H. Hänsel, V. Urban, V. Abetz, and G. Krausch, "The Influence of Incompatibility and Dielectric Contrast on the Electric Field Induced Orientation of Lamellar Block Copolymers." *Polymer* **47**, 849 (2006)

- K. Schmidt, H. G. Schoberth, F. Schubert, H. Hänsel, F. Fischer, T. M. Weiss, G. Sevink, A. V. Zvelindovsky, A. Böker, and G. Krausch, "Scaling Behavior of the Reorientation Kinetics of Block Copolymers exposed to Electric Fields." *Soft Matter*, **3**, 448 (2007)

- K. Schmidt, H. G. Schoberth, M. A. Ruppel, H. Hänsel, T. M. Weiss, V. Urban, G. Krausch, and A. Böker, "Reversible Tuning of Block Copolymer Domain Spacings via Electric Fields." accepted (2007)

Danksagung

Das Gelingen dieser Arbeit wäre ohne das passende Umfeld und die Unterstützung von vielen Seiten nicht möglich gewesen. Dafür möchte ich mich bedanken bei:

Prof. Alexander Böker für die hervorragende Betreuung, die intensive Förderung dieser Arbeit, zahlreiche Anregungen und Diskussion, sowie für viele Gespräche nicht-wissenschaftlicher Natur. Außerdem möchte ich mich bei ihm für die aufopferungsvolle Einführung in die Welt der Anionik, ebenso für viele großartige Ideen und Aufmunterungen in Grenoble, bedanken.
Prof. Georg Krausch danke ich für die Möglichkeit an einem spannenden Thema in seinem Arbeitskreis arbeiten zu können, die Diskussionsbereitschaft und die fürsorgliche Betreuung.

Für die außergewöhnlich gute „Rund-um-die-Uhr“Betreuung während der ESRF-Messzeiten und für viele anregende Diskussionen darüber hinaus möchte ich mich bei Thomas „*Mikey*“ Weiss bedanken.
Außerdem geht ein großes Dankeschön und die ganzen Grenoble-Teams, Alexander Böker, Frank Schubert, Heiko Zettl, Helmut Hänsel, Heiko Schoberth, Franz Fischer, Kerstin Schindler, Markus Ruppel und Adriana Mihut, ohne die die Messzeiten nie so erfolgreich und unterhaltsam verlaufen wären.

Ich möchte mich bei meinen zwei Büromitbewohnern, Frank Schubert und Helmut Hänsel, bedanken für die unglaubliche Hilfsbereitschaft bei den verschiedensten experimentellen Aufbauten und programmiertechnischen Problemen, für viele fruchtbare Diskussionen, für die gute Einführung in die Sys-Admin Tätigkeit, sowie für die unterhaltsame Büroatmosphäre und vor allem für die sehr gute Freundschaft.
Frank danke ich außerdem für die zahlreichen Freizeitaktivitäten, sei es beim Motorrad fahren, Ricochet spielen oder beim Tanzen, sowie für das schnelle und zu-

verlässige Korrekturlesen.
Helmut danke ich für die Einführung und die tausenden Hilfen in LabView, für das einmalige esrf.vi und ebenfalls für das Korrekturlesen, auch wenn diesmal der „Hänsel-Charme“ nicht ausgereicht hat.

Heiko Zettl danke ich für etliche gute Ideen, für die ebenfalls unglaubliche Hilfsbereitschaft bei den, öfters etwas unkonventionellen, experimentellen Aufbauten und Auswerteproblemen. Weiterhin danke ich ihm für viele schöne Spiele-, Koch- und Kinoabende, die gute Freundschaft und natürlich für die Beschaffung der Nervennahrung - Kaffee und kiloweise Gummibärchen.

Heiko Schoberth danke ich für die sehr gute Zusammenarbeit und für den Mut als Physiker bei einer Chemikerin Diplomarbeit zu machen. Außerdem danke ich ihm für die würdige Nachfolge von Helmut und Frank, sei es als Sys-Admin oder als Büronachbar.

Bei Franz Fischer möchte ich mich für die vielen unkonventionellen Aufbauten, ohne die etliche Messungen nicht erfolgt wären, und die hochspannenden Gespräche bedanken.
Außerdem danke ich den Mitarbeitern der Mechanik Werkstatt, die viele dieser Ideen in die Tat umsetzten.

Für die Einführung in die Neutronenstreuung danke ich Volker Urban, ebenso für die gute Betreuung in Oak Ridge und für seine gelassene Sichtweise der Dinge.

Ich danke Agur Sevink und Andrei Zvelindovsky für viele sehr fruchtbare Diskussionen und interessante Gespräche.

Ein ganz besonderer Dank gilt Sybille Zimmermann, dem guten Geist der PCII, für die Hilfsbereitschaft in bürokratischen und organisatorischen Belangen, für die Versorgung mit Nervennahrung, sowie für ihre liebenswerte Art und immer ein offenes Ohr.

Wolfgang Häfner und Markus Hund danke ich für die Hilfen, wenn LaTeX doch nicht tut, was es soll und für interessante Diskussionen.

Kerstin Schindler, Adriana Mihut und Volker Kuntermann, die mir ebenfalls sehr gute Freunde geworden sind, danke ich für viele kleine und auch größere Ablenkungen vom Büroalltag.

Weiterhin danke ich allen anderen Mitarbeitern der PCII, Arnaud Chiche, Anne Horn, Sven Hüttner, Ute Zettl, Denys Zimin, Andriana Horvat, Nicole Popp, Alexandra Sperschneider, John Bosco Stanislaus, Larisa Tsarkova, Nathalie Mougin, Günther Jutz, Sergej Kutuzov, Violetta Olszowka, Eva Max, Christian Karl, Thomas Czubak, Alexandra Schweikart und Carmen Kunert, besonders den Ehemaligen, Armin und Marina Knoll, Nico und Sabine Rehse und Robert Magerle, für die gute Arbeitsatmoshäre und Zusammenarbeit und für viele gemeinsame Kino-, Grill- und NfS-Abende.

Bei meinem Freund Matthias Kirchner möchte ich mich für die große Unterstützung und das Verständnis während des gesamten Studiums und der Promotion bedanken. Alexander Maurer, Markus Ruppel, Karsten Günther und Michaela Hoffmann danke ich für viele schöne gemeinsame Abende während der Studien- und Promotionszeit und für die langjährige Freundschaft.
Meinen Eltern und meinem Bruder danke ich für die unersetzliche Unterstützung bei allem was ich tue.

Erklärung

Die vorliegende Arbeit wurde von mir selbstständig verfasst und ich habe dabei keine anderen als die angegebenen Hilfsmittel und Quellen benutzt.
Ferner habe ich nicht versucht, anderweitig mit oder ohne Erfolg eine Dissertation einzureichen oder mich der Doktorprüfung zu unterziehen.

Bayreuth, den 21.11.2007

Kristin Schmidt